DOI:10.14753/SE.2024.2993

SEMMELWEIS EGYETEM

DOKTORI ISKOLA

Ph.D. értekezések

2993.

HUANG LUMEI

Funkcionális idegtudományok
című program

Program- és témavezető: Dr. Sperlágh Beáta, c. egyetemi tanár

DOI:10.14753/SE.2024.2993

The regulatory effect of purinergic P2X7Rs on the excitatory neurotransmission and the mouse model of schizophrenia

PhD thesis

Lumei Huang

Doctoral School of János Szentágothai
Semmelweis University

Supervisor: Beáta Sperlágh, MD, PhD, D.Sc

Official reviewers: Czirják Gábor, PhD, D.Sc
Judit Veres, PhD

Head of the Complex Examination Committee: László Köles, MD, PhD

Members of the Complex Examination Committee:
Dóra Zelena, PhD, D.Sc
György Lévay, PhD

Budapest
2024

DOI:10.14753/SE.2024.2993

Table of contents

DOI:10.14753/SE.2024.2993

DOI:10.14753/SE.2024.2993

List of abbreviations

ATP	Adenosine Triphosphate
ACSF	Artificial Cerebrospinal Fluid
Ach	Acetylcholine
Arg1	Arginase
AMPA	α-amino-3-hydroxy-5-methyl-4-isoxazolepropionic acid
ADP	Adenosine Diphosphate
AMP	Adenosine Monophosphate
BC	Basket cell
BzATP	2'(3')-O-(4-Benzoylbenzoyl)adenosine-5'-triphosphate tri(triethylammonium) salt
BSA	Bovine Serum Albumin
CNS	Central Nervous System
CD39	Ectonucleoside triphosphate diphosphohydrolase 1
CD73	Ecto-5′-Nucleotidase
CA1	Cornu Ammonis 1
CA3	Cornu Ammonis 3
CFA	Freund's adjuvant (CFA)
CO2	Carbon Dioxide
CNQX	6-cyano-7-nitroquinoxaline-2,3-dione
CCK	Cholecystokinin
Cx	Connexin
DISC1	Disrupted-In-Schizophrenia 1
DG	Dentate Gyrus
DIV	Day In Vitro
DIC	Differential Interference Contrast
DL-AP5	DL-amino-5-phosphonopentaoic acid
ERK	Extracellular Signal-Regulated Kinase
EC	Entorhinal Cortex
E-NTPD-1	Ectonucleoside triphosphate diphosphohydrolase-1
E-5’-NT	ecto-5′-nucleotidase
FBS	Fetal bovine serum
IN	Interneuron
IML	Inner molecular layer
GCPII	Glutamate carboxypeptidase II
GC	Granule cell
GCL	Granule cell layer
GABA	Gamma-Aminobutyric Acid

GWAS	Genome-Wide Association Studies
LEC	Lateral entorhinal cortex
LPP	lateral perforant path
MC	Mossy Cell
mEPSC	Miniature Excitatory Postsynaptic Current
MIA	Maternal Immune Activation
ML	Molecular layer
MAGUK	Membrane Associated Guanylate Kinase
MEC	Medial entorhinal cortex
MML	Middle molecular layer
MPP	Medial perforant path
NHS	Normal Horse Serum
NA	Norepinephrine
NMDG+	N-methyl-d-glucamine
NPC	Neural Progenitor Cell
NAAG	N-Acetylaspartylglutamic acid
NAA	N-acetylaspartic acid
NaN3	Sodium azide
NMDA	N-methyl-D-aspartate
OML	Outer molecular layer
PCP	Phencyclidine
PFA	Paraformaldehyde
PKC	Protein Kinase C
PLXNs	Plexins
PPR	Paired Pulse Ratio
PPF	Paired pulse facilitation
PPD	Paired pulse depression
PB	Phosphate-buffered saline
PV	Parvalbumin
Pan	Panxin
PWL	Paw withdrawal latency
QX314	N-Ethyllidocaine bromide
SEMA	Semaphorins family
sEPSC	Spontaneous Excitatory Postsynaptic Current
SuM	Supramammillary Nucleus
SCZ	Schizophrenia
SGZ	Subgranular zone
SST	Somatostatin
TTX	Tetrodotoxin
TBS	Tris-buffered saline
VTA	Ventral Tegmental Area
VNUT	Vesicular nucleotide transporter

1. Introduction

Purinergic signalling systems have received extensive research attention in both physiological and pathological conditions due to the discovery that "cellular energy currency" ATP could be released from cell into the extracellular space where it communicates with neighboring cells. As one of the most important receptors, ATP-gated ionotropic purinergic P2X7 receptor is particularly thought to be relevant to pathological conditions due to its low affinity to extracellular ATP. Although the protein and RNA expression of P2X7Rs in neurons have been documented in human excitatory neurons but not in inhibitory neurons (1), in rat hippocampal pyramidal cells (2), and in mouse P2X7R knock-in model (3), the neuronal expression of P2X7Rs and its contribution to neurotransmission are still controversial (4, 5). The dentate gyrus (DG), the "gate" of classic trisynaptic circuit (6, 7), serves as the important connection station between the entorhinal cortex (EC) of the temporal lobe and the rest of the hippocampus regions. However, it is unclear whether P2X7Rs express on DG and further participate in the regulation of excitatory neurotransmission. Moreover, the DG is subject to the development of schizophrenia (SCZ) in both patients and rodents (8-11). Although a few studies have reported that genetic ablation and pharmacological inhibition of P2X7Rs significantly alleviated phencyclidine (PCP)-induced schizophrenia symptoms (12-15), the role of P2X7Rs in PCP-induced neurodevelopment model of SCZ and the involvement of DG in this process are still largely unknown.

Therefore, the aim of this work was to investigate the role of axonal terminal P2X7Rs in excitatory neurotransmission in mouse dentate gyrus granule cells (DG-GC) and its potential mechanisms. In addition, the present study was aimed at investigating whether genetically deleted P2X7Rs could alleviate postnatal PCP-induced SCZ-like symptoms in mice and how DG synapse (EC-GC) responds to this postnatal PCP treatment.

1.1 Purinergic signaling system

1.1.1 The general concept of purinergic signalling system

Adenosine triphosphate (ATP) is recognized as the "energy currency" of the cell. However, since the 1920s, compelling evidence has shown that ATP can also be released

from the cell into the extracellular space, where it fulfils a variety of physiological roles. One important milestone is the identification of ATP or ATP-related nucleotides as transmitters released from intestinal nonadrenergic inhibitory nerves in 1970 (16). Subsequently, Burnstock first proposed the term "purinergic" in the journal Nature in 1971 (17). In addition to ATP release from intestinal nonadrenergic inhibitory nerves, a study demonstrated that ATP could be also released from excitatory nerves in bladder (18). Subsequent experiments uncovered that ATP acts as a transmitter and is released through an exocytotic process along with other transmitters such as ACh (acetylcholine) (19), NA (noradrenaline) (20), glutamate (21), dopamine (22), γ-aminobutyric acid (GABA) (23), and others.

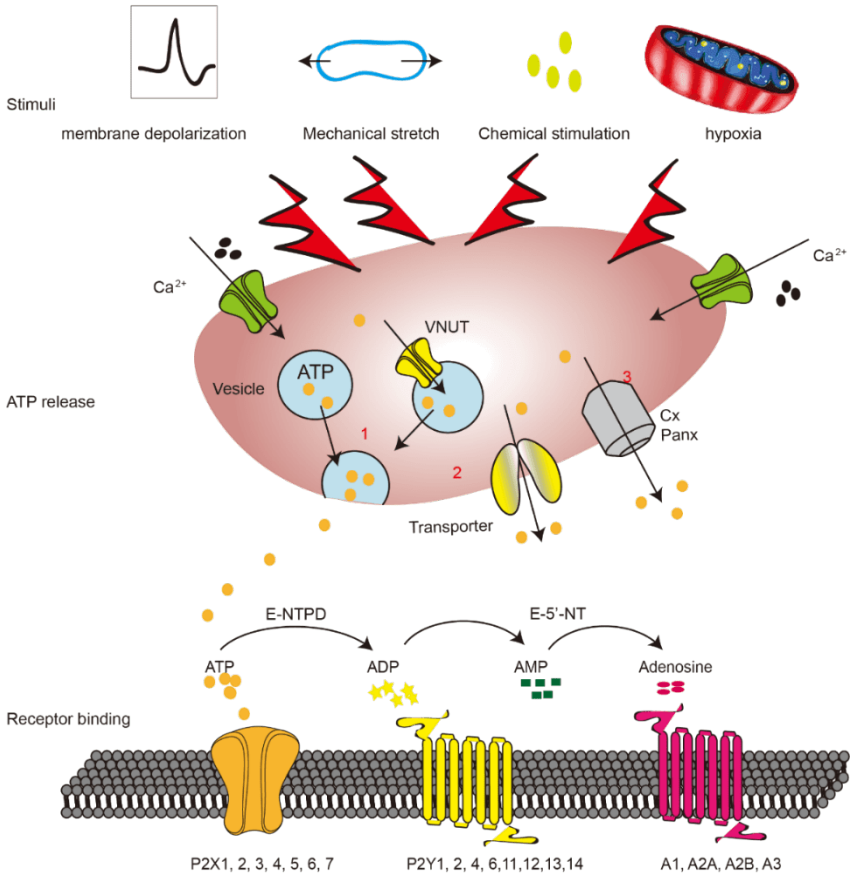

Figure 1. Schematic diagram of the purinergic system is quoted from Huang et al (24). Various factors stimulate cells to release ATP from the intracellular to the extracellular space through different mechanisms. ATP synthesized in mitochondria is actively transported into vesicles by vesicular nucleotide transporter (VNUT) and released via

conventional exocytosis process (1). ATP could also be transported directly through the transporter (eg., ATP-binding cassette transporters (ABC) transporter) (2) and released via connexin (Cx)/pannexin (Panx) channels (3). ATP released into the extracellular space is hydrolyzed by ectonucleoside triphosphate diphosphohydrolase (E-NTPD), and ecto-5′-nucleotidase (E-5'-NT) to ADP, AMP, and adenosine. Meanwhile, ADP, AMP, and adenosine bind to P2XRs, P2YRs, and adenosine receptors (P1 receptors), further triggering intracellular signal transduction processes.

Like other neurotransmitters, ATP and ATP-associated nucleotides transmit information through receptors. Because ATP can be sequentially hydrolysed to ADP, AMP, and adenosine by the exo-nucleotidases, such as ectonucleoside triphosphate diphosphohydrolase-1 (E-NTPD-1, aslo known as CD39) and 5'-nucleotidase (CD73) (25), two classes of receptors are identified to receive the released ATP (P2 receptors) and its breakdown product adenosine (P1 receptors), respectively (26). To date, there are four identified subtypes of P1 receptors (G protein-coupled receptors), including A1, A2a, A2b, and A3 (27). In addition to P1 receptors, the P2 receptor family consists of seven ligand-gated ion channel P2X receptors (P2X1, 2, 3, 4, 5 6, 7) (28) and eight G protein-coupled P2Y receptors ($P2Y_1$, $P2Y_2$, $P2Y_4$, $P2Y_6$, $P2Y_{11}$, $P2Y_{12}$, $P2Y_{13}$, and $P2Y_{14}$) (29). By binding to these receptors, ATP signalling is delivered to the target cell, resulting in a biological effect (Figure 1). Here, it is worth noting that exocytosis functions as one of the release processes, as ATP can be released directly through connexin /pannexin hemichannels and/or by transporters (24).

1.1.2 Purinergic P2X receptor family

Extracellular ATP molecules activate a variety of membrane surface receptors, including G protein-coupled receptors (P2Y receptor family) and ligand-gated ion channels (P2X receptor family). Although P2XRs share functional similarities with other ligand-gated ion channels, such as ACh and serotonin-gated channels (5-HT3), in terms of ion selectivity and channel gating kinetics, their unusual structure implies that P2X receptors are a novel class of ion channels gated by ATP. In general, extracellular ligand-gated ion channels, such as ACh receptors, 5-HT3, GABAA, and glycine, have four transmembrane structural domains (TM1-4) and a long extracellular N-terminus (30). Unlike these

receptors, the identification of P2X1R revealed a unique structure for members of the P2X receptor family (31). Surprisingly, each subunit of P2XRs cross the cell membrane only twice and contain intracellular N and C-termini (31, 32). Based on these unique structural features, six additional family members are subsequently identified (P2X2R, P2X3R, P2X4R, P2X5R, P2X6R and P2X7R) (28). Another unique property of the P2X receptor is that the P2X receptor is a trimer and can form hetero- or homotrimers. For example, quantitative real-time PCR analysis and whole-cell patch-clamp methods revealed that P2X1R and P2X5R form functional heteromeric P2X1/5 receptors in cerebral cortical astrocytes (33). Moreover, the P2X2R and P2X3R subunits can also form the heterotrimeric P2X2/3 receptor (27). The activation of P2X2/3 receptors contributes to the regulation of chronic pain due to the intermediate desensitisation kinetics of ATP-induced currents (28). Although the formation of P2X4/7R remains controversial (29-31), biochemical and electrophysiological evidence shows that P2X4R and P2X7R interact structurally and functionally in HEK cells (32).

1.2 Purinergic P2X7 receptors

Similar to all other P2X receptors, P2X7R has a common topology containing intracellular N and C-termini, two transmembrane structural domains (TM1 and TM2), and a large extracellular structural domain (34). In addition to these common features, the P2X7R exhibits a distinctive structural characteristic. The intracellular C-terminus contains an additional 200 amino acid residues, which are essential for the activation of intracellular signalling pathways (35, 36). For example, the novel 1-5-16 Ca^{2+}-dependent CaM-binding motif located between residues Ile-541 and Ser-560 has been identified in the rat P2X7R C-terminal end to facilitate P2X7R-mediated currents, although current facilitation also occurs in a Ca^{2+}/calmodulin-independent manner in human P2X7R (34, 37). Interestingly, P2X7R has a much lower affinity for extracellular ATP than other P2X receptors (38, 39) due to the highly conserved residues in the ATP binding pocket (40, 41). For example, as a unique residue of P2X7R, the D280A mutant in the left flip-flop produces a 15-fold ATP potency (41). Meanwhile, sustained activation of P2X7R further increases the permeability to cations (e.g., Na^{2+}, Ca^{2+}, and K^{+}) as well as to some macromolecules (e.g., $NMDG^{+}$ (N-methyl-D-glucosamine))(42-44).

In the CNS, P2X7Rs are found to be widely expressed in various brain areas, including the frontal cortex, hippocampus, amygdala, and striatum (45). In terms of cell type expression, it has been documented that P2X7Rs are abundantly present in microglia, astrocytes, and oligodendrocytes. Although the presence of P2X7Rs in neurons remains controversial (4, 5), a large body of data shows P2X7R expression in neurons. In situ hybridization, P2X7R-positive neurons are found in pyramidal cells from rat hippocampal CA1, CA3, and hilar regions, as well as other brain regions (2). Humanized mouse P2X7Rs are also detected through the P2X7R knock-in model (3). Recently, single nucleus RNA sequencing experiments revealed that P2X7R mRNA is expressed in human excitatory neurons but not in inhibitory neurons (1).

1.2.1 The distinct characteristics of P2X7Rs compared to other P2XRs

Due to its low affinity for ATP, endogenous activation of P2X7R is considered a “danger signal” and most research interest has focused on its role in pathological states, including Alzheimer's disease (46, 47), Huntington’s disease (48, 49)， Depression (50), Schizophrenia (13-15). The potential mechanisms of P2X7Rs under pathological conditions have been well-summarized (51). Various stimuli, such as membrane depolarization, mechanical stretch, chemical stimulation, and hypoxia, accelerate the release of ATP from the intracellular to the extracellular space. Consequently, excessive accumulation of ATP in the extracellular space further activates P2X7Rs expressed on neurons and glial cells. Activation of P2X7Rs leads to cell death mainly through the following pathways: First, the opening of P2X7Rs directly allows Ca^{2+} to flow into neuronal terminals, increasing the release of neurotransmitters, particularly glutamate. Glutamate released in the synaptic cleft activates AMPA and NMDA receptors, leading to more Ca^{2+} influx and eventually cellular excitotoxicity. Secondly, when extracellular ATP binds to P2X7R in the glia, the NLRP3-IL-1β inflammatory pathway is activated, which in turn results in neuroinflammation. Another common mechanism is oxidative stress caused by mitochondrial damage. The excessive reactive oxygen species generated by P2X7Rs activation further causes cell death via protein misfolding (51).

However, emerging data emphasizes that P2X7Rs also play an important role in physiology. In embryonic cells, upregulation of P2X7Rs maintains cell proliferation but

inhibits neural differentiation (52). By the contrary, stimulation of P2X7Rs in neural progenitor cells (NPCs) leads to Ca^{2+} influx, which further inhibits proliferation and enhances the expression of neuronal markers (e.g., MAP2) via activation of PKC-ERK1/2 (53). These data indicate that physiological expression of P2X7Rs contributes to the maintenance of development. Contrarily, the genetic deletion of P2X7Rs impairs cellular energy metabolism. In N13 microglia and primary mouse microglia, P2X7Rs gene deletion reduces resting mitochondrial potential and severely disrupts respiratory index (54). Furthermore, P2X7Rs have also been found to regulate cell morphology. Wild-type embryonic cultured hippocampal neurons showed that mRNA and protein expression of P2X7Rs peaked at DIV 4, declined at DIV 7 (day of in vitro culture), and remained unchanged at DIV 10 when dendrites were fully developed. In hippocampal slices, the presence of P2X7Rs plays a crucial role in the growth of neuronal dendrites. By analyzing the morphology of pyramidal cells, it was found that dendritic growth is impaired in CA1 but not in CA3 in those with P2X7Rs gene deletion compared to wild type counterparts (55). In dentate gyrus granule cells, P2X7R-deficient mice have fewer dendritic spines at the P9 stage compared to wild type (56). Besides, genetic ablation of P2X7Rs has also been reported to cause behavioural changes. Studies have reported that genetic deletion of P2X7Rs and pharmacological inhibition using their antagonists induce spatial memory deficits in mice (54) and impaired memory acquisition, consolidation, and retrieval in rat (57).

1.2.2 The pathophysiological role of P2X7Rs in CNS

Previous studies have reported that P2X7R is expressed in excitatory nerves and is involved in the regulation of excitatory neurotransmission (58-61). In cerebral cortical neurons, P2X7Rs were found to be present at glutamatergic termini, contributing to glutamate efflux (60). In brainstem slices, activation of P2X7Rs by BzATP, an agonist of P2X7Rs, increased the amplitude of evoked EPSCs and altered the paired-pulse ratio, suggesting that stimulation of P2X7Rs enhances the release of neurotransmitters from presynaptic sites (62). In hippocampal slices, activation of P2X7R significantly enhanced the release of glutamate and GABA in the CA1 and CA3 regions (58). Using patch-clamp approach, this study further demonstrates that activation of presynaptic P2X7Rs increases the frequency of sEPSC in hilar neurons (63). Controversially, the study from mossy fibre

suggested that activation of P2X7Rs inhibits synaptic transmission through activation of p38 MAP kinase (59). Interestingly, BzATP-induced frequency potentiation was completely abolished in CA1 neurons in the presence of the Krebs cycle inhibitor fluorocitric acid, which is preferentially taken up by glial cells. Furthermore, this paper also addressed that only CA1 neurons but not CA3 neurons showed an increase in PSC in response to BzATP (64). Taken together, it is plausible that P2X7Rs may have a dual effect on excitatory neurotransmission in hippocampal subregions.

1.3 The general information of dentate gyrus: with emphasis on excitatory inputs of dentate gyrus

The dentate gyrus (DG) is located between the entorhinal cortex of the temporal lobe and the CA3 region of the hippocampus, serving as the "gate" of classic trisynaptic circuit (EC → DG → CA3 → CA1) (6, 7). Typically, DG is made up of three main layers: the molecular layer, the granule cell layer, and the hilus. The molecular layer of DG mainly hosts dendritic plexus sending from granule cell layers, and axons projecting from the entorhinal cortex (EC) (65-68), the hilus, the supramammillary nucleus (SuM) (69, 70), and other brain regions, such as VTA GABAergic neurons (71) , although this layer also contains some interneurons, such as molecular layer perforant pathway cells (72) as well as semilunar granule cells in the inner part (67). The granule cell layer is characterised by the densely packed granule cells and a diverse group of interneurons (73). The hilus of DG mainly consists of mossy cells, mossy fibers from granule cells as well as different types of interneurons. As the main excitatory neurons in DG, the number of granule cells (GCs) in each hemisphere has been estimated to be approximately 1 million in the rat (74), which is twice as many as in the mouse (75), 15 times in the human DG (76), 7 times in the monkey DG (77). Typically, granule cells have elliptical soma and one to four primary dendrites spreading in the whole molecular layer. As it estimated, 63% of the dendritic branches are located in the inner third, 30% in the middle third, and 40% in the distal third of the molecular layer (78). These dendrites receive excitatory and inhibitory inputs from long-range projecting neurons and local neurons.

The major excitatory inputs of the dentate gyrus granule cells (DG GCs) originate from the entorhinal cortex (Figure 2). Axons from the lateral entorhinal cortex (LEC) primarily

project to the distal dendrites of GCs in the outer molecular layer (OML) (79-81) to form the lateral perforant path (LPP). In contrast, GCs dendrites in the middle layer of molecular layer (MML) mainly receive the excitatory projections from medial entorhinal cortex (MEC), which is also called medial perforant path (MPP) (81, 82). Apart from this anatomy difference, LPP and MPP are distinct in electrophysiology, neuropharmacology, and behavioural correlates. The early studies revealed that excitatory postsynaptic potentials (EPSP) elicited by MPP are different in slope, peak latency (83), and facilitation or suppression (84) when compared to MPP stimulation. Petersen et al. revealed that the paired pulse stimulation with an 50ms interpulse interval gives rise to the PPF in the LPP and the PPD in the MPP (85). In the long term potentiation (LTP) experiment, high-frequency stimulation-induced LTP was blocked in the presence of AP5 (a selective NMDA receptor antagonist) in the MPP but not in the LPP, suggesting the mechanism of LTP induction in MPP is NMDA receptor-dependent (86). Although the later study did not find the expression difference of NMDA receptor subunits, especially GluN1, GluN2A, and GluN2B subunits, at the MPP and LPP, GluN3a-containing NMDARs selectively expressed at MPP further enhance the MPP inputs to GC dendrites (87). Compared to NMDA receptor-dependent LTP induction in MPP, LTP induction in LPP requires the endogenous activation of delta (88) and mu opioid receptors (89). These electrophysiological and neuropharmacological characteristics determined that LPP and MPP carry different information and behaviour relevance (90, 91). Broadly speaking, MPP broadly carries spatial information and the LPP conveys non-spatial information. although this simple spatial–non-spatial dichotomy has been refined in the later well-summarized review (92).

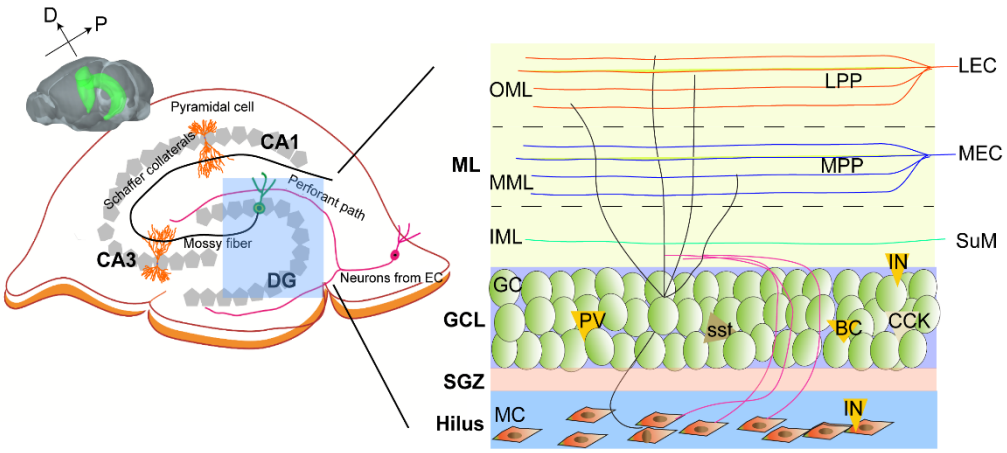

Figure 2. The schematic illustration of excitatory inputs to DG GCs. The DG is made up of three main layers: the molecular layer (ML), the granule cell layer (GCL), and Hilus. The molecular layer could be divided into three layers, including the inner molecular layer (IML), middle molecular layer (MML), and the outer molecular layer (OML). The IML receives the excitatory inputs from mossy cell in the Hilus, MML mainly distributes the fibers from the medial entorhinal cortex (MEC) to form the medial perforant path (MPP), and the OML receives the fibers from the lateral entorhinal cortex (LEC) to form the lateral perforant path (LPP). The inner molecular layer also contains the inputs from the supramammillary nucleus (SuM). GC, granule cell; PV, parvalbumin-expressing neuron; BC, basket cell; SST, somatostatin-expressing neuron; CCK, cholecystokinin-expressing neurons; IN, Interneuron (the figure modified from Figure 1 in (64)).

Importantly, DG GCs also primarily receive commissural/associational input from mossy cells in the hilus of DG (Figure 2). The mossy cells are another glutamatergic neuron type situated in the DG and characterized by thorny excrescences (93-95). However, mossy cells receive considerable interest due to their complex projections. The mossy cells terminate some of their axons in the hilus part of DG and send the collaterals to the inner molecular layer of DG, where they form synapses primarily with granule cells (96, 97) and inhibitory neurons (98). Of note, they also send the commissural projections to contralateral DG (95). Although sending the projections to the inner molecular layer is the common feature for ventral and dorsal mossy cells, the axons from the dorsal mossy cells have been found to have further projections into the MML, where they cooperate with PP in comparison with the axons from ventral mossy cells (99). These complex excitatory inputs play an important role in regulating DG output by increasing the excitation/inhibition balance, thus further facilitating dentate-dependent forms of learning and memory (100).

Additionally, the supramammillary nucleus (SuM) situated in the subcortical region also directly and strongly project to hippocampus, especially DG region (101, 102) (Figure 2). These axonal terminals innervate DG GCs in the inner molecular layer and characterized by release or co-release of glutamate and GABA as the neurotransmitters (103-105), which gave rise to the controversy whether these inputs exert net excitatory effect on DG

GCs. However, the optogenetic and electrophysiological evidence revealed that SuM afferents direct innervate GCs and interneurons in the DG and exert a net excitatory effect on both DG GCs and interneurons, further promoting GCs firing when associated with the inputs from entorhinal cortex (eg., PP) (106-108).

Besides, a different set of interneurons using GABA as a neurotransmitter is present in the DG, providing inhibitory control of granule cell activity. These neurons are usually distributed in the basal and molecular layers of the DG (73). From the perspective of firing property, it can be classified as fast-spiking (FS) and non-fast-spiking (non-FS) interneurons, respectively. Meanwhile, these interneurons can be further subdivided chemically. For example, soma-targeted interneurons include parvalbumin-expressing basket cells (PV+BCs) (109), whereas dendritic-targeted interneurons include cholecystokinin (CCK)-expressing neurons (110) and somatostatin-expressing neurons (111, 112) (Figure 2).

1.4 The general overview of schizophrenia

Schizophrenia (SCZ) is a debilitating mental illness characterized by persistent or relapsing psychotic episodes comprising positive symptoms (e.g., hallucinations, delusions, disorganized thinking, and speech), negative symptoms (e.g., social withdrawal, undermotivation, and impaired speech), and cognitive symptoms (e.g., memory loss, inattention). With a prevalence of 1-4% of the global population (113) and an early age of onset (typically from adolescence to early adulthood), SCZ poses a significant and lasting burden on both society and the patient. To date, the exact etiology of SCZ is unknown and is likely to be related to a combination of factors, including genetic predisposition, psychological, and environmental influences. Furthermore, the diagnosis of SCZ is still fairly subjective and difficult, although a significant amount of recent work introducing objective features, including biomarkers, neuroimaging, electrophysiology, biochemical methods, immunological, genetic approaches, and even artificial intelligence techniques (114) and machine learning techniques (115).

Moreover, the treatment of schizophrenia remains challenging. Currently, antipsychotic strategies have mainly focused on symptom reduction due to poor understanding of the

causes of the disease. So far, antipsychotics are divided into three categories: first-generation ("typical"), second-generation ("atypical"), and third-generation antipsychotics. First-generation antipsychotics primarily target the dopamine receptor D2 and reduce symptoms, especially positive symptoms (116, 117). Compared to first-generation antipsychotics, second-generation antipsychotics target the D2 receptor in a loose way or do not target the dopamine receptor, thereby releasing the side effects (118). In fact, the life-threatening side effects associated with some of second-generation drugs have largely limited their clinical use. For example, clozapine is considered the gold standard for treating refractory schizophrenia. However, the severe side effects, including myocarditis, cardiomyopathy, and agranulocytosis, induced by the administration of clozapine largely limits its prescription in the clinic, as more careful managements, such as dosage, plasma concentration and blood monitoring, are required (119). Additionally, approximately 30% of patients have only partial response to clozapine (120, 121). The main characteristic of third-generation drugs is that they are not dopamine D2 receptor antagonists, but rather D2 receptor partial agonists, which focus on alleviating negative symptoms (122, 123). Importantly, third-generation antipsychotics have been selected to use in combination with clozapine (124) and even in the treatment of clozapine-resistant schizophrenia. For example, a study found that augmentation therapy with amisulpride could alleviate the psychiatric symptoms and improve cognitive performance (125). Although treatment for schizophrenia includes psychiatric medication, training programmes, community support activities, psychotherapy and family education, more medication strategies are still needed to alleviate symptoms, minimize side effects and improve life quality.

1.4.1 Phencyclidine (PCP)-induced schizophrenia in rodents: Glutamatergic hypothesis of schizophrenia

In terms of the pathology of schizophrenia, there are a number of hypotheses, including neurotransmitters (Dopamine (126), glutamate (127, 128), serotonin (129) and GABA (130)) , neuroinflammation (131, 132), genetic (133, 134), neurodevelopment (135, 136), gut-brain axis (137, 138).

Although the dopamine hypothesis, which originates from the introduction of the antipsychotic drug phenothiazine in 1952, is the most predominant biological hypothesis for SCZ, the involvement of glutamatergic mechanisms could be traced back to 1949, when glutamate was used in the treatment of schizophrenic patients (139). The subsequent clinic trial reported that cerebrospinal fluid glutamate levels were reduced in patients with schizophrenia (140). However, this result was challenged by other research groups that were not able to reproduce it (141, 142). The breakthrough in the glutamatergic hypothesis was the discovery that dissociative anaesthetics ketamine and phencyclidine cause psychiatric symptoms (143, 144). Healthy volunteers infused with ketamine experience schizophrenia-like symptoms, including negative symptoms, subtle cognitive deficits, as well as some positive symptoms (145). Ketamine and phencyclidine primarily function as NMDA receptor antagonists (146), so more research attention has been focused on NMDA receptor dysfunction. A study of autopsy reported that glutamate carboxypeptidase II (GCPII), which catalyses the conversion of NAAG to NAA and glutamate, was reduced in the frontal cortex, hippocampus, and temporal cortex of patients with SCZ (147). Meanwhile, NAAG, as an agonist of the mGluR3 receptor, has been reported to be associated with the pathology of schizophrenia (148).

Similar to ketamine, the administration of phencyclidine (PCP) also causes schizophrenia-like symptoms (127). Unlike amphetamine-induced psychosis, PCP-induced psychosis in rodents incorporates positive, negative, and cognitive symptoms of SCZ. In rodents, PCP injection produces dose-dependent positive-like symptoms, such as hyper locomotor activity (149-151). In a forced swimming test, mice repeatedly treated with PCP increased the immobility that was reversed by atypical antipsychotics (152-154), suggesting that PCP can be used to produce negative symptoms of SCZ. In water maze tests, PCP treatment leads to impaired attention and latent learning (155), and disturbed spatial learning and memory (15). Therefore, the application of PCP to animals could also generate several cognitive-related impairments.

However, whether PCP administration produces the symptoms described above, particularly negative and cognitive symptoms, depends on a variety of factors, including dose, species, acute or chronic administration, and sex. In the sub-chronic PCP model,

PCP injection with 2-5 mg/kg (twice daily) for seven days followed by a seven-day washout resulted in persistent cognitive deficits in an operant reversal learning paradigm in rat, (156, 157) but not in mice with a background of C57BL/6J (158). Although the injection protocol differs, a higher concentration of PCP is required to cause the deficits of learning and memory. A study showed that 10 mg/kg but not 2-5 mg/kg of PCP injection severely impairs the spatial learning and memory (159). Besides, the strain difference has been found in PCP-induced hyperlocomotion and depressive symptoms (ddY>>C57BL/6N and 6J>ICR). In rodents, normal early postnatal development (first two weeks) is essential to undergo many key maturational changes. For example, brain growth spurt and gliogenesis will reach to the peak at postnatal day 7-10. At the same time, the density of axons and dendrites increases and the immune system is consolidated (160). Therefore, disturbances that occurs during this time period can lead to serious consequences in adulthood and postnatal interventions are widely used to establish neurodevelopmental models of disorders. In terms of postnatal PCP injection-induced SCZ model, the hyper locomotor activity and the impaired spatial memory are observed in juvenile rats treated with PCP from postnatal day 5 to day 15 (161) and the memory impairment remains in adulthood (162). Another commonly used postnatal PCP model protocol (daily injections of PCP on days 7, 9, and 11) also showed disturbance of spatial working memory in adult male mice, although this impairment is sex-specific (163). Notably, the strain difference is subtle in response to postnatal PCP injection, as ICR mice treated with the same protocol showed the impairments in spatial working memory and social interaction (164).

1.4.2 P2X7Rs in phencyclidine (PCP)-induced schizophrenia

Several lines of evidence suggest that P2X7Rs are involved in the development of schizophrenia. The largest genome-wide association study (GWAS) of schizophrenia patients identified genetic variations in P2X7 receptors (12). The pharmacological inhibition and genetic deletion of P2X7Rs could alleviate schizophrenia-like symptoms, including hyperlocomotion and stereotyped behaviours in acute and sub-chronic PCP models (13, 14). Additionally, postnatal injections of PCP have been utilized to establish a chronic model of SCZ, also called a neurodevelopmental model (165). In this chronic schizophrenia model, the blockade of P2X7Rs by the brain-penetrating antagonist JNJ-

4795567 significantly attenuated postnatal PCP-induced hyper motor activity and spatial memory impairment in adults (15). Finally, in another model of schizophrenia, poly(I:C)-induced MIA (maternal immune activation), the schizophrenia-like symptoms, including positive symptoms (excessive motor activity) and cognitive symptoms (working memory deficits and impairment of paired pulse facilitation (PPI)) were alleviated in animals genetically deficient in P2X7Rs (55).

Although the underlying mechanisms are not fully understood, there are several potential mechanisms. Firstly, the administration of PCP results in a direct increase in P2X7Rs mRNA and protein expression (15). Although the study did not mention the exact mechanism, the elevated expression of P2X7R by PCP treatment may be attributed to excessive release of ATP. Secondly, P2X7Rs regulates the expression of schizophrenia susceptibility genes. NMDA receptors are a tetramer consisting of two glycine-binding subunits GluN1, two glutamate-binding subunits, a combination of GluN2 subunit and one glycine-binding GluN3 subunit or two GluN3 subunits. Among these subunits, single nucleotide or dinucleotide-repeated polymorphisms of GluN1, GluN2A, and GluN2B subunits significantly increase susceptibility to schizophrenia in human. In the animal model, the upregulation of GluN1, GluN2A, and GluN2B was detected when animals were treated with the NMDA receptor antagonist PCP. The unregulated expression was suppressed in mice genetically deficient in P2X7 receptors (13). Thirdly, P2X7 receptors participate in the regulation of neuron excitability. C-Fos protein expression is commonly used as a marker of neuronal activity. In comparison with wild-type animals, P2X7R knockout mice had a lower number of c-Fos-positive neurons in the mPFC. However, this regulatory effect displayed a layer-specificity, as the decreased number of c-fos-positive neurons was only found in the ventral region of the second/third layer but not in the fifth layer. Individually, mPFC layer V neurons lacking P2X7Rs showed fewer action potentials in response to the same current step, suggesting that P2X7R gene deficiency results in reduced neuronal activation (14). Fourthly, P2X7Rs regulate the neuronal morphology under pathophysiological conditions. Under physiological conditions, gene ablation and pharmacological blockade of P2X7R lead to branching defects in primary cultures and acute slices. In contrast, primary cultured neurons dissected after poly I:C

treatment (MIA model) showed normal dendritic growth when animals were deficient in P2X7Rs (55).

1.4.3 Pathological changes in the dentate gyrus of schizophrenia

As an important excitatory input to the hippocampus, The EC is subject to the development of schizophrenia in patients and rodents. Smaller EC volumes and abnormalities in cytoarchitecture and cytoskeleton have been found to be positively correlated with the severity of delusions in patients (8). Besides, the hippocampus is also one of the important brain regions susceptible to the pathology of schizophrenia. Several schizophrenia-related abnormalities have been identified in the dentate gyrus, CA3, and CA1, including reduced volume, impaired inhibitory and excitatory neurotransmission, immature molecular signatures, and abnormalities in immunoreactivity (166). Furthermore, the study also pointed out the susceptible cell populations in DG. For example, impairment of GABAergic transmission was observed, and a reduced number of parvalbumin-positive (PV^+) cells in the DG was found in the MIA model (9) . Apart from inhibitory neurons, the abnormal glutamatergic system is also involved. The synapse-associated protein 97 (SAP97) is a membrane-associated guanylate kinase (MAGUK) protein that is a member of the glutamatergic postsynaptic density. This protein interacts directly with AMPA receptors (10) and controls dendrite growth (11). As one of the SAP97 isoforms, βSAP97 is abundantly expressed in DG CG dendrites compared to CA1 pyramidal dendrites. The mutation of SAP97 is highly related to the development of schizophrenia. In DG GC, SAP97 mutations have been found to increase the strength of rat glutamatergic synapses and interfere with the processing of contextual information (167). From the perspective of maturation, necropsy analyses showed a dramatic increase in the number of calreticulin-positive immature neuronal progenitors and a reduction in the number of calreticulin-positive mature neurons in DG. This pathological change has been termed the "immature dentate gyrus" (168).

Actin filaments are protein filaments in the cytoplasm of cells. They can form a network with other proteins beneath the plasma membrane and control cell movement. As a major candidate susceptibility gene for schizophrenia and bipolar disorder, DISC1 interacts with actin filaments, particularly girdin, to promote cell migration, localization, and axonal

guidance in the DG (169). In terms of axonal guidance, the semaphorin family (SEMA) and its receptor plexins (PLXNs) act as the axonal guidance regulator. Interestingly, SEMAs and plexins (PLXNs) also play a crucial role in mental disorders. Animals lacking the plxna2 gene in DG develop neuropsychiatric disorders, including the impairment of sensory-motor gating, abnormal social activity, and learning disabilities (170). Of note, the microglia activation regulated by microglia-specific arginase 1 (Arg1) in DG also contributes to schizophrenia-like symptoms (9).

DOI:10.14753/SE.2024.2993

2. Objectives

ATP-gated P2X7Rs play a crucial role in brain diseases and neuroinflammation. Although the role of P2X7Rs in the regulation of neurotransmission has been repeatedly reported, whether neuronal P2X7Rs are directly involved in this process remains controversial. Meanwhile, the role of P2X7Rs in neurodevelopmental models of schizophrenia remains unclear. Therefore, this study was designed with a variety of approaches including whole-cell patch clamp, viral injection, Ca^{2+} imaging, immunohistochemistry and animal models to achieve the following objectives:

2.1 To investigate the role of P2X7R in excitatory neurotransmission onto mouse DG GCs and understand whether the regulatory effect shows a pathway specificity in DG

2.2 To address the potential effects of P2X7Rs on postnatal phencyclidine (PCP)-induced schizophrenia model in mice and explore the potential underlying mechanism

3. Methods

3.1 Animals

In our project, we used only C57Bl/6J mice. Both wild-type mice and P2rx7-/- mice were homebred. However, the original breeding pair for the P2rx7-/- mice came from Dr Christopher Gabel. The P2rx7-/- mice consisted of P2X7-F1 (5′-CGGCGTGCGTTTTGACATCCT-3′) and P2X7-R2 (5′-AGGGCCCTGCGTTCTC-3′), which were validated in our previous paper (171). Based on different experimental designs, we had experimental groups of different ages. In the electrophysiological experiments, we used both sexes of the postnatal day P21-P28 and P58-P69 groups. In the viral injection experiments, we used only males in the P40-P47 age group of both genotypes to maintain the same injection coordinates. In Ca^{2+} imaging experiments, we used male mice at the age of P54-P61 for acute section preparation and Ca^{2+} imaging. Although the early study reported that C57Bl/6J strain showed less response to PCP treatment (158), the later studies from our group and other group could reproduce PCP-induced schizophrenia symptom (13-15, 172). Therefore, we utilized this strain to model phencyclidine-induced neurodevelopmental schizophrenia. We injected male pups at P7, P9, and P11 with PCP. Behavioural tests were performed when males grew to P67. All animals were kept under a standard 12 h light/12 h dark cycle with food and water provided ad libitum. In accordance with the European Communities Council Directive of 24 November 1986 (86/609/EEC), animal handling and sacrifices were carried out according to protocols approved by the Animal Welfare Committee of the Institute of Experimental Medicine and the relevant authorities (Budapest, Hungary, nos. PEI/001/778-6/2015, PE/EA/297-1/2021).

3.2 The methods employed to understand the role of P2X7R in excitatory neurotransmission onto mouse DG GCs

To investigate the role of P2X7R in excitatory neurotransmission onto mouse DG GCs and understand its underlying mechanisms, we mainly used the electrophysiological approach (whole-cell patch-clamp) with pharmacological method (drug application), immunostaining, Ca^{2+} imaging, and morphology approach.

3.2.1 Brain slices preparation and whole-cell patch-clamp recording conditions

Mice were anesthetized by inhaling forane. Whole brains were extracted after decapitation and were sliced in ice-cold cutting solution composed of (in mM: 85 NaCl, 2.5 KCl, 2 $MgCl_2$, 0.5 $CaCl_2$, 1.25 NaH_2PO_4, 24 $NaHCO_3$, 25 glucose and 75 sucrose). The pH of the solution was 7.4 and the osmotic pressure was 290-300 mOsm. The cutting solution was bubbling with 95% O2 + 5% CO_2. Hippocampal slices were cut into 300 μm by a Leica vibratome at 0.08 mm/s and an amplitude of 1.0 mm. Individual slices were transferred to artificial cerebrospinal fluid (ACSF) (in mM: 126 NaCl, 2.5 KCl, 2 $CaCl_2$, 2 $MgCl_2$, 1.25 NaH_2PO_4, 26 $NaHCO_3$ and 10 glucose, the pH of the solution was 7.4 and the osmolarity was 300-310 mOsm) bubbling with 95% O_2 + 5% CO_2 for 30 min at 34 °C. After incubation, the slices were kept at room temperature.

All recordings were performed at room temperature. Hippocampal slices were transferred to an oxygenated ACSF circulation chamber at 2.5 ml/min. Previous studies showed that the receptor affinity for its agonists was reduced in the presence of physiological concentration of extracellular Ca^{2+} (64, 173) and that blockade of NMDA receptors by Mg^{2+} is voltage-dependent. Therefore, we used a low divalent cation (X^{2+}) solution that removed Mg^{2+} from ACSF and reduced the Ca^{2+} concentration to 0.5 mM. This recipe was used in the BzATP puff experiment, extracellular stimulation experiment (input-specificity experiment), and the Ca^{2+} imaging experiment. However, normal ACSF containing 1.3 mM Ca^{2+} /2 mM Mg^{2+} has also been used for extracellular stimulation experiments (input-specificity experiment) and Ca^{2+} imaging experiments. For receptor inhibition, we diluted the drugs in ACSF. All recordings were performed using whole-cell patch-clamp technique. Axopatch 1D amplifier and Digidata 1322A data acquisition system were used for recording. DG GCs were visualized by Olympus BX50WI Differential Interference Contrast (DIC) microscope and a 40x water immersion objective. Borosilicate glass pipettes were pulled using a Sutter P-2000 micropipette puller. Glass pipettes have a resistance of approximately 4-7 mΩ, pipettes greater than 7 mΩ and less than 4 mΩ were discarded.

3.2.2 The AMPA receptor and NMDA receptor-mediated excitatory postsynaptic currents (s/mEPSCs) recordings

To understand whether genetic ablation of P2X7Rs has impact on DG GCs excitatory neurotransmission, we examined AMPA receptor and NMDA receptor-mediated excitatory postsynaptic currents in the presence (sEPSCs) and absence (mEPSCs) of action potential propagation at wild-type mice and P2rx7-/- mice, respectively. In this experiment, voltage-clamp configuration was used. The signals were filtered at 2 kHz and digitized at 10 kHz. The intracellular solution composed of (in mM): 120 CsCl, 8 NaCl, 10 HEPES, 0.3 Na-GTP, 4 Mg-ATP, 10 PO creatine, and 8 biocytin. The pH was adjusted to 7.2 and osmolarity was measured between 290–300 mOsm. To differentiate AMPA receptor-mediated sEPSCs under action potential generation or propagation, we pharmacologically blocked GABAA receptor and NMDA receptor by adding the GABAA receptor antagonist SR 95531 (10 μM) and NMDA receptor antagonist DL-AP5 (50 μM) to the ACSF. To record AMPA receptor-mediated miniature monosynaptic synaptic currents, which were not triggered by action potential, we added voltage gated sodium channel blocker TTX (1 μM) to the ACSF containing SR 95531 and DL-AP5. To record NMDA receptor-mediated sEPSCs, we added GABAA receptor antagonist SR 95531 (10 μM), the AMPA receptor antagonist CNQX (20 μM) and the NMDA receptor co-agonist D-serine (50 μM) to the ACSF. Similarly, TTX (1 μM) was added to ACSF containing SR 95531 (10 μM), CNQX (20 μM), and D-serine (50 μM) to record NMDA receptor-mediated mEPSCs. For both AMPA receptor and NMDA receptor-mediated mEPSCs, a sodium channel blocker QX314 (5 mM) was added to the internal solution. Using a 100 ms long -5 mV voltage steps were used to continuously monitor the series resistance. To check the direct participant of P2X7Rs in DG GC excitatory neurotransmission, we locally puffed P2X7Rs agonist BzATP (1 mM or 300 μM) for 30 s via the fast drug application system. For mEPSC/sEPSC analysis, we used template detection method and set the template match threshold at 4 for all the recordings.

3.2.3 Paired-pulse recording

To further clarify whether the change of excitatory neurotransmission from presynaptic site showed an input-specificity, we stimulated two main excitatory inputs onto DG GCs

(EC-GC fibers and MC-GC fibers) to check the presynaptic vesicle release by delivering paired pulses.

In this experiment, we used the internal solution contained (in mM): 115 Cs-methanesulfonate, 8 NaCl, 10 HEPES, 0.3 Na-GTP, 4 Mg-ATP, 10 PO creatine, 8 biocytin, 5 QX314. The pH was adjusted to 7.2 and osmolarity was 293 mOsm. GABAA receptors were blocked by SR 95531(10 μM). We patched DG GC to form the whole-cell configuration, then placed the microelectrode filled with aCSF on the surface of the middle and outer layer of molecular layer to stimulate EC-GC fibers (MPP and LPP) and at inner molecular layer to stimulate MC-GC fibers, respectively. The stimulating electrode connected to stimulation isolation unit from World Precision Instruments and the two consecutive stimuli composing of 100 μs duration stimulus of 40 uA amplitude with a 50 ms interpulse interval were delivered every 30s.

To pharmacologically distinguish EC-GC fibers and MC-GC fibers, DCGIV (1μM) (a selective agonist of group II metabotropic glutamate receptors) was also added to the ACSF at end of recording, since mGluR2/3 was expressed in the EC-GC fibers but not in the MC-GC fibers (106). The calculation of PPR referred to the second peak amplitude (P2) divided by the first peak amplitude (P1).

3.2.4 Virus injection

To determine the participant of PP and its Ca^{2+} mechanism, we specifically infected PP paths by using hSynapsin1 promoted and axon targeted GCaMP6s virus. pAAV-hSynapsin1-axon-GCaMP6s was a gift from Lin Tian (Addgene plasmid # 111262; http://n2t.net/addgene:111262; RRID: Addgene_111262). We aliquoted the virus contained solution once it arrived and stored at -80°C before experiments. ketamine/xylazine-hydrochloride (10 ml/kg i.p) was used to anesthetize the male mice at P40-47. Then stereotactic head frame was used to fix the position of the mouse. Eye ointment (Vidisic® Gel) was used to protect the eyes. We gently removed the head skin with the blade and exposed the skull. After removing the meninx with a cotton stick, we located the lambda with the glass capillary and adjust the position of the bregma to confirm both positions at the same horizontal level. We located the

coordinates of EC (LEC: -3.8 mm anteroposterior (AP), ±3.9 mm mediolateral (ML) and -4.7 mm dorsal-ventral (DV); MEC: -4.72 mm (AP), ±3 mm (ML), -4 mm (DV)). The bilateral craniotomies were made with a dental drill. The virus solution was diluted in the sterilized 0.1 mM PB buffer at a ratio of 1:10 for P2X7Rs immunostaining and Ca^{2+} imaging, as the dense labelling gave rise to the difficulty to detect the signals. The purified virus was used for location and expression check. The injection volume in different experiments was 60 nl in total for each side via the MicroSyringe Pump Controller system. The 60 nl was delivered by two steps: 20 nl was delivered at a rate of 57 nl/s, then 100 nl/min for 40 nl. After delivery, the virus-containing capillary was held in the place for 5 minutes before retraction. We closed the scalp incision with the surgical sew kit and released the animal from the head frame and placed to a stable-temperature pad. Once the animal woke up, we transferred it back to the home cage. In following two days, we applied analgesia to help the recovery. After two weeks' expression, the mice were anesthetized by carbon dioxide (CO_2) for immunostaining experiments. The mice were fixed on the board in hood. The chest wall was opened and the heart was exposed entirely. Transcardiac perfusion with 0.9% NaCl for 5 min to clear the blood, was followed by 4% PFA for 20 min to preserve the brain. The brain was extracted from the head and post-fixed with 4% PFA overnight at 4°C. After 12-24 h (less than 24 h), the brains were transferred into 24-well plate in 0.1 mM PB buffer. The brains were cut into 50 μm-thickness with the Leica vibratome (Leica VT1200s, Germany).

3.2.5 Synaptic markers Vglut1 and Homer1 staining

To identify that the pAAV-hSynapsin1-axon-GCaMP6s efficiently infect axons and boutons but not the dendrites, we stained presynaptic marker Vglut1 and postsynaptic marker Homer1. The brain sections with a thickness of 40 μm were washed in 0.1 M PB buffer, followed by 0.5 M TBS prior to blocking. The brain slices were further incubated in blocking buffer containing 10% normal horse serum (NHS) and 0.3% Triton X-100 diluted in 0.5 M TBS for 1 h at RT, and then incubated with primary antibodies at 4 °C for at least 72 h. Primary antibodies used: guinea-pig anti-Vglut1 (Millipore, AB_2301751,1:1000), rabbit anti-Homer1 (Synaptic System, AB_887730, 1:500) and chicken anti-GFP (Biozol, GFP-1020, 1:10000). Slices were further rinsed in 0.5 M TBS and incubated with secondary antibodies at 4 °C for overnight. Secondary antibodies used

were: Cy™3 AffiniPure Donkey Anti-Guinea Pig IgG (H+L) (Jackson Immuno Research, AB_2340460, 1:500), Alexa Fluor® 647 AffiniPure Donkey Anti-Rabbit IgG (H+L) (Jackson Immuno Research, AB_2492288,1:500) and Alexa Fluor® 488 AffiniPure Donkey Anti-Chicken IgY (IgG) (H+L) (Jackson Immuno Research, AB_2340375, 1:500). Sections were further washed in 0.5 M TBS, followed by 0.1 M PB. Then we mounted the slices with ProLong™ Gold Antifade (Thermo Fisher Scientific, Massachusetts, US) for visualization with a C2 confocal microscope. Z-stack images obtained at an interval of 0.125 μm, 0.08 pixel/um with a 60x objective were used for deconvolution with Huygen Professional software (Huygens Computer Engine 4.2.1p764b).

3.2.6 P2X7Rs staining

We next did the P2X7Rs antibody immunostaining to identify the expression of P2X7Rs on the EC-GC axonal terminals. Instead of using the same protocol from 3.2.5, we employed the protocol for better P2X7Rs antibody immunostaining (55). The post-fixed brains from both WT and P2rx7-/- injected with virus were sliced at 40 μm by using Leica vibratome in the presence of 0.01 mM PBS buffer. The slices were rinsed with 0.01 mM PBS 3 times (10 minutes each time). Then the slices were incubated in citrate buffer (pH 6) for 30 minutes at 85 °C. After another 3 x 10 minutes wash with 0.01 mM PBS, brain slices were blocked in 0.01 mM PBS buffer consisting of 1% BSA, 5% FBS and 0.2% Triton X-100 for 1h at room temperature. We next incubated the slices with primary antibody. The primary antibody rabbit anti-P2X7Rs (1:100, Alomone Labs, Cat. #. APR-004; RRID: AB_2040068) and chicken anti-GFP (1:1000, Aves Labs, Cat. #. GFP-1020; RRID: AB_10000240) were diluted in above blocking buffer for 2 nights at 4°C. The slices were washed for 3 times (10 minutes each time) with 0.01 mM PBS. The biotinylated antibody containing 10% BSA, goat serum, and biotinylated anti-rabbit IgG were used to incubate the slices for 1h at room temperature. After rinsing the slices 3 x 10 minutes with 0.01 mM PBS, the slices were incubated with the secondary antibodies Alexa Fluor 594-conjugated streptavidin (1:500) and Alexa Fluor® 488 goat anti-chicken antibody (1:1000) for 1h at RT. Subsequently, sections were mounted on glass slides with ProLong Gold for C2 confocal imaging. Z-stack images were used for the deconvolution by using Huygen Professional software (Huygens Computer Engine 4.2.1p764b). We

next imported the deconvoluted images into NIS software for XYZ dimension identification.

3.2.7 Ca^{2+} imaging

After two weeks' virus expression, mice were anesthetized by forane and hippocampal slices were prepared as described previously to detect the Ca^{2+} influx in EC boutons. We utilized an upright A1R MP+ multiphoton confocal microscope (NIKON) with a water immersion objective of NA 1.10, WD 2.0 (CFI75 Apochromat 25XC W 1300) and a 680-1040 nm titanium sapphire laser view and scan slices with axonal GCaMP reporter. We used a resonant scanner, at 30 Hz sampling rate, 920 nm wavelength, and 15 mW laser power to detect the Ca^{2+} related fluorescence. A monopolar stimulus isolator unit (BioStim STE-7c, Supertech Instruments UK Ltd, UK) equipped with a sharp capillary placed either at the middle layer (MPP) or outer layer of molecular layer (LPP), was used to deliver the electric pulses. 5 pulses of frequencies among 10–100 Hz (10, 30, 60, 100 Hz) were used to test the saturation of the Ca^{2+} indicator. For each scanning, the scanning duration lasts for 10 seconds (300 frame in the length) and was repeatedly scanned 15 times. Scanning images were captured by NIS software for further data analysis. The average NIS image with nd format from 15 times' scan for each plane was converted into tif format by edited script in python spyder (Pierre Raybaut, The spyder Development Team, python 3.8) under anaconda platform (Anaconda, Inc, version 3.8). The tif movies were subsequently imported into the suite2p software ((suite2p, version 0.8.0, RRID: SCR_016434) for the imaging registration. This software detected regions of interest (ROI) based on the anatomy where pixels are correlated across time. To meaure the boutons precisely, we set the diameter of regions of interest (ROIs) as 4-6 pixel size. As this setting also will detect some parts of axonal shafts, we manually deleted the ROIs on shafts in the automatically generated GUI panel. To extract fluorescence traces and spikes in ROIs with the equation of: $F_c = F - 0.7 * F_{neu}$ (F_c means corrected fluorescence value; F stands for the raw fluorescence intensity; F_{neu} means the neuropil-induced fluorescence intensity; 0.7 is the neuropil coefficient). To further calculate electrical pulse-induced fluorescence intensity, we used python spyder script (Pierre Raybaut, The Spyder Development Team, python 3.8) under anaconda platform (Anaconda, Inc, version 3.8)

to subtract baseline fluorescence from peak fluorescence, subsequently obtained the change of fluorescence intensity also known as ΔF.

3.3 The methods used to exclude the involvement of postsynaptic sites

Regarding that the frequency change of AMPA receptor and NMDA receptor-mediated s/mEPSC also could be attributed to the reduction of dendritic spine number, we examined the dendritic morphology of DG GCs in both WT mice and P2rx7-/- mice. Then we checked whether genetic ablation of P2X7Rs has impact on DG GCs neuronal excitability by recording the action potential and whether P2X7Rs potentially interact with NMDA receptors on soma.

3.3.1 Biocytin-labelling cell staining and spine number quantification

Since our internal solution contained biocytin, we fixed the slice after recording with 4% PFA overnight at 4 °C for immunostaining experiments. The streptavidin was reconstructed with 0.1 M phosphate-buffered (PB) containing 2 mM sodium-azide (NaN3). After overnight fixation, the slices were kept in the 24-well plate and gently washed with 0.1 M PB for 3 times 10 min each. The slices were washed with 0.5 mM tris buffered saline (TBS) for another 3 times (10 minutes each). After this process, we blocked the slices in the blocking buffer containing 5% normal goat serum and 0.03% triton X-100 in 0.5 mM TBS for 2h at room temperature. Subsequently, the slices were incubated with Alexa Fluor 594 streptavidin (Invitrogen, Cat. #. S11227) with a concentration of 1:500 for 3-4h at room temperature or overnight at 4 °C. 0.5 mM TBS was used for another 3 times wash (10 minutes each), followed by 0.1M PB 3 times (10 minutes each). Then the slices were mounted onto gelatin-coated glass slides by using the vectashield mounting medium. After visualization with confocal microscope, the neurons were identified based on the morphology.

To further count the dendritic spines of DG GCs from the same slices mentioned above, we had to re-slice the 300 µm slice into 50 µm for the sake of better confocal visualization. Therefore, we stripped the hippocampal slices from the glass slides after morphology visualization and then transferred in 24-well plate filled with 0.1 mM PB and washed for 3 times 10 min each on shaker. 2% agarose gel was prepared to embed the slices which

were further cut into 50 μm slices with with Leica vibratome. The resection slices were mounted in a sequential way with vectashield mounting medium. The slides were further visualized under Nikon C2 confocal microscope with 60x oil immersion objective, 0.07-pixel size, and 0.125 μm between steps. The whole dendritic branches were manually divided into 100, 150, 200 μm away from neuronal soma. The confocal images were deconvolved by using Huygens Professional program prior to importing into Neurolucida software for the quantification. Neurolucida software tracked the branches and labelled the spines within 30 μm segments. In this process, we only counted the total number of spines and did not do spine type classification.

3.3.2 Action potential recording

To record the action potentials of DG GC, we used current clamp. A glass pipette was filled with internal solution (in mM: 126 K-gluconate, 4 KCl, 10 HEPES, 0.3 Na-GTP, 4 Mg-ATP, 10 PO creatine, 8 biocytin). pH was adjusted to 7.2, and osmolality was between 290-300 mOsm. To stimulate action potentials, the somatic current was increased from -100 pA to +280 pA in 20 pA increments for a duration of 450 ms. When the holding current was more negative than -100 pA, neurons were excluded.

3.3.3 Drug puff application

To examine the potential interaction between P2X7 receptors and NMDA receptors on DG GC soma, we used fast drug application system to locally puff NMDA at 10 μM or 100 μM to evoke NMDA receptor-mediated current response. We puffed 20 s for each sweep with a 5 min's interval between two sweeps to make sure the currents could be completely recovered. After two stable sweeps, we bath-applied P2X7Rs agonist BzATP (1 mM) or antagonist JNJ47965567 (10 μM) to either activate or inhibit P2X7Rs. In this experiment, we used internal solution composed of (in mM): 115 Cs-methanesulfonate, 8 NaCl, 10 HEPES, 0.3 Na-GTP, 4 Mg-ATP, 10 PO creatine, 8 biocytin, 5 QX314. NMDA was dissolved into normal ACSF solution containing (in mM: 126 K-gluconate, 4 KCl, 10 HEPES, 0.3 Na-GTP, 4 Mg-ATP, 10 PO creatine, 8 biocytin).

3.3.4 Western blot

Previous studies reported that the expression of P2X7Rs and P2X4Rs were mutually regulated and both receptors are BzATP sensitive (174). Additionally, we also found that BzATP application increased the frequency of EPSC in P2X7R deficient mice. Therefore, we check the protein expression of P2X4Rs in WT and P2X7R deficient mice.

As our previous paper described (55), Animals were euthanized with CO_2 inhalation and decapitated. After dissecting the hippocampus tissue, it was snap frozen in liquid nitrogen. Then the samples were lysed in radioimmunoprecipitation assay (RIPA) buffer composed of 150 mM NaCl, 50 mM Tris-HCl (pH 7.4), 5 mM EDTA, 0.1 % (w/v) SDS, 0.5 % sodium deoxycholate and 1 % Triton X-100 and protease inhibitors (10 mg/ml leupeptin, pepstatin A, 4-(2-aminoethyl) benzensulfonyl-fluorid and aprotinin). Sodium dodecyl sulfate-polyacrylamide gel electrophoresis was employed to separate the Total lysates. Protein was transferred onto nitrocellulose membranes. To block unspecific binding, 5 % non-fat dry milk was used for 1h at room temperature (RT), followed by overnight incubation with primary antibodies anti-P2X4R (1:200, Alomone Labs) and anti-β-actin (1:1000, Cell Signalling Technology Inc.). Membranes were incubated with horseradish peroxidase-conjugated secondary antibodies (Cell Signaling Technology Inc., Danvers, MA, USA) for 1 hour at RT and were developed using the ECL detection system (Thermo Scientific Pierce, Life Technologies). Protein band intensities were analyzed by ImageJ software (NIH). Intensity values of bands representing P2X4R proteins (50-55 kDa) were normalized to the intensity of the band representing total protein (β-actin: 42-45 kDa).

3.4 The methods employed to test potential effects of P2X7Rs on postnatal phencyclidine (PCP)-induced schizophrenia model in mice

After understanding the regulatory effect of P2X7Rs on excitatory neurotransmission and its underlying mechanism, we next aimed to investigate the potential role of P2X7Rs in phencyclidine (PCP)-induced mouse model of schizophrenia. We subcutaneously injected the PCP 10 mg/kg or an equal volume of saline into the male pups at P7, P9, and P11. At 3 weeks of age, the mice were weaned and separated into 3-5 mice per cage. The electrophysiology experiment was performed at juvenile (P25-28), the schizophrenia

DOI:10.14753/SE.2024.2993

related behaviour tests have been performed at both juvenile (P25-28) and young adult (after P67) (Figure 3).

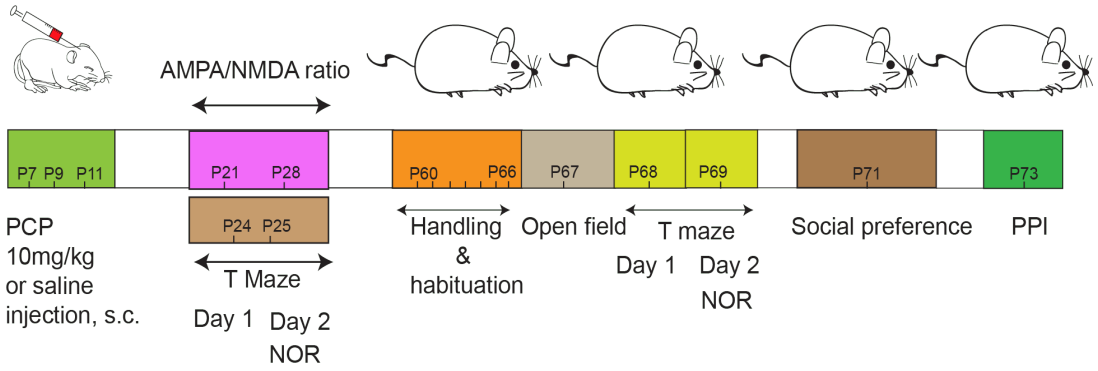

Figure 3. Scheme of the PCP injection, patch clamp experiments, and behaviour tests in juveniles and young adults.

3.4.1 AMPA/NMDA ratio recording

In the previous section, we found P2X7Rs in EC terminal boutons participate in the regulation of DG GCs neurotransmission from presynaptic sites and the involvement of postsynaptic sites was unlikely under the physiological condition. Therefore, we tested DG GCs synapse strength by recording the AMPA/NMDA ratio in the mouse model of postnatal PCP-induced schizophrenia. In this experiment, we sacrificed the juvenile mice from P21-28 to prepare the slice as the previously describe in section 3.2.1. To block GABAA receptor, SR 95531(10 μM) was added to the ACSF. The microelectrode filled with aCSF was placed on the surface of molecular layer of DG. Once the whole-cell configuration formed on DG GC, the stimulating electrode connecting to stimulation isolation unit from World Precision Instruments delivered the pulse which was 100 μs duration stimulus of 40 uA amplitude delivered every 30s. We first held the DG GC neuron at −80 mV for 10-15 sweeps and then switched to +40 mV for another 10-15 seeps. The AMPA receptor mediated-EPSCs were identified at the peak evoked by -80 mV. The NMDA receptor mediated-EPSCs were determined 50 ms after the peak evoked at +40 mV, where the AMPA receptor component was gone due to the rapid kinetics of AMPA receptor components (175-177). AMPA/NMDA ratio was calculated by AMPA receptor amplitude divided by NMDA receptor amplitude at 50 ms post-stimulus.

3.4.2 Spontaneous alteration and Novel object recognition tests

To test the memory related tasks for juvenile mice, we used the three-arm T-maze with a 30 cm L×7 cm W×5 cm H per arm to measure spontaneous alteration at the day 1 and the novel object recognition test at day 2. EthoVision XT 10 system was used to define/calibrate each arena and set the 10 minutes track protocol with a 2 s delay. For the first day, mice were transported into the experiment room 10 minutes before the experiment. Then, the mouse was placed into the middle arm and moved freely through the three arms for another 10 minutes (Figure 4A). For spontaneous alteration analysis, we analysed the entries to each arm in a consecutive sequence manner. For instance, ACBCAC=ACB, CBC, BCA, CAC. However, we calculated the spontaneous alteration only when the mouse entered A, B, and C in any different orders, but not when the same arm was entered more than once. We used the following formula to calculate: Alternations (%) = (Total number of arm entries-2) * 100. To minimize the stress, we did not perform the independent open field in juvenile. Alternatively, we used the videos acquired from day 1 to analyse the total moving distance and calculated the average velocity in 10 minutes.

The novel object recognition test was performed on the second day. This test included two sessions (Figure 4B). In session one, the mouse was placed into the T- maze which contained two identical legos at the end of each arms for 10 minutes free exploration. After 10 minutes, the mouse was back to the home cage for 3 minutes. Then one of the familiar lego was replaced with a new one which had different shape and colors for 10 minutes video recording. We calculated the discrimination index which referred the percentage of time spent in the new object to the time spent in both objects as below: Discrimination index (%) =Time $_{new}$/ (Time $_{new}$ + Time $_{old}$) *100%. Note: This two-days protocol also was used in adult mice.

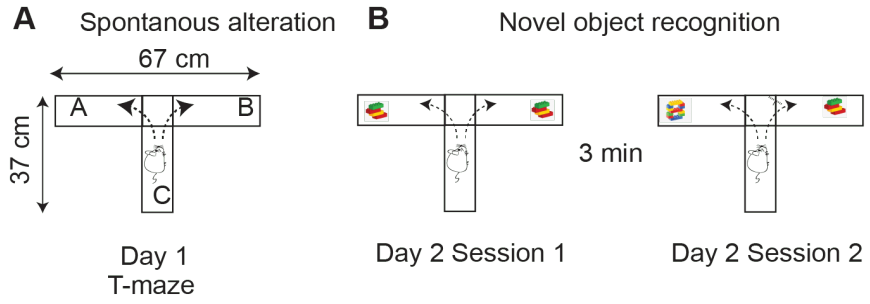

DOI:10.14753/SE.2024.2993

Figure 4. Scheme of the T-maze test. A, spontaneous alteration test and locomotor activity test at day 1. B, novel object recognition test at day 2.

3.4.3 Locomotor activity test

To check the postnatal PCP treatment-induced positive symptom in adult mice, such as hyper locomotor activity, we used four squares arenas with 40 × 40 cm for each arena to measure the locomotor activity in adults (Figure 5A). EthoVision XT 10 system was used to set the same recording protocol as previous described in section 3.5.2. The mice were transported to the experimental room 10 minutes prior to the experiments. After 10 minutes, the mice were placed into the center of each arena for 10 minutes of video recording. Between two runs, the arenas were cleaned totally with 20% alcohol and water. We calculated the total moving distance and the average velocity.

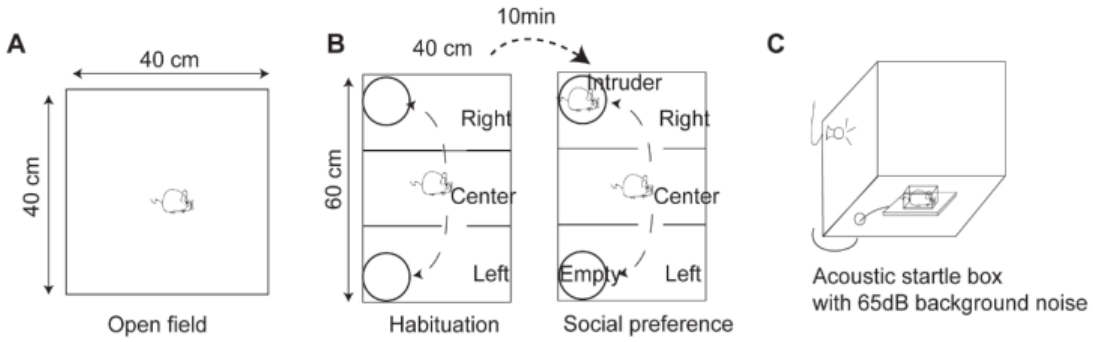

Figure 5. Scheme of open field (A), social preference test (B), and acoustic startle reflex box (C).

3.4.4 Social preference

To clarify whether animals could occur the impairment of social affiliation (one of the indexes for negative symptoms) by PCP treatment, we tested the social preference in three-chambered social box apparatus (40 × 60 cm). There were two doors that allowed animal to freely travel through three chambers (Figure 5B). EthoVision XT 10 was used to define/calibrate each chamber, the intruder cage and empty cage, and the sniffing zones surrounding the cages. After 10 minute's habituation to the experiment room, mouse was

placed into the chamber to freely explore for 10 minutes. Then, the mouse was locked in the middle chamber with two closed doors. Meanwhile, the intruder mouse with the same gender and age was placed into the cage positioned at the corner. Subsequently, we opened the doors and allowed the experimental mouse travel freely for 10 minutes. Between two runs, the arenas were cleaned totally with 20% alcohol and water. We finally calculated social preference percentage based on the time spent in intruder and time spent in both intruder and empty as the following formula: Social preference (%) = (Time $_{intruder}$)/(Time $_{intruder}$ + Time $_{empty}$)*100% .

3.4.5 Prepulse inhibition (PPI)

Although sensory gating deficit did not exclusively occur in schizophrenia, impaired prepulse inhibition (PPI), acts as a hallmark of behavioural deficits in human SCZ (175-179). Although the startle box connected the SR-LAB software was used for the startle experiments (Figure 5C). The whole protocol includes 5 blocks under the 65 dB background noise. The block 1 and 5 contained 5 times 120 dB; the block 2 consisted of to 80, 90, 100, 110, and 120 dB intensities; the block 3 was preceded by pre-pulse (3, 6, 12 dB) and followed by 120 dB; the block 4 was preceded by 73 dB pre-pulse with 25, 50, 100, 200, or 500-ms interval. Before running the blocks, the mice were placed on the platform for 5 min acclimatization. We calculated PPI as a percentage from block 3 by using the following formula: PPI (%) = (100-(average startle magnitude in prepulse trial/average startle magnitude to pulse alone trial) *100)

3.5 The methods used for co-author papers

To understand whether genetic ablation of P2X7Rs altered synaptic strength in CA1 region under the physiological condition, we tested AMPA/NMDA ratio in CA1 pyramidal neurons (55) . In addition to PCP-induced schizophrenia model, we also examined the role of P2X7Rs in complete Freund's adjuvant (CFA)-induced inflammatory pain model (180).

3.5.1 AMPA/NMDA ratio in CA1 pyramidal neurons

The protocol used in this paper (55) was the same as previously described in section 3.4.1. The microelectrode filled with aCSF was placed on the surface of on the surface of radiatum and lacunosum-molecular layer to stimulate Schaffer collaterals and the recorded the response from CA1 pyramidal cells. Although we used -70 mV but not -80 mV to record AMPA receptor-mediated current amplitude due to the cell type difference, we kept all the conditions consistent in different papers.

3.5.2 Acute thermal pain test: the paw withdrawal latency

To understand that P2X7Rs might play important role in other pathological state, we used CFA to establish inflammatory pain model (Figure 6). In this project, we mainly used adult male Sprague–Dawley rats (180–220 g of weight). After measuring the baseline of Paw withdrawal latency (PWL) with thermal laser stimulation, we injected 100 µl CFA into left hind paw of rats and subsequently returned rats back the home cage for 24h. Then, we measured the change of PWL to evaluate the success of the model. The thermal stimulus instrument was preheated for at least 30 min. The percentage of light beam was set for 30% with 20 s cut-off time to avoid over-heat induced tissue damage. All animals were placed on the platform and accustomed to the transparent plastic enclosure. The left hind paw surface was measured. Each animal was measured 3 times at 0, 30, 60, 90, and 120 min with 5 minutes interval. The pH of the PBS was 7.4. The antagonist of P2X3R (A-317491) and P2X7R (A-438079) were dissolved into PBS buffer.

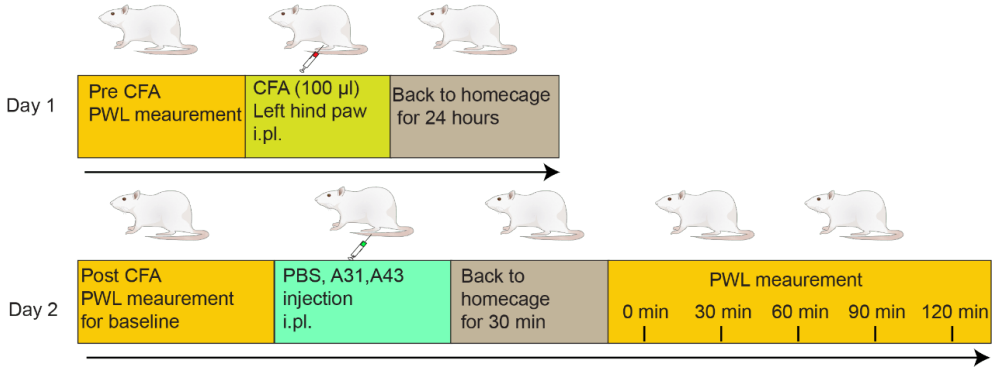

Figure 6. Diagram of the CFA injection, drug injection, and paw withdrawal latency measurement.

3.6 Statistics analysis

The pClamp 10.2 was used to analysis electrophysiological recordings. GraphPad Prism 8.0.2 was used for statistical analyses. Before going parametric and non-parametric, we examined all the data with normality test and not all the data were normally distributed. Therefore, we performed non-parametric methods for statistical analysis. Wilcoxon matched-pairs signed rank test was used for the paired t-test and Mann-Whitney test were used for unpaired t-test. Kruskal-Wallis or Friedman test was used for one-way ANOVA (with or without repeated measures) and two-way ANOVA. The Kolmogorov-Smirnov test was used for cumulative probability. Wilcoxon matched-pairs signed rank test was used for the paired t-test and Mann-Whitney test were used for unpaired t-test. Kruskal-Wallis or Friedman test was used for one-way ANOVA (with or without repeated measures) and two-way ANOVA, followed by the Dunnett-test and Tukey test were used. The data are presented as the means ± SEMs. Sample sizes were chosen based on the value sufficient to observe statistical significance in prior studies (55, 181, 182). Statistical significance was determined when $p^{*}<0.05$; $p^{**}<0.03$; $p^{***}<0.01$, ns: not significant.

DOI:10.14753/SE.2024.2993

3.7 Drugs and description

Name	**description**
2′(3′)-O-(4-Benzoylbenzoyl)adenosine 5′-triphosphate triethylammonium salt （BzATP）	P2X7R potent agonist
5-BDBD	P2X4R selective antagonist
A 438079 hydrochloride	P2X7R selective antagonist
ARL 67156 trisodium salt	selective NTPDase inhibitor
CNQX disodium salt	AMPA/Kainate Receptor Antagonist
DL-AP5	Competitive NMDA Receptor Antagonist
DCG IV	group II metabotropic glutamate receptors (mGluR2/3)
D-serine	Potentiator of NMDA recepors
JNJ 47965567	P2X7R selective and brain permeable antagonist
QX 314 chloride	Na+ channel blocker
SR 95531 hydrobromide	Competitive and selective GABAA antagonist
Tetrodotoxin citrate	Na+ channel blocker
ω-agatoxin TK	Blocker of P/Q-Type Ca^{2+} Channels
ω-conotoxin GVIA	Blocker of N-Type Ca^{2+} Channels

DOI:10.14753/SE.2024.2993

4. Results

4.1 P2X7R activation changes excitatory neurotransmission onto DG GCs by directly increasing the Ca^{2+} influx via the receptor itself

4.1.1 Genetic ablation of P2X7Rs changes excitatory neurotransmission onto DG GCs

All results in this section have been published (183). To understand whether the genetic ablation of P2X7Rs could change the excitatory neurotransmission onto DG GCs, we examined AMPA receptor-mediated excitatory postsynaptic currents in the presence (sEPSC) and absence (mEPSCs) of action potential propagation, respectively, in both WT and P2X7R deficient mice at P21-28. Compared to WT, ablation of P2X7Rs robustly reduced the number of events in AMPA receptor-mediated s/mEPSC, but did not change the amplitude of events (Figure 7A-C).

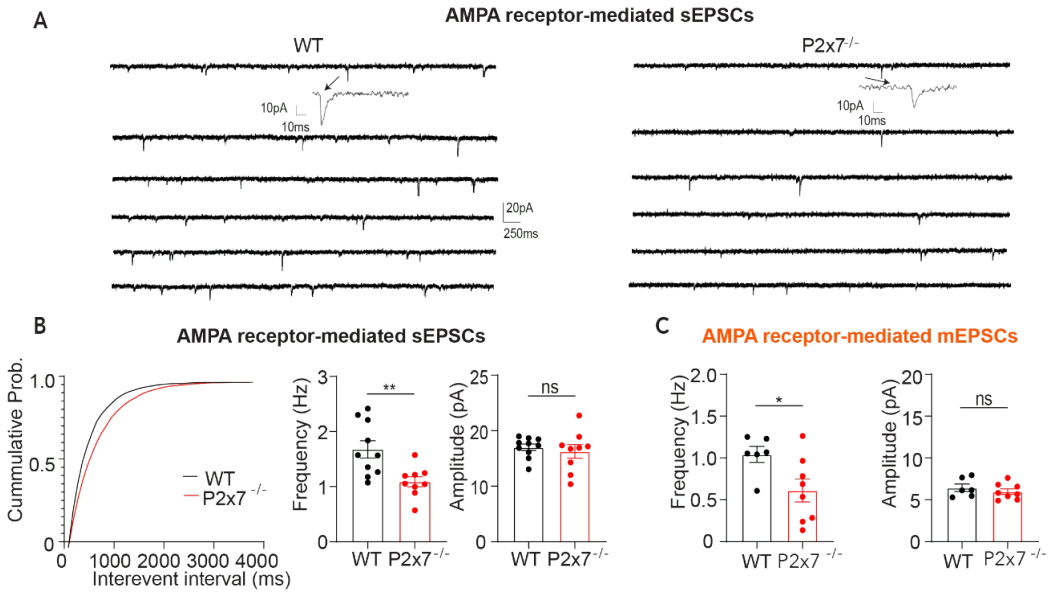

*Figure 7. AMPA receptor-mediated s/mEPSC on DG GCs in both WT and P2X7 deficient mice. (A) Representative traces for AMPA receptor-mediated sEPSC in mice of both genotypes. (B) Cumulative probability of interevent interval for sEPSC in both WT and P2x7-/-. (C) Summary columns for mEPSC frequency and amplitude. Cumulative probability was assessed using the Kolmogorov-Smirnov test. Dots represent the number of the cells. Summary data were expressed as the mean ± SEM. Unpaired t-test was used to compare two groups. * marks significant difference. * $p<0.05$, ** $p<0.03$. ns, no significance.*

DOI:10.14753/SE.2024.2993

We next investigated whether P2X7Rs deficiency also could impair NMDA receptor-mediated neurotransmission. To address this, we recorded NMDA receptor-mediated s/mEPSCs by blocking AMPA receptor components in company with NMDA co-agonist D-serine. Compared to AMPA receptor-mediated s/mEPSC, the frequency of events were lower and amplitude of events were smaller. Importantly, the NMDA receptor-mediated events could be abolished by NMDA receptor blocker DL-AP5. This suggested that the detected events were NMDA receptor-mediated events (Figure 8D). Compared to WT, P2x7-/- mice showed fewer events and the amplitude remained unchanged (Figure 8A-C). To further understand whether P2X7Rs affected neurotransmission in an age-dependent manner, we also examined NMDA receptor-mediated mEPSC in adult. Similarly, we observed the decreased number of events in P2x7-/- mice in comparison with the WT counterparts at the same age. Again, the amplitude remained unchanged. Compared to two different ages, we did not observe significant alteration in either WT or P2x7-/- mice (Figure 8E). These results suggested that P2x7-/- altered DG GC neurotransmission and the regulatory effect was not age-dependent.

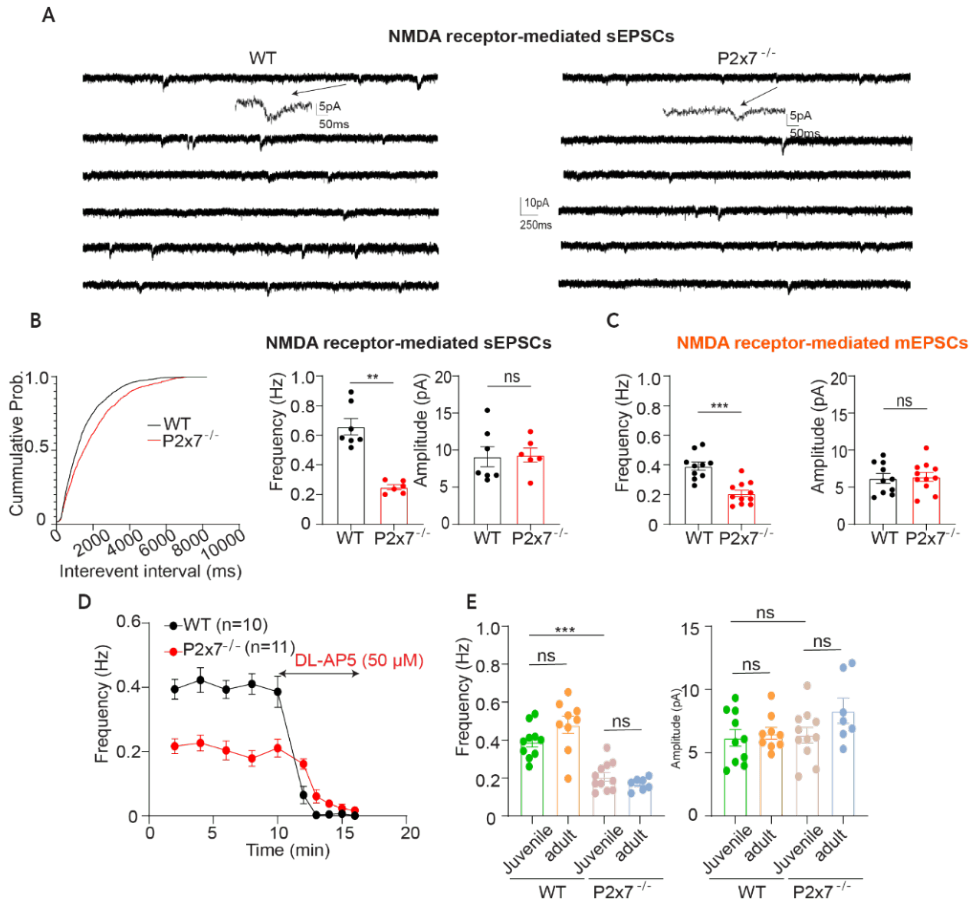

*Figure 8. NMDA receptor-mediated s/mEPSC on DG GCs in both WT and P2X7 deficient mice. (A) Representative traces for NMDA receptor-mediated sEPSC in two genotypes, respectively. (B) Cumulative probability of interevent interval and summarized columns for frequency and amplitude in NMDA receptor-mediated sEPSC. (C) Summary data for frequency and amplitude of NMDA receptor-mediated mEPSC. (D) Change of NMDA receptor-mediated mEPSC frequency over the time in two genotypes in the presence of DL-AP5. (E) NMDA receptor-mediated mEPSC frequency and amplitude in two genotypes at different ages. The cumulative probability was assessed using the Kolmogorov-Smirnov test. Dots represent the number of the cells. Summary data are shown as the mean ± SEM. Unpaired t-test and One-way ANOVA by Dunnett's test used for two groups and multiple groups comparison. * marks significant difference. * $p<0.05$, ** $p<0.03$, *** $p<0.01$. ns, no significance.*

4.1.2 Activation of P2X7R modulated DG GC excitatory neurotransmission from presynaptic site

All results in this section have been published (183). The results from the P2X7Rs deficient animals could not exclude the possibility that the removal P2X7Rs indirectly changes the excitatory neurotransmission, we next investigate the direct participant of P2X7Rs in this process by using the P2X7Rs potent agonist BzATP and selective antagonist JNJ-47955567. It is well-known that ATP becomes hydrolysed into ADP in the presence of nucleoside triphosphate diphosphohydrolase1 (NTPDase1, CD39). The ARL67156 is a commonly used ecto-ATPase inhibitor and could protect BzATP from hydrolysis into Bz-adenosine (62, 184), since it will inhibit the neurotransmission once the Bz-adenosine further activates adenosine receptor 1 (185, 186). Therefore, we added ARL67156 into ACSF to minimize the BzATP hydrolysis. Under this condition, we directly applied BzATP (1 mM) via a fast drug application system (Figure 9A) to the molecular layer of DG for 30s after baseline recording, we found that the frequency of NMDA receptor-mediated sEPSC dramatically increased and was washed out completely (Figure 9B-D). Remarkably, 1mM BzATP-induced potentiation was efficiently suppressed by bath application of P2X7R selective antagonist JNJ-47955567 (Figure 9E and F).

DOI:10.14753/SE.2024.2993

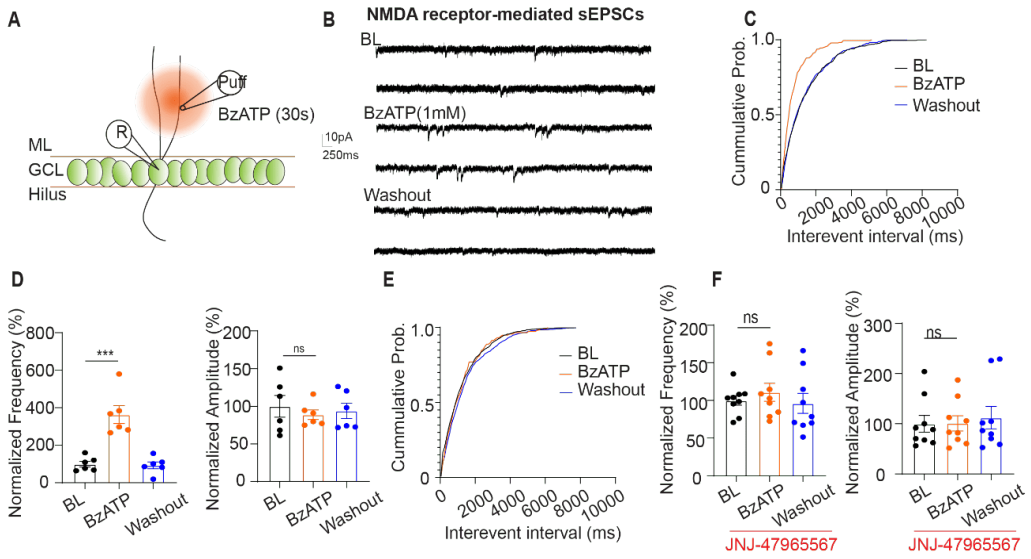

*Figure 9. NMDA receptor-mediated sEPSC on DG GCs by pharmacological manipulation of P2X7Rs. (A) The scheme of puff in the DG region. (B) Representative traces for NMDA receptor-mediated sEPSC by 1 mM BzATP puff for 30s. (C) Cumulative probability of interevent interval for sEPSC and (D) summarized data for frequency and amplitude. (E and F) Frequency and amplitude change in the presence of 10 μM JNJ47965567. Cumulative probability was assessed using the Kolmogorov-Smirnov test. Dots represent the number of the cells. Summary data are shown as the mean ± SEM. Multiple groups comparison were tested by one-way ANOVA repeated measures by Dunnett's test. * marks significant difference. ** $p<0.03$, *** $p<0.01$. ns, no significance.*

To understand the direct activation of P2X7Rs also could change the NMDA receptor-mediated mEPSCs without action potential propagation, we used the same puff method as previous described in section 3.2.2. Unsurprisingly, we also found that 1 mM BzATP increased the frequency of NMDA receptor-mediated mEPSCs and the increase was reversed by P2X7Rs antagonist JNJ-47965567 (Figure 10A and B). These data suggested that P2X7Rs directly participate in the regulation of DG GC excitatory neurotransmission from the presynaptic sites. However, BzATP-induced effect showed a concentration dependent manner, since 300 uM BzATP puff did not change the frequency (Figure 10C).

DOI:10.14753/SE.2024.2993

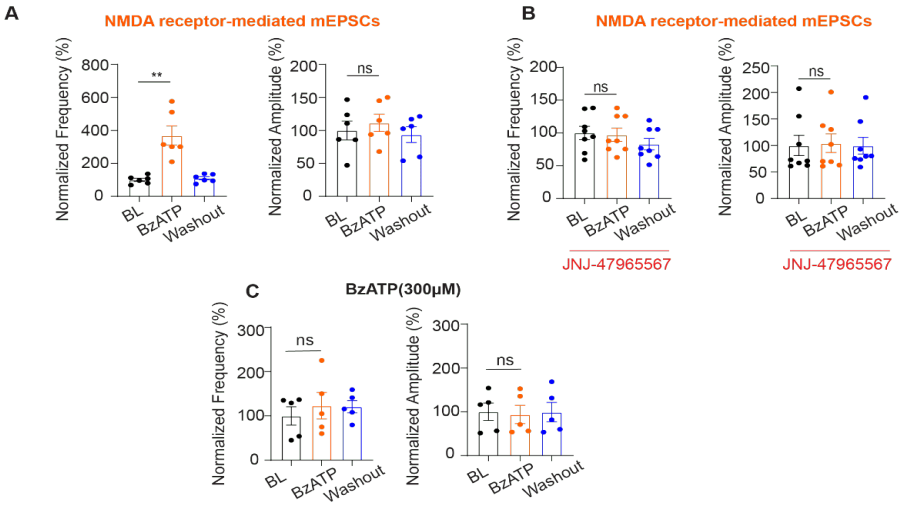

*Figure 10. NMDA receptor-mediated mEPSC on DG GCs by pharmacological manipulation of P2X7Rs. (A and B) 1 mM BzATP puff induced the frequency and amplitude change of NMDA receptor-mediated mEPSC in the absence and presence of 10 μM JNJ-47965567. (C) 300 μM BzATP application-induced change of NMDA receptor-mediated sEPSC. Cumulative probability was assessed using the Kolmogorov-Smirnov test. Dots represent the number of the cells. Summary data are expressed as the mean ± SEM. Multiple groups comparison have been tested by using one-way ANOVA repeated measures by Dunnett's test. * marks significant difference. ** p<0.03, *** p<0.01. ns, no significance.*

We also examined the frequency potentiation induced by 1 mM BzATP in P2x7-/- mice (Figure 11A). This was presumably due to the activation of other P2X receptors by high concentration of BzATP. To clarify this possibility, we checked the involvement of other P2 receptors with an emphasis on BzATP sensitive P2X4 receptors for following reasons. Firstly, P2X7/4Rs could form the heteromeric receptors with P2X7Rs and the receptor expression is regulated by each other (174). Secondly, BzATP sensitive P2X4Rs also participate in the regulation of synaptic neurotransmission in the CNS (187-189). As expected, we found that the protein expression of P2X4R was upregulated in P2x7-/- mice (Figure 11B). Additionally, the 1 mM BzATP-induced NMDA receptor-mediated sEPSC frequency potentiation in P2x7-/- was inhibited when the slices were perfused with P2X4R selective antagonist 5-BDBD (Figure 11C). Altogether, these data pointed out the potential involvement of P2X4Rs.

DOI:10.14753/SE.2024.2993

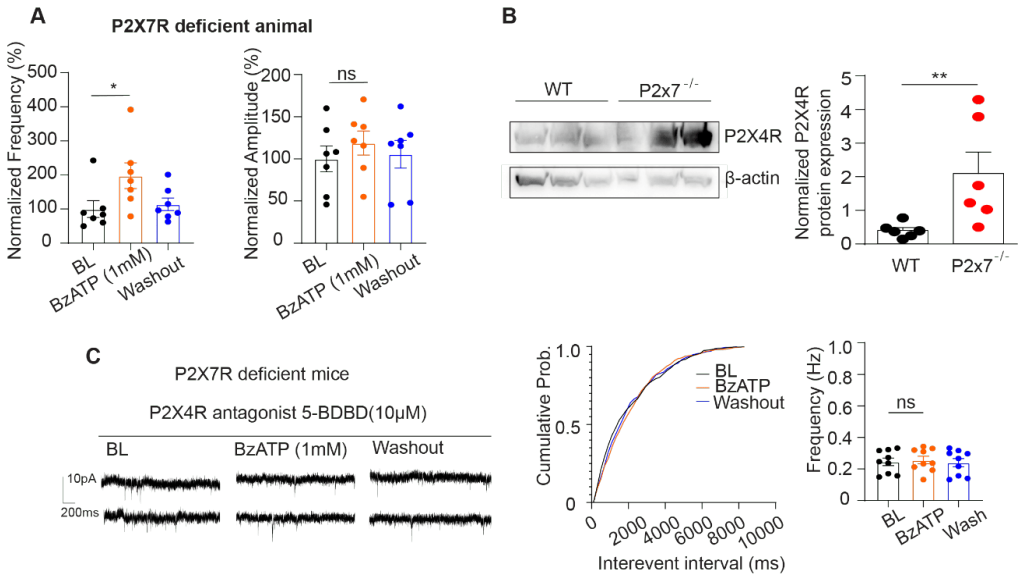

*Figure 11. Involvement of P2X4Rs in DG GCs neurotransmission. (A) 1 mM BzATP-induced NMDA receptor-mediated sEPSC in P2x7-/- mice. (B) P2X4 protein expression bands and the quantitative data. This experiment was performed by Dr. Andras Iring. (C) Left, the representative traces for NMDA receptor-mediated sEPSC in P2x7-/- mice. Right, cumulative probability of frequency and the summarized data in the presence of 5-BDBD. The cumulative probability was assessed using the Kolmogorov-Smirnov test. Dots represent the number of the cells. The data dots from B represent the number of wels from 3 animals. Summary data are shown as the mean ± SEM. One-way ANOVA repeated measures by Dunnett's test and unpaired t-test were used. * marks significant difference. * $p<0.05$, ** $p<0.03$. ns, no significance.*

4.1.3 Regulation of DG GC excitatory neurotransmission by P2X7Rs activation originates from the EC-GC pathway (perforant path)

All results in this section have been published (183). Previous data has shown that acute activation of P2X7Rs lead to the increase of DG GCs glutamate release by changing the frequency, indicating the involvement of the presynaptic site, but it is still unclear whether this regulatory effect displays the input specificity. Indeed, DG GCs receive several excitatory inputs from the entorhinal cortex (EC-GC, also called perforant path), the hilar mossy cell (MC-GC) as well as the supramammillary nucleus (69, 70). In this project, we mainly focused on EC-GC and MC-GC pathway inputs to record extracellular stimulation-evoked currents and measure their paired pulse ratio, which referred to

presynaptic mechanism. To distinguish two different inputs, we placed the stimulating electrode in outer (LPP) and middle (MPP) molecular layers where perforant path are present (Figure 12A) and in inner molecular layer of the DG where MC-GC axons innervate (Figure 14A), respectively. Meanwhile, we employed DCG-IV, a selective agonist of group II metabotropic glutamate receptors (mGluR2/3), at end of recording to identify the fibers, since mGluR2/3 is expressed in the EC GC but not in the MC-GC pathway (100).

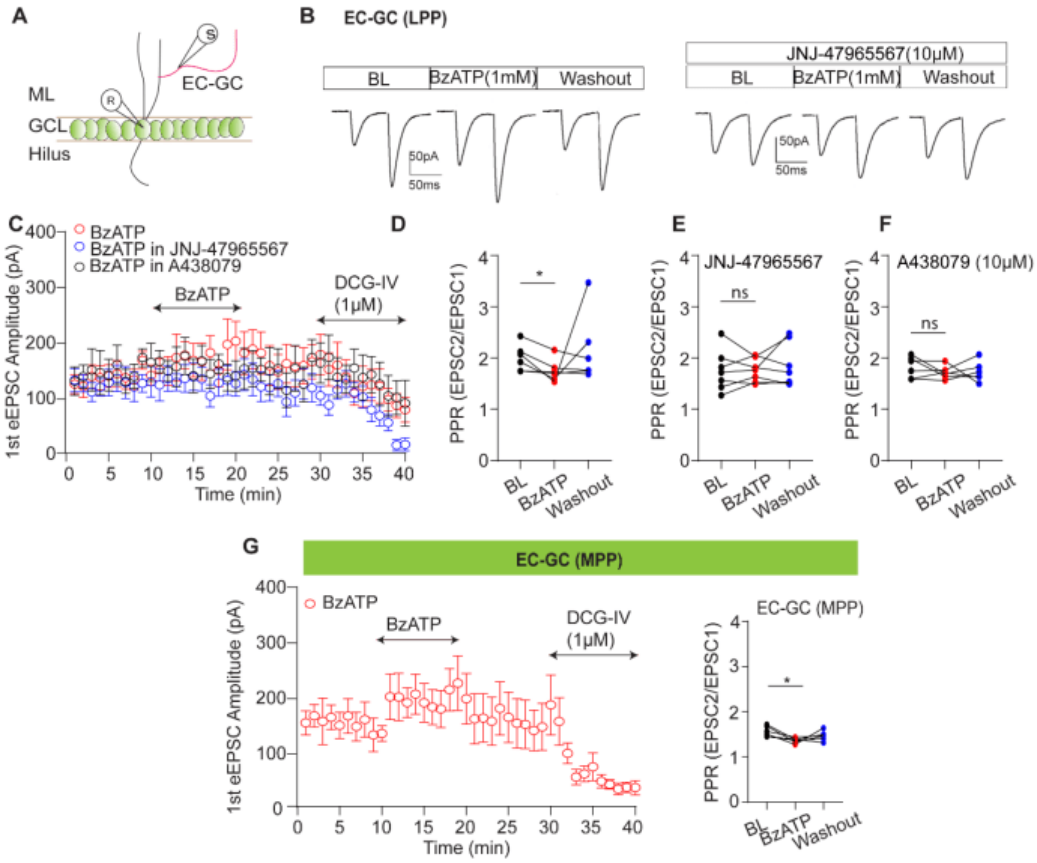

Figure 12. P2X7Rs regulate excitatory neurotransmission through the EC-GC pathway (LPP and MPP). (A) Stimulation diagram for EC-GC pathway. (B) The representative traces for BzATP and JNJ-47965567 application. (C) 1st pulse-induced EPSCs amplitude over the recording time in different conditions in LPP. (D) Summary data for PPR. (E and F) The summary data for PPR in the presence of two P2X7Rs antagonists JNJ-47965567 and A438079, respectively. (G) 1st pulse-induced EPSCs amplitude over the recording time and the PPR value in MPP. Dots represent the number of the cells. Summary data are showed as the Mean ± SEM. One-way ANOVA repeated measures by

*Dunnett's test were used to test the statistical difference. * marks significant difference. * $p<0.05$. ns, no significance.*

We found that the first pulse-induced current amplitude dramatically decreased when applied to DCG-IV in EC-GC fibers (Figure 12C). On the contrary, DCG-IV application did not change the first pulse-induced current amplitude in MC-GC fibers (Figure 14B). These suggested that we could successfully distinguish two inputs neuroanatomically and pharmacologically. In the LPP, we found that 1 mM BzATP application potentiated the 1st pulse-induced EPSC current amplitude, contributing to the decrease of PPR (Figure 12B-D). However, the P2X7Rs antagonists JNJ-47965567 (Figure 12E) and A438079 incubation inhibited the effect of BzATP (Figure 12C). Moreover, we had the similar observation when the MPP was targeted. (Figure 12G).

Previous studies have shown that the P2X7R affinity for its agonists was reduced in the presence of physiological concentration of extracellular Ca^{2+}, thus the low Ca^{2+} (0.3 or 0.5 mM) solution was used (64, 173). To check whether the effect of BzATP on P2X7Rs could be augmented by low Ca^{2+} solution, we decreased the extracellular concentration of Ca^{2+} from 1.3 mM to 0.5 mM. Under this condition, we still observed that BzATP efficiently elevated the 1st pulse-induced current amplitude (Figure 13A) in EC-GC pathway, but not in MG-GC pathway (Figure 14B). Additionally, this effect was blocked by JNJ-47965567 (Figure 13A). Of note, the eEPSC amplitude was much smaller than in ACSF solution containing 1.3 mM Ca^{2+}. However, the BzATP-induced effect was no longer occurred when we increased the extracellular Ca^{2+} concentration from 1.3 mM to 2.6 mM in EC-GC pathway (Figure 13B). Together with the results from 1.3 mM Ca^{2+} these data indicated that Ca^{2+} concentration-dependent blockage of P2X7Rs to BzATP occurred in a higher extracellular Ca^{2+} concentration.

Remarkably, when we placed the stimulating electrode into the inner molecular layer of DG where the MC-GC fibers present, we did not obtain the similar results with EC-GC fibers stimulation. Instead, we found that 1 mM BzATP application did not change the 1st pulse induced EPSC amplitude (Figure 14B) and PPR value in both normal ACSF containing 1.3 mM Ca^{2+} (Figure 14C) and ACSF containing 0.5 mM Ca^{2+} (Figure 14D).

DOI:10.14753/SE.2024.2993

These results suggest that MC-GC pathway was not linked to P2X7R activation induced increase of excitatory neurotransmission in DG GCs.

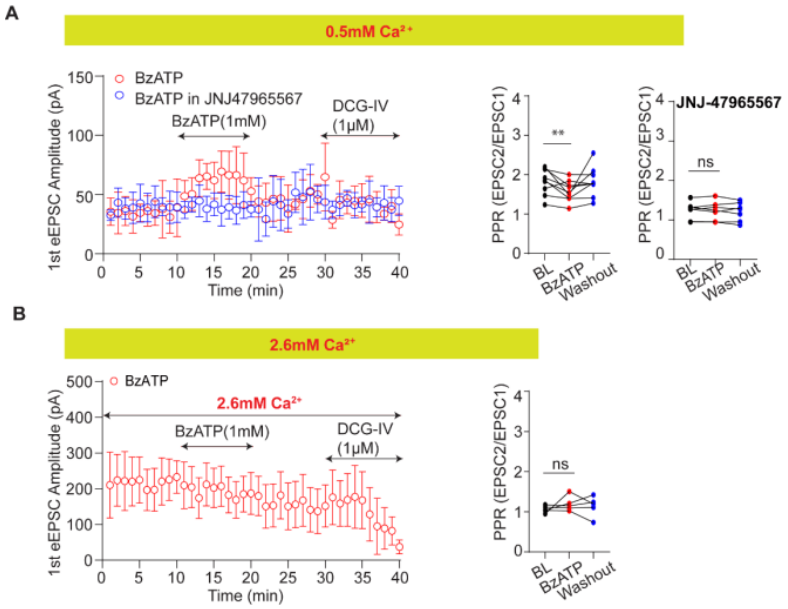

*Figure 13. PPR data in extracellular solution containing 0.5 mM and 2.6 mM Ca^{2+} in LPP. (A) PPR value in BzATP and JNJ-47965567 application in 0.5 mM Ca^{2+} solution. (B) Time course of 1st pulse-induced EPSCs amplitude in the presence of 2.6 mM Ca^{2+}. Each data dot represents the number of the cell. Summary data are expressed as the mean ± SEM. one-way ANOVA repeated measures by Dunnett's test was used. * marks significant difference. ** p<0.03, ns, no significance.*

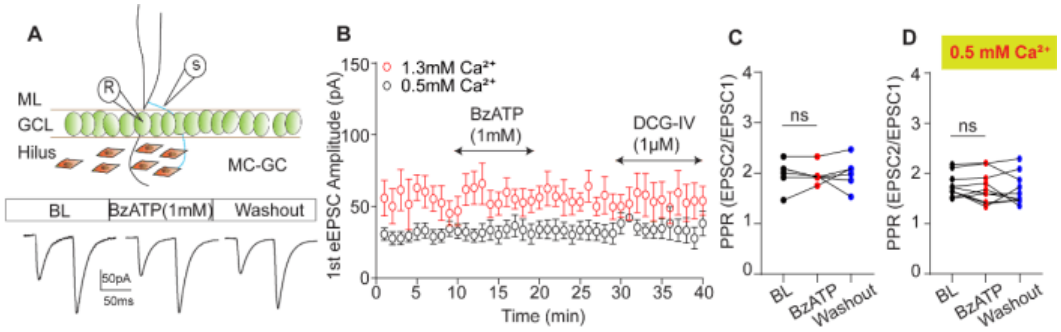

Figure 14. MC-GC pathway did not contribute to P2X7Rs-regulated DG-GC neurotransmission. (A) Diagram for stimulating and recording electrodes in DG for MC-GC pathway. (B) Time of course of 1st pulse-induced EPSCs amplitude in the MG-GC pathway. (C and D) Summary data for PPR in the presence of 1.3 mM $Ca^{2+}$and 0.5 mM

Ca^{2+}, respectively. Dots represent the number of the cells. Summary data are shown as the Mean ± SEM. One-way ANOVA repeated measures by Dunnett's test was used. ns, no significance.

4.1.4 Activation of P2X7Rs on EC boutons directly promoted the Ca^{2+} influx

All results in this section have been published (183). A line of evidence suggest that the activation of P2X7Rs caused Ca^{2+} influx via the channel itself, but no data has indicated whether P2X7Rs directly express on EC GC (perforant path) boutons to elicit the influx of Ca^{2+} into these boutons, followed by the increasing of neurotransmission. To clarify this, we injected virus pAAV1-hSynapsin1-axon-GCaMP6s in EC and expressed Ca^{2+} indicator on PP. In DG molecular layer, the fibers originated from LEC (LPP) and the fibers derived from MEC (MPP) carry distinct information. Therefore, we injected the virus into LEC and MEC based on different coordinates in different animals (Figure 15A and B). After 2 weeks of expression, we sacrificed animals to check virus expression. In the LEC, we found the GCaMP6s positive axons mainly innervated the outer part of DG molecular layer where LPP expressed. Similarly, GCaMP6s positive axons expressed in middle part of molecular layer where MPP present when we injected the virus into MEC.

Although the possibility of these LPP or MPP fibers contaminate with somatodendritic part is quite low, we double stained presynaptic marker Vglut1 and postsynaptic marker Homer1. The staining result showed that the presynaptic marker Vglut1 localized at GCaMP6s positive boutons and Homer1 positive puncta closed to boutons (Figure 15C). These results confirmed that the fibers were axons with boutons, but not dendrites. We next checked the expression of P2X7Rs on these boutons with P2X7R antibody. we found that P2X7R positive puncta were localized on boutons in WT animals but not P2X7R deficient mice (Figure 15D). To further address whether the expression of P2X7Rs in MPP and LPP was different, we randomly quantified the number of P2X7Rs positive puncta in every 50 boutons in each picture and found that there was no expression difference in both MPP and LPP (Figure 15E).

DOI:10.14753/SE.2024.2993

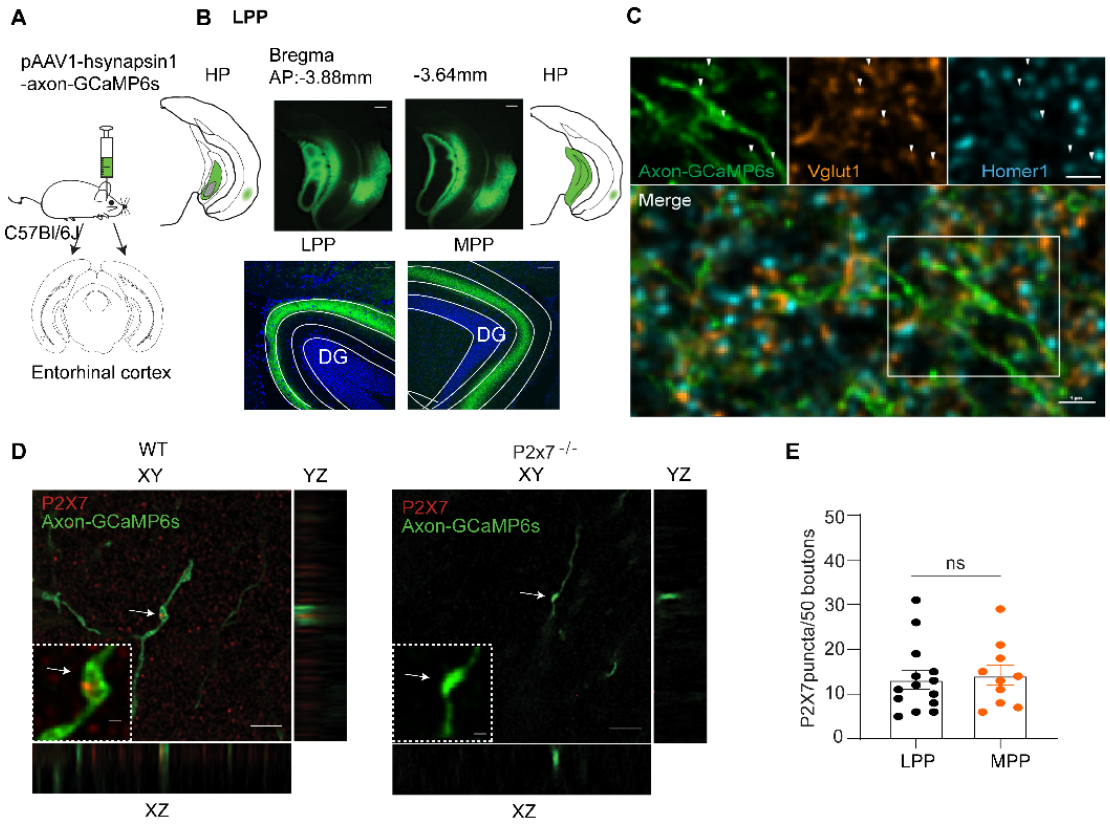

Figure 15. pAAV1-hSynapsin1-axon-GCaMP6s and expression in DG. (A) Scheme for virus injection in EC. (B) Upper panel, the injection point in the LEC (Scale: 200 µm). Lower panel, the axon expression in hippocampus (scale: 50 µm). (C) Representative double staining pictures, showing that presynaptic marker Vglut1 located on boutons but postsynaptic marker Homer1 just close to boutons (scale: 1 µm), this experiment was performed by Dr. Antónia Arszovszki. (D) Representative P2X7Rs staining images from both WT and P2X7R deficient mice (scale: 20 µm and 1). (E) Quantification of P2X7Rs positive puncta in LPP and MPP boutons in WT mice. Dots represent the number of P2X7 positive puncta. Summary data are expressed as the mean ± SEM. Unpaired t-test was used. ns, no significance.

Next, we tested the functionality of GCAMP6s indicator in acute hippocampal slices with multiphoton microscope in company with extracellular stimulation. We placed the stimulating electrode 200 µm away from the scanning area to deliver 5 electrical pulses with different frequencies in a random order (60 Hz>10 Hz>100 Hz>30 Hz) (Figure 16A). In the presence of normal ACSF solution composed of 1.3 mM Ca^{2+}/2 mM Mg^{2+}, 5 pulses

DOI:10.14753/SE.2024.2993

of 60 Hz dramatically saturated the axonal GCaMP6s indicator and there was no further increase of fluorescence intensity when applied to 100 Hz (Figure 16B-D). Therefore, we chose to use 5 pulse of 10 Hz as our stimulating protocol for all experiments. In our preliminary experiment, we found that Z direction drift induced by upright microscope when the protocol was more than 10 minutes. To minimize instability, we ended each experiment within 5 minutes. Under this condition, we did control group and found that fluorescence intensity-related amplitude did not change in 5 minutes (Figure 16E and F). Therefore, we used this 5 minute's protocol for following experiments.

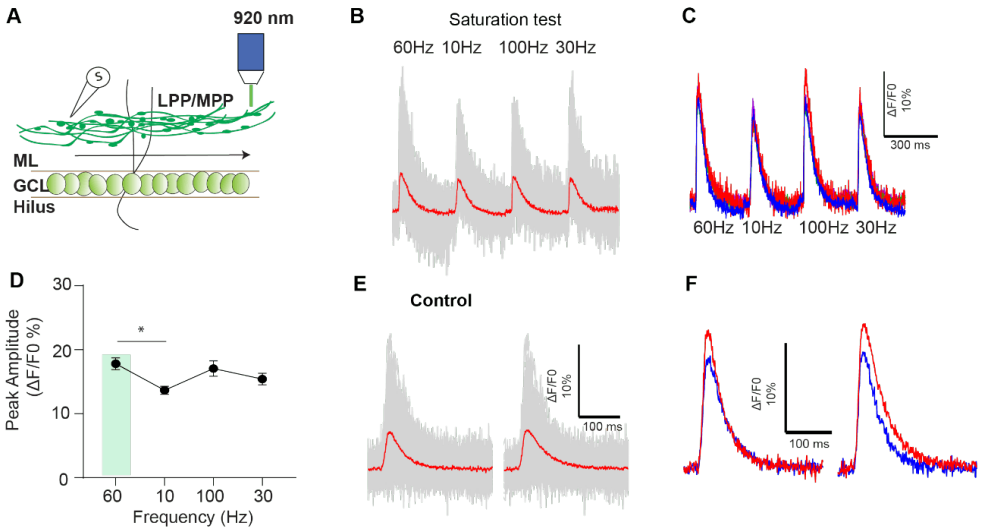

*Figure 16. Electric stimulus-induced Ca^{2+} influx related fluorescence intensity. (A) Diagram for electrical stimulation and multi-photon scanning. (B) Representative traces (the grey curves represented the response from individual bouton, the red curve was the average for all boutons in one slice) for 5 pulses of 10, 30, 60, 100 Hz induced-Ca^{2+} influx spikes in a random sequence. (C) Original traces from different slices (each curve represented the average response of all boutons in one slice). (D) Summary data for the Ca^{2+} spikes by different frequencies. (E and F) Representative traces generated from 5 pulses of 10 Hz in control recording (E: Representative traces from one slice; F: each curve represented the average response of all boutons in one slice). Summary data were showed as mean ± SEM. One-way ANOVA repeated measures by Dunnett's test was used. * marks significant difference. * $p<0.05$.*

DOI:10.14753/SE.2024.2993

According to the immunostaining result showing the P2X7Rs expression on boutons, we expected that stimulation-evoked Ca^{2+} influx should be elevated once the receptors are activated by agonist. To test this, we applied to 1 mM BzATP to activate the receptors and scanned the fluorescence intensity change in the LPP. We found that 1mM BzATP application increased the peak of the action potential relevant GCaMP-fluorescence intensity in comparison with the baseline (Figure 17A and B). The BzATP-induced elevation was inhibited by pre-incubation of P2X7Rs antagonist JNJ47965567 (Figure 17C and D). In addition to the kinetics of fluorescence curves, BzATP application did not change the area under the curve, suggesting that the activation of P2X7Rs did not change the kinetics of Ca^{2+} spikes induced by electric pulses (Figure 17B and D). Additionally, we observed the similar results when we targeted the MPP (Figure 17E and F). Together, all these data suggested that the activation P2X7Rs on boutons by agonist directly increased the stimulation evoked Ca^{2+} influx in both LPP and MPP in the presence of ACSF solution composed of 1.3 mM Ca^{2+}/2 mM Mg^{2+}.

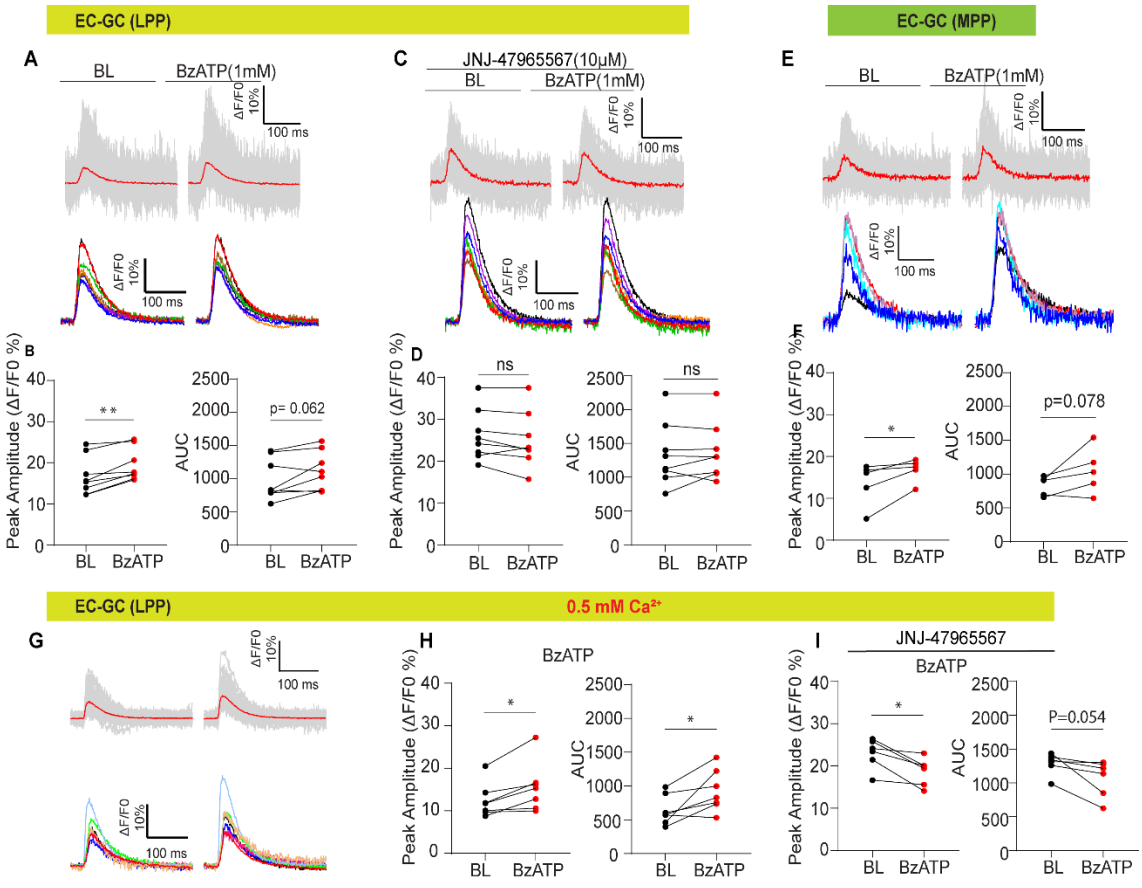

DOI:10.14753/SE.2024.2993

*Figure 17. P2X7Rs activation induced-Ca^{2+} influx on LPP and MPP axonal boutons. (A and C) Representative individual Ca^{2+} spike-related traces and averaged traces from different slices. (B and D) Summary data for peak amplitude and area under the curve. (E and F) Representative traces and data column for peak amplitude and area under the curve in the MPP. (G and H) Representative traces and summary data for peak amplitude and area under the curve in 0.5 mM Ca^{2+} in the LPP. (I) Dots represent the number of the slices. Summary data are shown as the mean ± SEM. Paired t-test was used. * marks significant difference. * $p<0.05$, ** $p<0.03$. ns, no significance.*

Although we also found that BzATP application also increased the Ca^{2+} spike amplitude in the presence of ACSF containing 0.5 mM Ca^{2+}/0 mM Mg^{2+} in the LPP (Figure 17G-I), the increase was not higher than in the presence of normal Ca^{2+} (1.3 mM) group. However, the low Ca^{2+} groups significantly changed the kinetics of the spikes, as the area under the curve was larger in BzATP application compared to baseline and the increase of area under the curve was blocked by JNJ47965567.

When we analysed the individual boutons, we found that not all the boutons have response to BzATP. We found that 48 out of 228 boutons showed an increased fluorescence intensity in control group in WT mice. However, the proportion of boutons positively responding to BzATP was significantly higher than in WT control group. The blockage of P2X7Rs by JNJ47965567 dramatically decreased the number of BzATP-sensitive boutons (76 of the total 397 boutons), suggesting the direct involvement of P2X7Rs. We also detected that 189 boutons of the total 610 boutons displayed a positive response to BzATP in P2X7R deficient mice. Although the proportion is slightly larger than in control, it was still less than in BzATP WT group (Figure 18A and B).

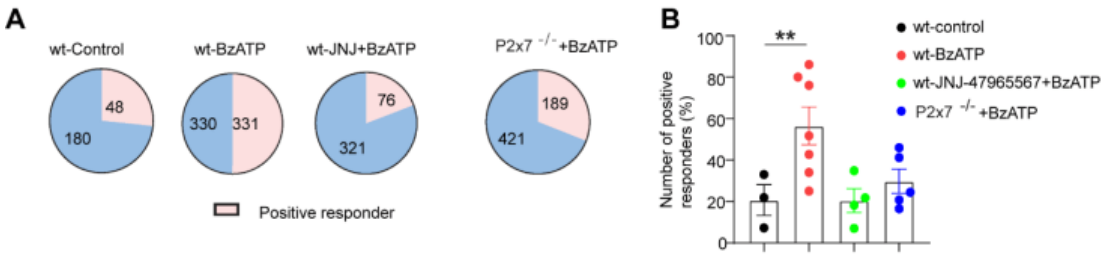

*Figure 18. Bouton numbers referring to increasing fluorescence intensity (positive responder) in different conditions. (A) Proportion of positive responders in total detected boutons in WT-control, WT-BzATP, WT-JNJ-BzATP and P2rx7-/--BzATP groups. (B) Summary data for the number of positive responders in each condition. Dots represent the number of the slices.Summary data are shown as the mean ± SEM. One-way ANOVA by Dunnett's test was employed. * marks significant difference. ** p<0.03.*

4.1.5 P2X7R has no interaction with P/Q and N-type voltage-gated Ca^{2+} channels

All results in this section have been published (183). Although previous data showed that P2X7Rs activation directly increased the influx of Ca^{2+}, it is unclear whether P2X7Rs function together with the voltage-gated Ca^{2+} channels (VGCCs). Additionally, the motor synapse study has reported that activation of P2X7Rs could potentiate presynaptic L-type Ca^{2+} channels by Ca^{2+}/CaMkII (190). We next checked whether this interaction also occurs in EC GC synapses, where P/Q-type and N-type VGCCs are the predominant Ca^{2+} sources to trigger neurotransmitter release (191). We placed the stimulating electrode in the molecular layer of DG to evoke the EPSCs and then activated P2X7Rs by 1 mM BzATP (Figure 19A). Unsurprisingly, 1 mM BzATP significantly increased the peak amplitude of eEPSCs and the potentiation induced by BzATP was suppressed when blocked P2X7Rs by JNJ-47965567 (Figure 19B-D). Then, we employed ω-Aga TK and ω-CTX GVIA to block P/Q type and N-type Ca^{2+} channel, respectively. After 30 minute of slice incubation with 200 μM ω-Aga TK or 100 μM ω-CTX GVIA dissolved into BSA (Figure 19E), we found the amplitude of eEPSCs dramatically decreased and maintained after 30 minutes. Subsequently, we applied to 1 mM BzATP. Compared to baseline (after 30 min incubation) (Figure 19F and G), BzATP elevated the amplitude of eEPSCs in both ω-Aga TK and ω-CTX GVIA conditions, despite that the later one did not show statistical significance. These results indicated that P2X7Rs affected eEPSC via the receptor itself and did not interact with P/Q and N-type voltage-gated Ca^{2+} channels.

DOI:10.14753/SE.2024.2993

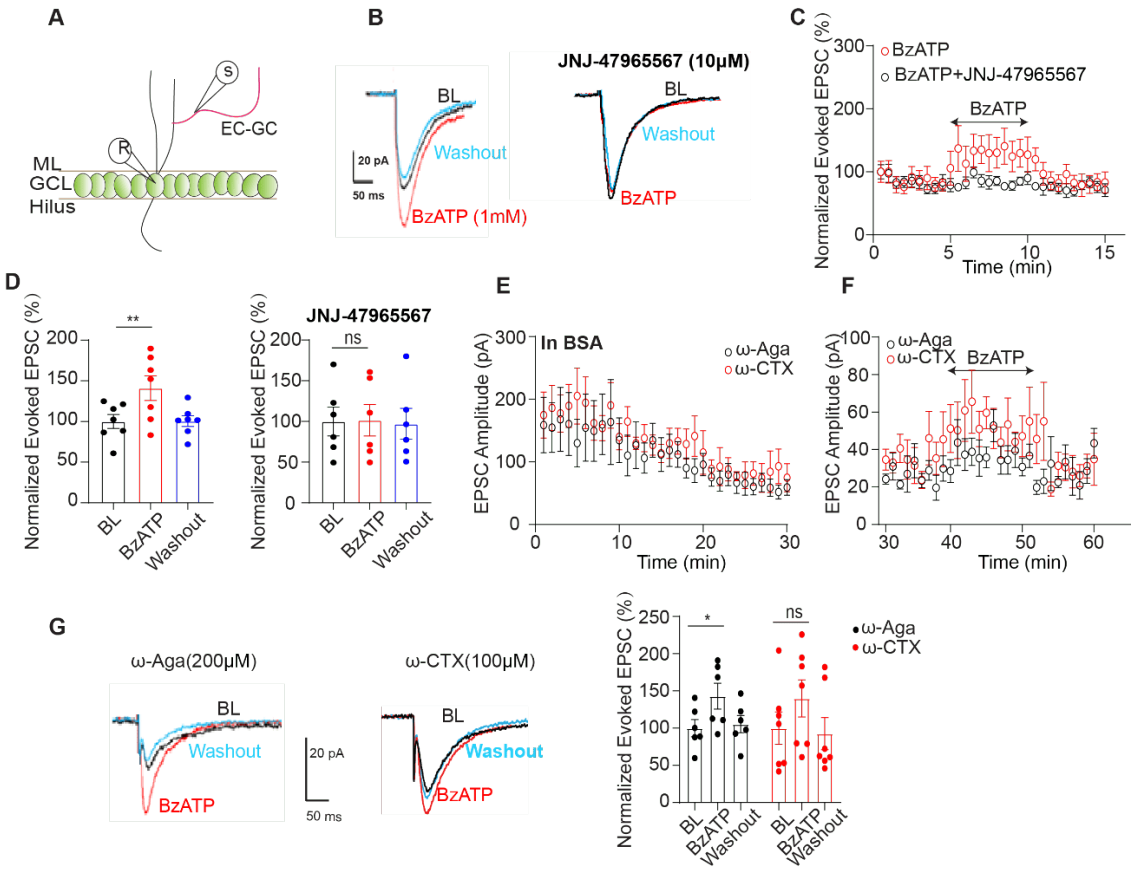

*Figure 19. P2X7Rs did not interact with P/Q and N-type Ca^{2+} channels in EC-GC. (A) Diagram for stimulating and recording electrodes. (B) Representative eEPSC traces. (C) The eEPSCs change over the time in different conditions. (D) Summary data showing the eEPSCs change induced by BzATP traces in the absence and presence of P2X7Rs antagonist. (E) eEPSCs amplitude change in the presence of ω-Aga TK and ω-CTX GVIA, respectively. (F) Effect of BzATP on eEPSCs when blocked P/Q type Ca^{2+} channel and N-type Ca^{2+} channel. (G and H) Representative eEPSC traces and the summary data for eEPSC induced by BzATP in the presence of two Ca^{2+} channels blockers. Dots represent the number of cells. Data are shown as the mean ± SEM. One-way ANOVA repeated measures by Dunnett's test was used. * marks significant difference. * $p<0.05$, ** $p<0.03$. ns, no significance.*

DOI:10.14753/SE.2024.2993

4.2 Involvement of P2X7R in postsynaptic site depends on cell type and pathophysiological conditions

4.2.1 Genetic ablation of P2X7Rs does not alter the number of DG GC dendritic spine under physiological conditions

All results in this section have been published (55, 183). Regarding that a decrease in the postsynaptic spine number can also contribute to a lower neurotransmitter release frequency, we next examined biocytin-labelled GC morphology and counted the number of dendritic spines. We found that the length and number of intersections of DG GC dendrites were not altered in the P2X7R-deficient group in comparison to the WT group (Figure 20A). Subsequently, quantification of the spine numbers showed that there was no change in spine density of dendrite at distances of 100, 150, and 200 µm from the soma in mice of the two genotypes (Figure 20B and C).

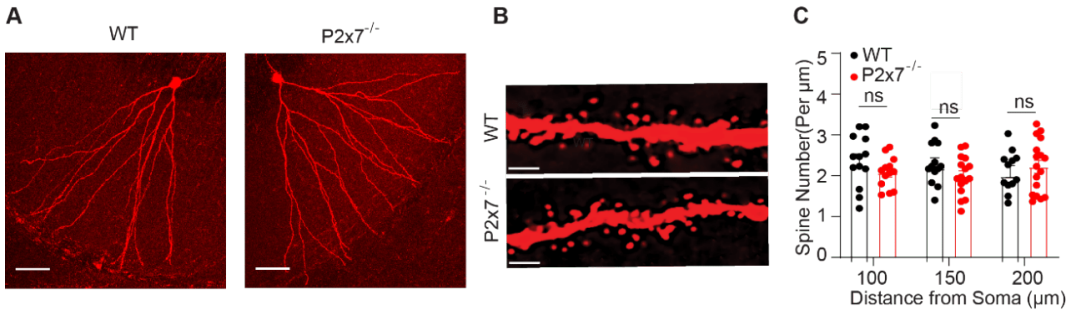

Figure 20. Morphology of DG GC in WT and P2rx7-/- mice. (A) Representative dendritic branches in two genotypes (Scale: 50 µm). (B) Representative images from the dendrites with spines (Scale: 10 µm). (C) Summary spine number from proximal and distal dendritic branches. Dots represent the number of spines. Data are shown as the Mean ± SEM. Two-way ANOVA multiple comparison by Dunnett's test was employed. ns, no significant difference.

Previous electrophysiological studies reveal a potential link between P2X7Rs and NMDARs in pyramidal neurons (13) and neural progenitor cells (NPCs) in the subgranular zone of the DG (192). However, whether these receptors directly interact with one another in DG GCs soma is unclear. Thus, we applied NMDA at concentrations of 10 and 100 µM for 10 s to evoke NMDARs-mediated currents (Figure 21A and B), which were dramatically inhibited by the NMDA antagonist DL-AP5 (Figure 21C). After

DOI:10.14753/SE.2024.2993

two stable baseline current responses, 1 mM BzATP (Figure 21D) or 10 μM JNJ47965567 (Figure 21E) was applied. We found that NMDARs currents were unaffected by pharmacological manipulation of P2X7Rs (activation or inhibition), suggesting that there was no direct interaction between P2X7Rs and NMDARs in DG GCs soma.

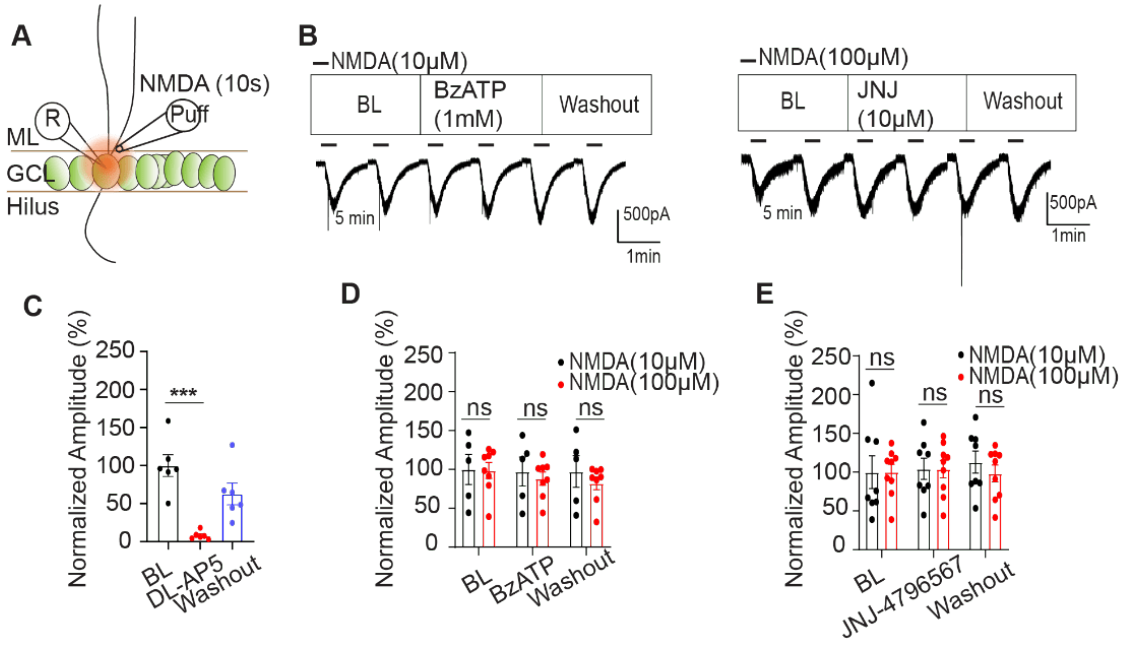

*Figure 21. Interaction between P2X7Rs and NMDA receptors in DG GCs somata. (A) Scheme of NMDA puff. (B) Exogenous NMDA-triggered currents before, during and after BzATP application. (C) Summary data indicating the blockage of NMDA currents by NMDA receptor antagonist D-AP5. (D and E) Data showing the change in BzATP and JNJ-4796556 application. Dots represent the number of cells. Data are shown as the Mean ± SEM. One-way ANOVA repeated measures and Two-way ANOVA multiple comparison by Dunnett's test were utilized. *** P<0.01. ns, no significance.*

Additionally, previous study found that genetic absence of P2X7Rs specifically change the excitability of mPFC layer V neurons. Thus, we checked whether the genetic ablation of P2X7Rs also changed the intrinsic excitability of the DG GCs. We did not observe difference between the two genotypes, although the adult mice showed a slightly higher action potential amplitude compared to the juveniles in WT but not in P2X7R deficient

DOI:10.14753/SE.2024.2993

mice (Table 1). Therefore, the postsynaptic mechanism is unlikely to be associated with P2X7R-mediated modulation of excitatory neurotransmission demonstrated above.

DOI:10.14753/SE.2024.2993

	WT		Significance (ANOVA)	P2x7-/-		Significance (ANOVA)
	P20 (23)	P60 (20)		P20 (15)	P60 (14)	
RMP (mV)	-74.98 ± 1.26	-74.43 ± 1.11	P= 0.74	-74.26 ± 1.29	-73.71 ± 1.75	P= 0.79
IR (MΩ)	249.76 ±11.66	226.16 ± 14.81	P= 0.21	262.45 ±10.36	239.35 ± 8.67	P= 0.10
Maximal Freq (Hz)	31.69 ±1.03	31.55 ± 0.72	P= 0.91	30.56 ± 1.07	30.16 ± 0.86	P= 0.77
Threshold (mV)	-43.54 ± 1.71	-40.67 ± 1.29	P= 0.19	-42.58 ± 1.70	-40.70 ± 1.09	P= 0.37
Amplitude (mV)	78.00 ± 2.70	87.27 ± 2.62	p= 0.01	83.01 ± 2.40	87.00 ± 2.36	P= 0.24
Rise time (ms)	0.88 ± 0.020	0.85 ± 0.028	P= 0.87	0.88 ± 0.02	0.84 ± 0.03	P= 0.27
Half-width time (ms)	1.48 ± 0.03	1.48 ± 0.04	P= 0.62	1.49 ± 0.03	1.45 ± 0.05	P= 0.90
AHP (mV)	6.24 ± 0.36	9.78 ± 0.61	P < 0.0001	6.48 ± 0.29	8.94 ± 0.85	P= 0.01

Table 1. Membrane properties and intrinsic excitability of DG GCs in each group. Data shown as mean ± SEM, Two-way ANOVA multiple comparison by Dunnett's test, p value has been showed in the table.

DOI:10.14753/SE.2024.2993

4.2.2 Genetic deletion of P2X7R restores AMPA/NMDA ratio in PCP-treated animal

All results in this section have been published (55, 183). We next investigated whether genetic ablation of P2X7Rs changed synaptic plasticity. We first measured the AMPA/NMDA ratio at EC GC synapses on P21-28 after postnatal PCP or saline treatment. We found AMPA/NMDA ratio robustly increased when animals were treated with PCP in WT, indicating postanal PCP treatment impaired the EC GC synapse by altering AMPA/NMDA ratio (Figure 22A and B). To analyse components, we found that NMDA receptor components instead of AMPA receptor components were inhibited. Importantly, P2X7R deficiency rescued NMDA receptor components, further contributing to recovery of the AMPA/NMDA ratio. These data addressed that P2X7Rs deficiency resisted the alteration of synapse plasticity under pathological condition.

Compared to WT mice treated with saline, we did not detect any genotype-related change in AMPA/NMDA ratio, AMPA or NMDA receptor-mediated current amplitude, rise time and decay time in P2X7Rs deficient mice. This suggested the genetic absence of P2X7Rs did not change the property of the EC GC synapse (Table 2). In our previous study, we found that CA1 pyramidal cell showed less dendrites and spines in P2X7Rs deficient mice compared to WT counterparts (55). Therefore, we aimed to clary whether genetic ablation of P2X7Rs could change synapse property in a cell type-specific manner. Compared to EC GC synapses, the synapses from CA1 displayed genotype difference. Although AMPA/NMDA ratio did not change (Figure 22C and D) (55), the amplitude of AMPA and NMDA receptor-mediated currents were smaller in P2X7Rs deficiency mice (Table 2). Nevertheless, the rise time and decay time did not change. Together, these data indicated that the genetic ablation of P2X7Rs altered the synaptic plasticity in a cell-type specific manner under physiological condition.

DOI:10.14753/SE.2024.2993

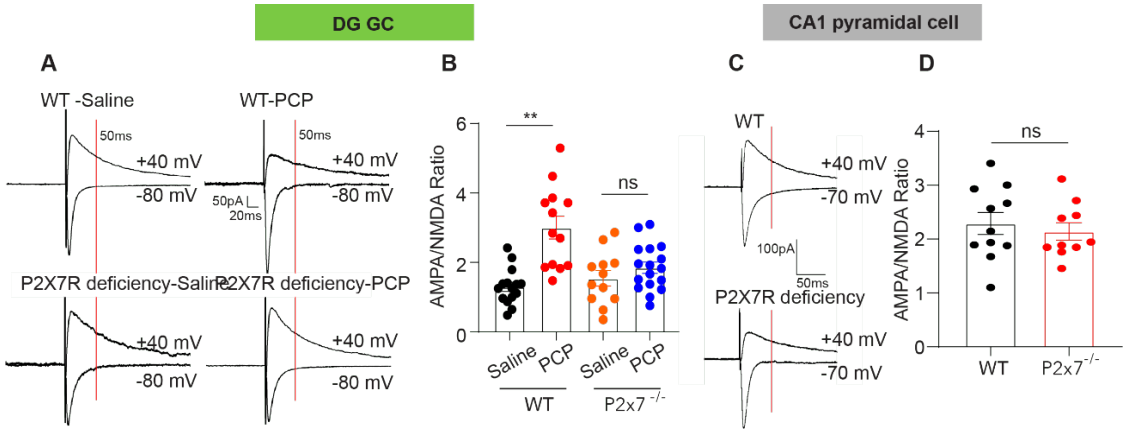

*Figure 22. AMPA/NMDA ratio in DG GCs and in CA1 regions pyramidal cells. (A) Original traces for AMPA and NMDA receptor-mediated currents in DGs. (B) Summary data for AMPA/NMDA ratio in DG GCs. (C and D) Representative traces and summary data for AMPA/NMDA ratio in CA1 pyramidal cells. Dots represent the number of cells. Data are shown as the mean ± SEM. One-way ANOVA by Dunnett's test and unpaired t-test were used. ** P<0.03. ns, no significance.*

DOI:10.14753/SE.2024.2993

		WT			P2x7-/-		
		Amplitude (pA)	Rise time (ms)	Decay time (ms)	Amplitude (pA)	Rise time (ms)	Decay time (ms)
DG GCs + Saline	AMPA	232.1 ± 34.21	3.126 ± 0.25	49.69 ± 5.4	212.9 ± 36.09	3.06 ± 0.43	45.37 ±11.35
	NMDA	199.1 ± 29.11	6.27 ± 0.36	146.3 ± 13.8	157.1 ± 31.88	5.47 ± 0.38	125.9 ± 11.57
DG GCs + PCP	AMPA	185 ± 31.34	3.77 ± 0.36	35.08 ± 4.42	178.6 ± 28.53	3.03 ± 0.19	33.25 ± 3.25
	NMDA	66.06 ± 11.56 **	7.28 ± 0.45	118.9 ± 1.75	98.79 ± 11.43	7.53 ± 0.38	122.8 ± 1.39
CA1 Pyramidal cells	AMPA	157 ± 30.7	3.93 ± 0.42	55.30 ± 3.45	56.29 ± 6.89 ##	3.84 ± 0.306	56.54 ± 1.77
	NMDA	64.67 ± 9.10	8.72 ± 0.35	127 ± 2.37	27.25 ± 3.55 ##	8.51 ± 0.42	124 ± 2.38

*Table 2. Parameters of AMPA/NMDA ratio in both DG GCs and CA1 pyramidal cells. NMDA receptor-mediated amplitude in DG GCs+PCP compared to DG GCs+Saline. One-way ANOVA by Dunnett's test and paired-t test. ** p<0.03. NMDA and AMPA receptor amplitude in WT and P2x7-/- mice. ## p<0.03.*

4.3 The potential therapeutic effect of P2X7Rs blockage/deletion on different pathological models.

To identify the role of P2X7Rs in pathological conditions, we mainly established PCP-induced schizophrenia model in mice and CFA-induced inflammatory pain model in rats.

4.3.1 Genetic ablation of P2X7R attenuates postnatal PCP-induced schizophrenia-like symptoms in mice

All results in this section have been published (183). To establish a neurodevelopmental model of SCZ, we injected PCP into male pups at P7, 9, 11 and checked the behaviour alterations in both juveniles and adults. We monitored the body weight change over the growing up period. After an acute injection, the body weight of WT mice treated with PCP slightly decreased but did not show significant difference when animals reached to adulthood (Figure 23).

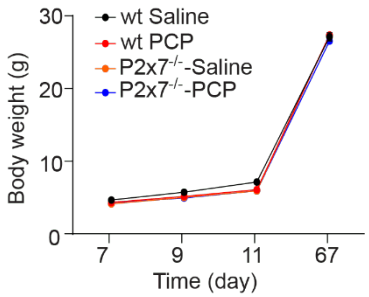

Figure 23. Body weight of animals at different time points in each group.

In WT groups, PCP treatment showed significantly longer moving distance in 10 minutes compared to saline treatment in both T-maze and open field diagram. This displayed that the PCP treatment successfully resulted in hyper locomotor activity which remained in adulthood (Figure 24A). We also examined working memory and recognition paradigms, including spontaneous alteration and novel object recognition in T maze. In juvenile mice, PCP treatment decreased the percentage of spontaneous alteration, suggesting that the ability to remember the previous arm travelled was impaired due to PCP treatment (Figure 24B left). Interestingly, we found that PCP-induced deficit of spontaneous alteration did not show in young adults (Figure 24B right). This indicated that the maturation process somewhat reduced the susceptibility to PCP in this paradigm. In novel object recognition test, PCP treated animals did not show disturbance in the ability to discriminate the novel object in either juvenile or young adults

DOI:10.14753/SE.2024.2993

(Figure 24C). To minimize the stress, we did not include other paradigms in juvenile mice. Nevertheless, we added social preference and acoustic startle reflex in young adult mice. In three chamber social preference test, we did not observe the impairment of social affiliation, suggesting that PCP treatment in our model did not affect the social interaction (a negative symptom) (Figure 24D). Given that sensorimotor gating disturbance is a common feature for schizophrenia patients and prepulse inhibition normally was employed to as operational measurement of sensorimotor gating, we utilized acoustic startle box to test the acoustic startle reflex, especially prepulse inhibition. In comparison with saline-treated animals, postnatal PCP injection slightly disturbed prepulse inhibition in response to 3dB and 6dB, and severely impaired prepulse inhibition when animals received 12 dB prepulse stimulation (Figure 24E). These data suggested that animals were unable to suppress the motor response when the startle-eliciting pulse was preceded by a weaker prepulse. To sum up, postnatal PCP injection could successfully reproduce schizophrenia-like symptoms.

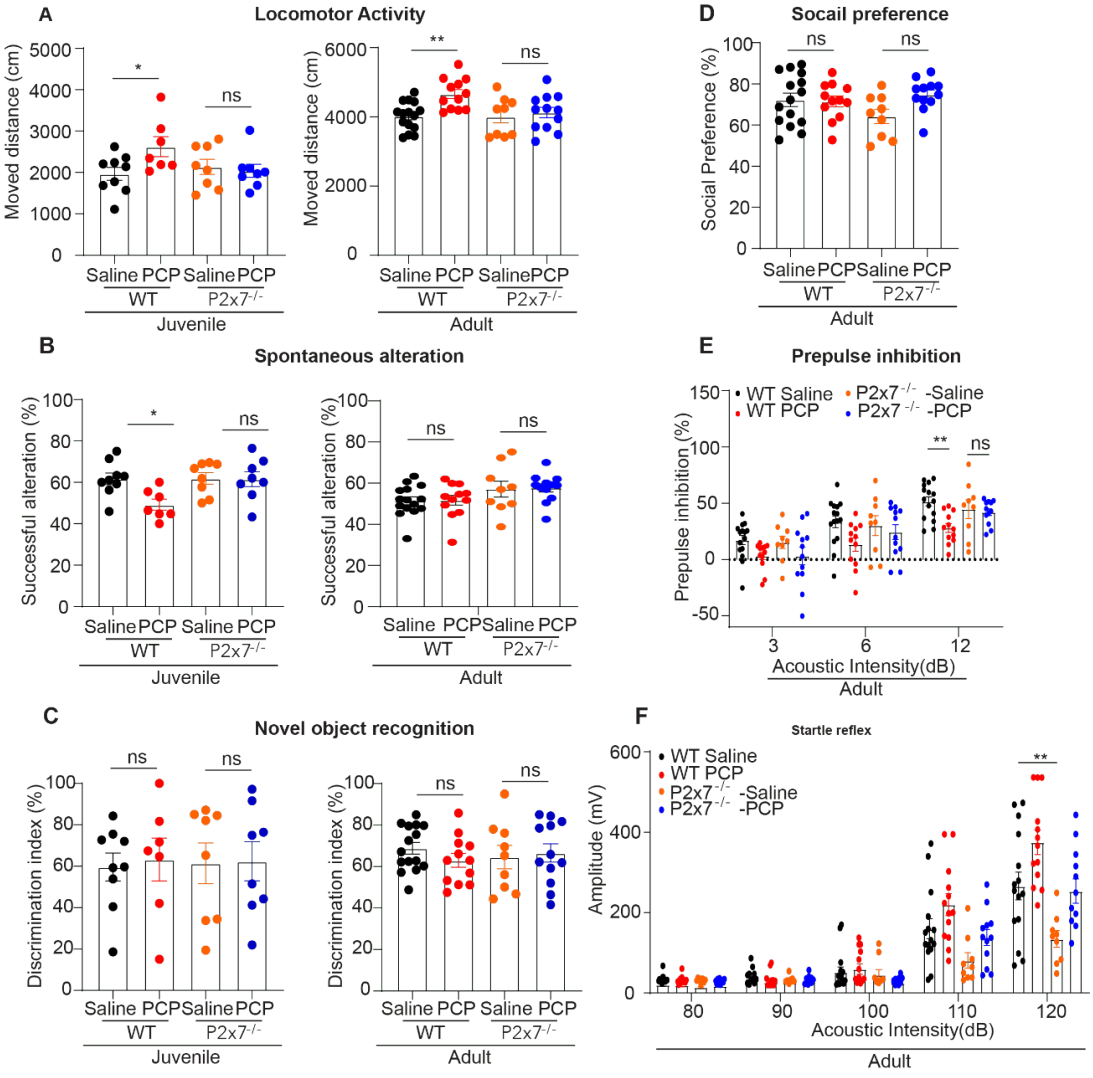

*Figure 24. Behavioural testing of two genotypes at different ages. (A) Summary data from the distance travelled. (B) Summary column for arm spontaneous alteration test. (C) Statistic data for novel object recognition test. (D) Data column for social preference test. (E) Summary data demonstrating the prepulse inhibition test. (F) Data summary for the startle interstimulus interval. Behavior from juveniles were performed by Dr. Bibiána Török. Dots represent the number of animals. Summary data are shown as the mean ± SEM. One-way ANOVA by Dunnett's test was used. * marks significant difference. * $p<0.05$, ** $p<0.03$. ns, no significance.*

Remarkably, we found that the absence of P2X7Rs alleviated the above behaviour alterations induced by postnatal PCP injection. In contrast to WT groups, we found that PCP treatment-induced hyper locomotor activity was missing in P2X7R deficient mice (Figure 24A), suggesting that the genetic ablation of P2X7Rs alleviated PCP-induced positive symptoms. Additionally, P2X7Rs deficient animals did not show disturbance of spontaneous alterations after PCP treatment (Figure 24B). This suggested that the genetic absence of P2X7R also suppressed the PCP-induced working memory impairment. Furthermore, P2X7R deficient mice treated with PCP did not exhibit prepulse inhibition impairment as we observed in WT groups (Figure 24E), addressing that the absence of P2X7Rs also attenuated the PCP-induced alteration of sensory gating. Moreover, we found that P2X7R deficient mice treated by saline did not show different behaviour paradigms, which excluded the influence of gene ablation under physiological condition, although we observed decreased response to higher acoustic stimulus (120 dB) in P2X7Rs deficient mice (Figure 24F). Together, these data indicated that the genetic ablation of P2X7Rs alleviated postnatal PCP induced schizophrenia-like symptoms in both juvenile and young adults.

4.3.2 Blockage of P2X7R relieves Complete Freund's adjuvant (CFA)-induced inflammatory nociception in rat

All results in this section have been published (180). To understand the role of P2X7Rs in another pathological condition, we established inflammatory pain model (arthritic rat model) by injecting CFA into the left hind paw intra-plantar. Compared to pre-CFA injection, CFA injection decreased the paw withdrawal latency (PWL) in all groups, suggesting CFA injection successfully led to thermal hypersensitivity. Remarkably, the injection of 300 nM A438079

(The IC50 of A438079 is 300 nM), the selective antagonist of P2X7Rs which was available in Prof. Tang's lab in China, acutely relieved the pain as the time of PWL increased at 0 min (Figure 25). Although the effect gradually decreased after 30 min, it was still higher than in CFA-alone group. These data indicated that blockage of P2X7Rs relieved CFA-induced acute thermal pain. Although the participation of P2X3Rs in pain sensation has been described by others (193, 194), we also tested the effect of P2X3Rs blockage by its antagonist A317491 300 nM (the IC50 for A317491 is 300 nM) on CFA-induced pain. Unsurprisingly, the PWL time increased when P2X3Rs were blocked by antagonist, indicating the regulatory effect of P2X3Rs on this model. Furthermore, we found that the co-application of P2X3Rs and P2X7Rs antagonists caused a larger effect (Figure 25) (180).

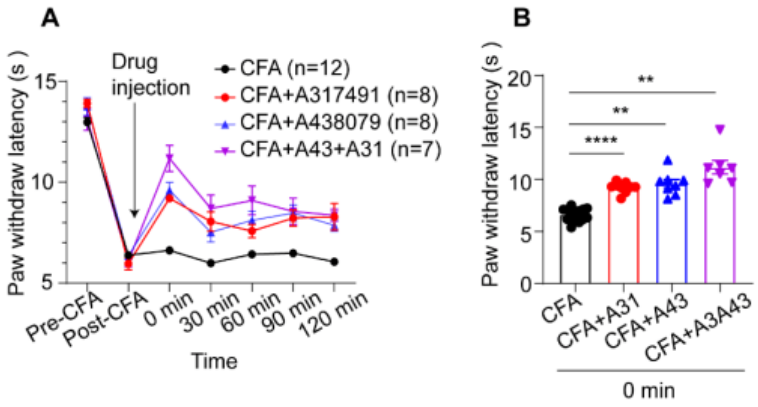

*Figure 25. PWL measurements. (A) PWL value at different time points. (B) PWL at 0 min in each group. Dots represent the number of animals. Data shown as the mean ± SEM. One-way ANOVA by Tukey test was used. * marks significant different. ** $p<0.03$.*

5. Discussion

5.1 The modulatory effect of P2X7Rs activation in the excitatory neurotransmission

Whether P2X7Rs mediate neurotransmitter release remains a matter of long-standing debate. Previous studies have shown that activation of P2X7Rs by their potent agonist BzATP induces neurotransmitter release in the hippocampus (58, 63, 195) and in cortical synaptosomes (60, 196), suggesting that P2X7Rs play a crucial role in neurotransmitter regulation. Importantly, Ca^{2+} influx through P2X7Rs is directly involved in neurotransmission via vesicular exocytosis and channel-mediated processes (e.g., release of ATP by P2X7R itself and by hemichannel connexin/pannexin). However, within the hippocampus, neurons in different subregions show an opposite effect in response to the P2X7Rs agonist BzATP. For example, whole-cell patch-clamp experiments have shown that activation of P2X7Rs by BzATP increases excitatory neurotransmission in the hilar neurons but decreases in the CA3 neurons (59). There are two main issues regarding these inconsistent results. First, the breakdown products of BzATP have an inhibitory effect on neurotransmission. Notably, BzATP can be catabolized by E-NTPDase and E-5'NTase to ADP, AMP, and ultimately adenosine (197). Subsequent activation of adenosine A1Rs by adenosine inhibits the release of neurotransmitters, mainly glutamate (198, 199) and GABA (200). To prevent the breakdown of BzATP, we perfused acute brain slices with the NTPDase inhibitor ARL-67156, which has minimal effects on synaptic transmission (201). In control experiments, we also validated that ARL-67156 alone did not affect synaptic transmission. In the presence of ARL-67156, we found that BzATP application increased the excitatory neurotransmission in the frequency, but not in the amplitude, and the increase was blocked by the P2X7Rs selective antagonist, JNJ-47965567. Second, different subregions of the hippocampus may respond differently to BzATP. To test this region/input-specific effect, we targeted the EC-GC and MC-GC pathways in the DG region. Surprisingly, we found that only the EC-GC pathway was mediated by P2X7Rs. However, further investigations of other brain regions are needed to clarify whether EC-GC is the only pathway influenced by P2X7Rs manipulation. Recently, a study reported that astrocytic P2X7Rs, but not neuronal P2X7Rs, regulate neurotransmission in the CA1 and CA3 region of the hippocampus, because the BzATP-induced increase in the frequency of sEPSCs can be significantly inhibited by the glial metabolism inhibitor fluorocitrate (64). Although we did not examine this possibility, we provide direct support for neuronal P2X7Rs expression; that is the presence of P2X7Rs-immunoreactive puncta on WT EC-GC boutons, but not on P2X7Rs-deficient boutons.

It is well-known that MC-GC does not express mGluR2/3, allowing us to differentiate between EC-GC and MC-GC pathways by mGluR2/3 agonist DCG-IV pharmacologically (100, 202-205). However, type 1 cannabinoid receptor (CB1) agonist, such as WIN 55,212-2, is needed to specifically identify the MC-GC pathway, as hilar mossy cells express CB1 receptor (206, 207). The EC-GC pathway, known as the perforant path, can be divided into the medial perforant path and the lateral perforant path depending on whether the fibres innervate the middle molecular layer or project to the outer molecular layer, respectively. Two pathways can be distinguished pharmacologically and electrophysiologically. In present work, we have mainly used paired-pulse protocols, in which two consecutive stimuli were delivered with an inter-stimulus interval (ISI) of 50 ms. This conventional protocol is thought to induce paired pulse depression (PPD) of the MPP and paired pulse facilitation of the LPP (84, 205, 208-210). However, a later study showed that both pathways induce PPF of field excitatory postsynaptic potentials (fEPSPs) at 50 ms ISI protocol (85). In our system, we found that the PPR values of both LPP and MPP showed PPF, although the PPR values of MPP were slightly lower than those of LPP. To note, this protocol was recorded in the presence of ACSF containing 2 mM Ca^{2+}. In fact, the physiological concentration of Ca^{2+} varies from state to state, ranging from 1.3 mM to 1.8 mM (211-213). Therefore, the reason we did not observe the expected results is that our recording conditions were different. However, the Ca^{2+} imaging results combined with the immunostaining results of hSynapsin1-axon-GCaMP6s specifically infected with the LPP and the MPP underlined a direct involvement of P2X7Rs in both MPP and LPP.

5.2 The role of P2X4R neurotransmission

P2X7Rs have a low affinity for ATP, so we had to use high concentrations of BzATP to activate the receptor. Thus, this may activate other members of the P2XRs family (214) as well as the metabotropic P2Y2Rs (39, 215, 216). Among different P2 receptors, we focused on the P2X4 receptor for two reasons. Firstly, P2X7R can form a heterodimer with P2X4R (174, 217) and their expression can be mutually regulated (218). Secondly, P2X4 receptors also regulate synaptic transmission and plasticity in the hippocampus, suggesting that it may have implications for our experimental observations (187-189). In accordance with our assumption, we found that P2X4Rs expression was upregulated in P2X7Rs-deficient mice. Moreover, direct evidence for the involvement of P2X4Rs is obtained by inhibition of the BzATP-induced effect in P2X7Rs-deficient mice using the P2X4R selective antagonist 5-BDBD. Thus, the compensatory expression of P2X4Rs in the absence of P2X7Rs may contribute to the BzATP-

induced effect. While both P2X4Rs and P2X7Rs have similar sensitivity to BzATP P2X receptors, but ATP is relatively more potent for P2X4Rs than for P2X7Rs. Therefore, further experimental work with ATP application would be needed to address the exact role of P2X4R in the absence of P2X7R. Additionally, we did not investigate other BzATP-sensitive P2 receptors in the present project, therefore, we cannot completely rule out their involvement in regulation of excitatory transmission onto DG GCs.

5.3 Ca^{2+} influx via P2X7 receptor acts as a key role in the modulation of neurotransmitter release

Unlike other P2XRs, extracellular Ca^{2+} acts as a negative allosteric modulator of P2X7R by decreasing the affinity of the receptor for orthosteric ligand agonists (173, 219). Consequently, low Ca^{2+} (0.5 or 0.1 mM)/0 Mg^{2+} ACSF is routinely used to study the electrophysiological effects of P2X7Rs in acute brain slices from rodents (64, 192, 220, 221). In fact, this particular composition of ACSF might impair the release of neurotransmitters from presynaptic terminals due to the non-physiological Ca^{2+} concentration. Depending on arousal/sleep or other situations (211-213), physiological Ca^{2+} concentrations vary from 1.3 mM to 1.8 mM (normally below 1.8 mM) in the extracellular space. In the present project, we first used normal ACSF consisting of 1.3 mM Ca^{2+} /2 mM Mg^{2+}. Under this condition, we were still able to detect BzATP-induced effects. However, when we increased the Ca^{2+} concentration from 1.3 mM to 2.6 mM, the BzATP-induced effect was abolished completely. Conversely, the BzATP-induced effect occurred when we decreased the Ca^{2+} concentration to 0.5 mM and 0 Mg^{2+}, although the effect in the presence of ACSF containing low Ca^{2+} (0.5 mM)/0 Mg^{2+} was not significantly different from that of 1.3 mM Ca^{2+}/2 mM Mg^{2+}. Therefore, we speculate that the Ca^{2+} concentration-dependent blockade of P2X7Rs occurs largely in a high extracellular Ca^{2+} environment.

P2X7R is a Ca^{2+}-permeable channel whose activation leads directly to Ca^{2+} influx and subsequently enhances neurotransmitter release. The C-terminus of P2X7R is the structural domain mainly responsible for cytoplasmic regulation of Ca^{2+}, leading to the phosphorylation of CaMKII (222). A previous study reported that P2X7Rs-mediated Ca^{2+} influx affects the function of L-type voltage-gated Ca^{2+} channels in motor synapses, suggesting a possible interaction between P2X7Rs and VGCCs. Moreover, the α1C-subunit of neuronal L-type VGCCs interacts with CaMKII, further increasing the opening probability of L-type Ca^{2+} channels. Thus, Ca^{2+}/CaMKII may play an important role in the interaction of P2X7Rs and VGCCs (190). In the hippocampal slices, we did not find the similar interaction between

P2X7Rs and P/Q and N-type VGCCs. Therefore, further studies are needed to investigate whether this interaction functions a channel-specific or synapse-specific manner.

5.4 The potential role of P2X7Rs in postsynaptic sites

An earlier report by Sebastian Serrano et al. showed that the number of spines in hippocampal DG neurons were significantly reduced at P9 in P2X7R-deficient mice (56). Inconsistent with these data, we did not find a significant difference in the number of spines between WT mice and P2X7R-deficient mice. To support this conclusion, we first labelled the neurons with biocytin and examined the morphology of the neurons by Sholl analysis. P2X7R-deficient mice did not show difference in the number of crossings, average length, cell body area, or number of endings in comparison to WT mice (183). We then divided the dendritic branches into three sections that correlated with the distance of the dendrites from the soma and did not find differences at different distances. However, we cannot exclude the possibility of quantitative changes in certain spine subtypes, as we did not distinguish between spine subtypes in this work.

Moreover, it is likely that age may contribute to this discrepant result. The animals we used are young juveniles rather than 9-day pups. It is also worth noting that genetic P2X7Rs deletion may alter the number of dendritic spines in certain regions. Our recent paper found that P2X7R-deficient mice showed morphological defects only in the pyramidal cells of CA1, but not in those of CA3 compared to WT mice (55). Thus, we suspect that the regulation of P2X7R on dendritic spines varies by brain regions. Our electrophysiological recordings of CA1 pyramidal cells and dentate gyrus granule cells also showed this region-specific modulation. In CA1 pyramidal cells, the absence of P2X7Rs did not alter the AMPA/NMDA ratio but decreased the amplitude of AMPA and NMDA receptor-mediated currents, which is consistent with the number reduction of dendritic spines. In contrast, we did not observe the same phenomenon in dentate gyrus granule cells.

Pathological conditions may also alter the role of P2X7Rs in DG GCs. In WT mice, we puffed NMDA directly into granule cells and recorded the amplitude of NMDA receptor-induced currents. When P2X7Rs were acutely blocked or activated using the antagonists JNJ-4795567 or BzATP, we did not find changes in current amplitude, suggesting that there is no direct interaction between two receptors on somata. Notably, this modulation was initiated when

animals were injected with PCP postnatally. In contrast to saline-treated animals, injection of PCP increased the AMPA/NMDA ratio by inhibiting the NMDA receptor component. Genetic deletion of P2X7Rs, however, rescued this inhibitory effect, as we could not observe changes in AMPA/NMDA ratio in P2X7Rs-deficient mice. Thus, the involvement of P2X7Rs in the regulation of postsynaptic mechanisms also depends on physiopathological conditions.

5.5 The involvement of P2X7R in pathological conditions: a model of schizophrenia and a model of inflammatory pain

While schizophrenia is known to be a human disease, translating this disease to rodents is challenging. Firstly, the etiology of schizophrenia is a combination of physiological, genetic, psychological, and environmental factors. Therefore, it is difficult to replicate a perfect model that meets all the requirements. Secondly, patients typically have impairments in higher brain functions, including hallucinations, delusions, and language disorders, which are difficult to measure in rodent models. Nonetheless, rodent models are still used in the laboratory to better understand etiology, pathology, diagnosis, and treatment. NMDA receptor hypofunction has been widely used in different animal models to support the glutamatergic hypothesis of schizophrenia (127).

As a noncompetitive NMDA receptor blocker, PCP has been widely used as acute, subacute, and chronic animal models of schizophrenia (223-225) and to recapitulate schizophrenia-like symptoms, including positive (13-15, 226), negative symptoms (227), and cognitive symptoms (15, 226). In the present study, we also selected to us the chronic PCP model with an emphasis on the neurodevelopmental aspect to understand whether early NMDA receptor hypofunction affects the onset of schizophrenia in adolescents and adults. We subcutaneously injected male pups with PCP at P7, P9, and P11 and observed behavioural changes in juveniles (P25-26) and young adults (P60 onwards). Consistent with previous acute, chronic, and neurodevelopmental models (13-15), our postnatal PCP injections also resulted in hyperlocomotion in juveniles and young adults. Thus, postnatal PCP injection reproduced a positive symptom (hyperactivity) after weaning and the symptom persisted into adulthood.

In addition, we observed that postnatal injection of PCP also disturbed working memory, although this symptom occurred only in early childhood and disappear in adulthood. A recent study using a similar model showed that postnatal injection of PCP impaired spatial memory in

the water maze in adulthood (15). This difference may be linked to the injection model and behavioural paradigm. In the reported animal model, PCP was injected at a dose of 10 mg/kg at P7, P9, P11, P13, and P15. Intensive repeated exposure to PCP in infancy may lead to more severe consequences in adulthood compared to our less invasive procedure (P7, P9, P11). We utilized the T-maze to detect spontaneous changes compared to the water maze which focuses primarily on spatial memory and includes a learning/training component. We also tested negative symptoms (social withdrawal) and sensory-gated function (prepulse inhibition) in adult mice. Although we were unable to produce social interaction deficits in this model, we found that postnatal injection of PCP severely impaired prepulse inhibition (PPI), which is a hallmark of behavioural deficits in human SCZ (175-179). These data are consistent with previous reports in rodents (228-231). Thus, by using a model of postnatal injection of PCP, we were able to simulate positive symptoms (hyperlocomotion), cognitive symptoms (working memory, but not novel object recognition), and sensory-gating symptoms (prepulse inhibition). Besides, we found that schizophrenic episodes occurred during weaning and this symptom persisted into adulthood.

Remarkably, we found that P2X7R deficiency suppressed hyper motor activity, alleviated memory deficits, and attenuated prepulse inhibition impairment. These observations are consistent with previous studies in other models (13, 14, 232). A two-stage genome-wide association study of subjects with schizophrenia found that genetic polymorphisms in P2RX7 are associated with this psychiatric disorder (12), suggesting that P2X7Rs contribute to the pathogenesis of schizophrenia from a human genetic perspective. In rodent models, pharmacological blockade and genetic deletion of P2X7Rs attenuates PCP-induced symptoms, including hyperactivity, PPI impairment, and spatial memory deficits, in both acute and subchronic models (13-15).

Several previous studies have been devoted to exploring the role of P2X7Rs in PCP-induced schizophrenia-like behavioural changes. First, P2X7Rs regulate the neuronal excitability. In the medial prefrontal cortex, the number of c-fos-positive pyramidal neurons was reduced in PCP-treated P2X7R-deficient animals compared with WT animals (14). To further investigate the excitability of these pyramidal neurons, this study showed that P2X7R-deficient animals generated fewer action potentials when injected with the same current (14). However, the effect of P2X7R on neuronal excitability may vary in different brain regions and neuron types. In the present project, WT mice and P2X7Rs-deficient mice showed no change in excitability of the

DG GC at the same age, although there were age-related changes in the amplitude of action potentials. Secondly, P2X7Rs interact with NMDA receptors in pathophysiological states (183). By examining NMDA receptor-induced changes in prefrontal cortex (PFC) pyramidal neuron currents in the presence of genetic deletion and pharmacological blockade of P2X7Rs, an interaction between P2X7Rs and NMDA receptors in pyramidal neurons was proposed (13). However, we did not detect any interaction on DG GCs, suggesting that the interaction between P2X7Rs and NMDA receptors varies by cell type and brain region. Notably, pathophysiological conditions could also affect this interaction, as the higher AMPA/NMDA ratio induced by postnatal injection of PCP was suppressed by inhibiting the NMDA receptor component in P2X7Rs-deficient mice. However, the exact mechanism of the interaction between P2X7Rs and NMDARs requires further investigation.

In contrast to NMDA receptor hypofunction model of schizophrenia, injection of CFA in the hind paw induces inflammation, which has been widely used to study pain and analgesia. Although there are compelling data suggesting that P2X7Rs are involved in studies of different pain models, including neuropathic pain and pain induced by cervical incision (233, 234), there are relatively few studies of CFA-induced pain (235). Consistent with the previous study (235), we also found that blockade of P2X7Rs acutely alleviated CFA injection-induced thermal hypersensitivity, although we used A-438079 rather than A-839977. In addition, we found that blockade of the P2X3Rs with the selective antagonist, A-317491, also relieved thermal nociception. Notably, co-injection of P2X7Rs and P2X3Rs antagonists effectively suppressed thermal sensitization, suggesting that both P2X7Rs and P2X3Rs play a key role in CFA-induced pain. The potential underlying mechanism might be that CFA-induced a substantial increase in ATP release, which further activated ATP-sensitive P2 receptors, particularly P2X7Rs and P2X3Rs (180). In conclusion, pharmacological interference with the signalling pathways of P2X3 and P2X7 receptors may be beneficial to abolish thermal or ATP-induced pain both under acute and sub-chronic inflammatory conditions.

DOI:10.14753/SE.2024.2993

6. Conclusions

The data presented in this thesis highlights the important role of presynaptic P2X7Rs in excitatory neurotransmission and pathological states, particularly in postnatal PCP-induced schizophrenia-like symptoms.

By integrating different approaches, we found that AMPA and NMDA receptor-mediated neurotransmission onto DG GCs is subject to regulation by P2X7Rs at presynaptic sites, whereas P2X7R-mediated modulation is input specific. The potential regulatory mechanism involves the expression of P2X7 receptors on axon terminals and the modulation of influx of Ca^{2+} due to the direct activation of P2X7R by BzATP. Meanwhile, we also found that P2X7Rs could affect postsynaptic sites by changing the dendritic morphology and receptors property depending on cell types and pathophysiological conditions.

In postnatal PCP injection-induced mice model of SCZ, we found that genetic ablation of P2X7Rs restored phencyclidine-induced EC-GC synapse alterations and alleviated phencyclidine-induced symptoms in juvenile and adulthood. In CFA-induced inflammatory model of pain, we found that local blockade of P2X7Rs also significantly alleviated CFA-induced pain sensation.

These findings pave the way for a better understanding of P2X7Rs in pathophysiology. The input-specific expression of neuronal P2X7Rs in the dentate gyrus may indicate some specific functions of P2X7Rs in this region, providing a perspective for future studies. In addition, the modulatory effects of P2X7Rs on pathological conditions, such as schizophrenia-like disorders and inflammatory pain, provide potential therapeutic relevance where blockade of P2X7Rs may be beneficial in the treatment of certain types of disorders.

DOI:10.14753/SE.2024.2993

7. Summary

ATP-gated P2X7Rs play a crucial role in brain disorders, mainly by regulating glial cell activity. However, their neuronal mechanisms remain controversial and unclear. Therefore, we investigated the involvement of P2X7Rs in excitatory neurotransmission in dentate gyrus granule cells (DG-GCs) of the hippocampus and in a postnatal phencyclidine (PCP)-induced schizophrenia mouse model.

To address these questions, we first recorded AMPA and NMDA-receptor-mediated spontaneous excitatory postsynaptic currents (sEPSCs) and miniature excitatory postsynaptic currents (mEPSCs) in both WT and P2X7R-deficient mice utilizing the in vitro whole-cell patch-clamp technique. We found that genetic ablation of P2X7Rs decreased the frequency, but not the amplitude, of AMPA and NMDA receptor-mediated EPSCs. The direct involvement of P2X7Rs was confirmed by a pharmacological approach. Paired pulse ratio (PPR) analysis further indicated that the entorhinal cortex (EC)-GC pathway (perforant path), but not the mossy cell (MC)-GC pathway, was associated with DG neurotransmitter regulation mediated by P2X7Rs. To further understand the intracellular mechanism of the EC GC pathway, we injected pAAV1-hSynapsin1-axon-GaMP6s into EC and measured the Ca^{2+} influx of the EC GC pathway with a multiphoton microscopy. Ca^{2+} imaging showed that activation of P2X7Rs directly increased the Ca^{2+} influx into EC-GC boutons. To validate the role of P2X7R in pathological states, we established a neurodevelopment model of schizophrenia by postnatal PCP injection and tested the behaviour changes in juveniles and young adults. We observed that P2X7Rs deletion restored the AMPA/NMDA ratio at EC-GC synapses and attenuated PCP-induced schizophrenia-like behaviours. We also established a rat model of CFA-induced inflammatory pain and found that pharmacological inhibition of P2X7Rs significantly relieved CFA-induced acute thermal pain sensation.

Taken together, P2X7Rs are involved in the modulation of excitatory neurotransmission onto the DG GC through the EC-GC pathway by directly increasing the Ca^{2+} influx. In addition, P2X7Rs may be potential therapeutic targets for the treatment of schizophrenia and pain.

DOI:10.14753/SE.2024.2993

8. Összefoglalás

Az ATP-érzékeny P2X7 receptorok (P2X7R) fontos szerepet játszanak az agyi rendellenességekben, főként a gliasejtek aktivitásának szabályozásán keresztül. Neuronális működésekben betöltött szerepük azonban továbbra is ellentmondásos és tisztázatlan. Kísérleteinkkel a P2X7R-ek részvételét vizsgáltuk a gyrus dentatus szemcsesejtekben (DG-GC-k) a serkentőp neurotranszmisszióban, illetve a posztnatális fenciklidin (PCP) által kiváltott szkizofrénia egérmodellben.

E kérdések megválaszolása érdekében először AMPA és NMDA-receptorok által közvetített spontán serkentő posztszinaptikus áramokat (sEPSC-k) és miniatűr serkentő posztszinaptikus áramokat (mEPSC-k) regisztráltunk vad típusú (WT) és P2X7R-hiányos egerekben in vitro teljes sejtes patch-clamp technikát alkalmazva. Megfigyeltük, hogy a P2X7R-ek genetikai hiánya csökkentette az AMPA és NMDA receptorok által közvetített EPSC-k frekvenciáját, de nem az amplitúdóját. A P2X7R-ek közvetlen részvételét farmakológiai megközelítéssel igazoltuk. A páros impulzusarány (PPR) elemzés továbbá azt mutatta, hogy az entorhinális kéreg (EC)-GC útvonal, de nem a mohasejt (MC)-GC útvonal, áll kapcsolatban a P2X7R-ek által közvetített DG neurotranszmitter felszabadulás szabályozással. Az EC GC útvonal intracelluláris mechanizmusának további megértése érdekében pAAV1-hSynapsin1-axon-GaMP6s vírust injektáltunk az EC-be, és multifoton mikroszkópiával vizsgáltuk az EC GC útvonal kalcium beáramlását. Eredményeink igazolták, hogy a P2X7R-ek aktiválása közvetlenül növelte a kalcium beáramlását az EC-GC boutonokba. A P2X7R kóros állapotokban betöltött szerepét vizsgálva a szkizofrénia idegrendszeri fejlődési modelljét hoztuk létre posztnatális PCP injekcióval, és a viselkedésváltozásokat fiatalkorú és fiatal felnőtt állatok esetében vizsgáltuk. Megfigyeltük, hogy a P2X7Rs delécója helyreállította az AMPA/NMDA arányt az EC-GC szinapszisokban és mérsékelte a PCP által kiváltott szkizofrénia-szerű viselkedésformákat. Vizsgáltuk továbbá a CFA-indukált gyulladásos fájdalom rágcsáló modelljét, és megállapítottuk, hogy a P2X7R-ek farmakológiai gátlása jelentősen enyhítette a CFA kezelés-indukált akut termikus hiperszenzitivitást.

Összességében megállapítottuk, hogy a P2X7R-ek részt vesznek a GC excitatórikus neurotranszmisszió modulációjában a DG-ben az EC-GC útvonalon keresztül, közvetlenül a kalciumionok beáramlásának fokozásával. Ezenkívül a P2X7R-ek potenciális terápiás célpontok lehetnek a skizofrénia és a fájdalom kezelésében.

9. References

1. Hodge RD, Bakken TE, Miller JA, Smith KA, Barkan ER, Graybuck LT, Close JL, Long B, Johansen N, Penn O, Yao Z, Eggermont J, Hollt T, Levi BP, Shehata SI, Aevermann B, Beller A, Bertagnolli D, Brouner K, Casper T, Cobbs C, Dalley R, Dee N, Ding SL, Ellenbogen RG, Fong O, Garren E, Goldy J, Gwinn RP, Hirschstein D, Keene CD, Keshk M, Ko AL, Lathia K, Mahfouz A, Maltzer Z, McGraw M, Nguyen TN, Nyhus J, Ojemann JG, Oldre A, Parry S, Reynolds S, Rimorin C, Shapovalova NV, Somasundaram S, Szafer A, Thomsen ER, Tieu M, Quon G, Scheuermann RH, Yuste R, Sunkin SM, Lelieveldt B, Feng D, Ng L, Bernard A, Hawrylycz M, Phillips JW, Tasic B, Zeng H, Jones AR, Koch C, Lein ES. (2019) Conserved cell types with divergent features in human versus mouse cortex. Nature, 573: 61-68.
2. Yu Y, Ugawa S, Ueda T, Ishida Y, Inoue K, Kyaw Nyunt A, Umemura A, Mase M, Yamada K, Shimada S. (2008) Cellular localization of P2X7 receptor mRNA in the rat brain. Brain Res, 1194: 45-55.
3. Metzger MW, Walser SM, Dedic N, Aprile-Garcia F, Jakubcakova V, Adamczyk M, Webb KJ, Uhr M, Refojo D, Schmidt MV, Friess E, Steiger A, Kimura M, Chen A, Holsboer F, Arzt E, Wurst W, Deussing JM. (2017) Heterozygosity for the Mood Disorder-Associated Variant Gln460Arg Alters P2X7 Receptor Function and Sleep Quality. J Neurosci, 37: 11688-11700.
4. Illes P, Khan TM, Rubini P. (2017) Neuronal P2X7 Receptors Revisited: Do They Really Exist? J Neurosci, 37: 7049-7062.
5. Miras-Portugal MT, Sebastian-Serrano A, de Diego Garcia L, Diaz-Hernandez M. (2017) Neuronal P2X7 Receptor: Involvement in Neuronal Physiology and Pathology. J Neurosci, 37: 7063-7072.
6. Eichenbaum H. (1993) Thinking about brain cell assemblies. Science, 261: 993-994.
7. Lisman JE. (1999) Relating hippocampal circuitry to function: recall of memory sequences by reciprocal dentate-CA3 interactions. Neuron, 22: 233-242.
8. Prasad KM, Patel AR, Muddasani S, Sweeney J, Keshavan MS. (2004) The entorhinal cortex in first-episode psychotic disorders: a structural magnetic resonance imaging study. Am J Psychiatry, 161: 1612-1619.
9. Xia Y, Zhang Z, Lin W, Yan J, Zhu C, Yin D, He S, Su Y, Xu N, Caldwell RW, Yao L, Chen Y. (2020) Modulating microglia activation prevents maternal immune activation induced schizophrenia-relevant behavior phenotypes via arginase 1 in the dentate gyrus. Neuropsychopharmacology, 45: 1896-1908.
10. Leonard AS, Davare MA, Horne MC, Garner CC, Hell JW. (1998) SAP97 is associated with the alpha-amino-3-hydroxy-5-methylisoxazole-4-propionic acid receptor GluR1 subunit. J Biol Chem, 273: 19518-19524.
11. Zhou W, Zhang L, Guoxiang X, Mojsilovic-Petrovic J, Takamaya K, Sattler R, Huganir R, Kalb R. (2008) GluR1 controls dendrite growth through its binding partner, SAP97. J Neurosci, 28: 10220-10233.
12. Trubetskoy V, Pardinas AF, Qi T, Panagiotaropoulou G, Awasthi S, Bigdeli TB, Bryois J, Chen CY, Dennison CA, Hall LS, Lam M, Watanabe K, Frei O, Ge T, Harwood JC, Koopmans F, Magnusson S, Richards AL, Sidorenko J, Wu Y, Zeng J, Grove J, Kim M, Li Z, Voloudakis G, Zhang W, Adams M, Agartz I, Atkinson EG, Agerbo E, Al Eissa M, Albus M, Alexander M, Alizadeh BZ, Alptekin K, Als TD, Amin F, Arolt V, Arrojo M, Athanasiu L, Azevedo MH, Bacanu SA, Bass NJ, Begemann M, Belliveau RA, Bene J, Benyamin B, Bergen SE, Blasi G, Bobes J, Bonassi S, Braun A, Bressan RA, Bromet EJ, Bruggeman R, Buckley PF, Buckner RL, Bybjerg-Grauholm J, Cahn W, Cairns MJ, Calkins ME, Carr VJ, Castle D, Catts SV, Chambert KD, Chan RCK,

Chaumette B, Cheng W, Cheung EFC, Chong SA, Cohen D, Consoli A, Cordeiro Q, Costas J, Curtis C, Davidson M, Davis KL, de Haan L, Degenhardt F, DeLisi LE, Demontis D, Dickerson F, Dikeos D, Dinan T, Djurovic S, Duan J, Ducci G, Dudbridge F, Eriksson JG, Fananas L, Faraone SV, Fiorentino A, Forstner A, Frank J, Freimer NB, Fromer M, Frustaci A, Gadelha A, Genovese G, Gershon ES, Giannitelli M, Giegling I, Giusti-Rodriguez P, Godard S, Goldstein JI, Gonzalez Penas J, Gonzalez-Pinto A, Gopal S, Gratten J, Green MF, Greenwood TA, Guillin O, Guloksuz S, Gur RE, Gur RC, Gutierrez B, Hahn E, Hakonarson H, Haroutunian V, Hartmann AM, Harvey C, Hayward C, Henskens FA, Herms S, Hoffmann P, Howrigan DP, Ikeda M, Iyegbe C, Joa I, Julia A, Kahler AK, Kam-Thong T, Kamatani Y, Karachanak-Yankova S, Kebir O, Keller MC, Kelly BJ, Khrunin A, Kim SW, Klovins J, Kondratiev N, Konte B, Kraft J, Kubo M, Kucinskas V, Kucinskiene ZA, Kusumawardhani A, Kuzelova-Ptackova H, Landi S, Lazzeroni LC, Lee PH, Legge SE, Lehrer DS, Lencer R, Lerer B, Li M, Lieberman J, Light GA, Limborska S, Liu CM, Lonnqvist J, Loughland CM, Lubinski J, Luykx JJ, Lynham A, Macek M, Jr., Mackinnon A, Magnusson PKE, Maher BS, Maier W, Malaspina D, Mallet J, Marder SR, Marsal S, Martin AR, Martorell L, Mattheisen M, McCarley RW, McDonald C, McGrath JJ, Medeiros H, Meier S, Melegh B, Melle I, Mesholam-Gately RI, Metspalu A, Michie PT, Milani L, Milanova V, Mitjans M, Molden E, Molina E, Molto MD, Mondelli V, Moreno C, Morley CP, Muntane G, Murphy KC, Myin-Germeys I, Nenadic I, Nestadt G, Nikitina-Zake L, Noto C, Nuechterlein KH, O'Brien NL, O'Neill FA, Oh SY, Olincy A, Ota VK, Pantelis C, Papadimitriou GN, Parellada M, Paunio T, Pellegrino R, Periyasamy S, Perkins DO, Pfuhlmann B, Pietilainen O, Pimm J, Porteous D, Powell J, Quattrone D, Quested D, Radant AD, Rampino A, Rapaport MH, Rautanen A, Reichenberg A, Roe C, Roffman JL, Roth J, Rothermundt M, Rutten BPF, Saker-Delye S, Salomaa V, Sanjuan J, Santoro ML, Savitz A, Schall U, Scott RJ, Seidman LJ, Sharp SI, Shi J, Siever LJ, Sigurdsson E, Sim K, Skarabis N, Slominsky P, So HC, Sobell JL, Soderman E, Stain HJ, Steen NE, Steixner-Kumar AA, Stogmann E, Stone WS, Straub RE, Streit F, Strengman E, Stroup TS, Subramaniam M, Sugar CA, Suvisaari J, Svrakic DM, Swerdlow NR, Szatkiewicz JP, Ta TMT, Takahashi A, Terao C, Thibaut F, Toncheva D, Tooney PA, Torretta S, Tosato S, Tura GB, Turetsky BI, Ucok A, Vaaler A, van Amelsvoort T, van Winkel R, Veijola J, Waddington J, Walter H, Waterreus A, Webb BT, Weiser M, Williams NM, Witt SH, Wormley BK, Wu JQ, Xu Z, Yolken R, Zai CC, Zhou W, Zhu F, Zimprich F, Atbasoglu EC, Ayub M, Benner C, Bertolino A, Black DW, Bray NJ, Breen G, Buccola NG, Byerley WF, Chen WJ, Cloninger CR, Crespo-Facorro B, Donohoe G, Freedman R, Galletly C, Gandal MJ, Gennarelli M, Hougaard DM, Hwu HG, Jablensky AV, McCarroll SA, Moran JL, Mors O, Mortensen PB, Muller-Myhsok B, Neil AL, Nordentoft M, Pato MT, Petryshen TL, Pirinen M, Pulver AE, Schulze TG, Silverman JM, Smoller JW, Stahl EA, Tsuang DW, Vilella E, Wang SH, Xu S, Indonesia Schizophrenia C, PsychEncode, Psychosis Endophenotypes International C, Syn GOC, Adolfsson R, Arango C, Baune BT, Belangero SI, Borglum AD, Braff D, Bramon E, Buxbaum JD, Campion D, Cervilla JA, Cichon S, Collier DA, Corvin A, Curtis D, Forti MD, Domenici E, Ehrenreich H, Escott-Price V, Esko T, Fanous AH, Gareeva A, Gawlik M, Gejman PV, Gill M, Glatt SJ, Golimbet V, Hong KS, Hultman CM, Hyman SE, Iwata N, Jonsson EG, Kahn RS, Kennedy JL, Khusnutdinova E, Kirov G, Knowles JA, Krebs MO, Laurent-Levinson C, Lee J, Lencz T, Levinson DF, Li QS, Liu J, Malhotra AK, Malhotra D, McIntosh A, McQuillin A, Menezes PR, Morgan VA, Morris DW, Mowry BJ, Murray RM, Nimgaonkar V, Nothen MM, Ophoff RA, Paciga SA, Palotie A, Pato CN, Qin S, Rietschel M, Riley BP, Rivera M, Rujescu D, Saka MC, Sanders AR, Schwab SG, Serretti A, Sham PC, Shi Y, St Clair D, Stefansson H,

Stefansson K, Tsuang MT, van Os J, Vawter MP, Weinberger DR, Werge T, Wildenauer DB, Yu X, Yue W, Holmans PA, Pocklington AJ, Roussos P, Vassos E, Verhage M, Visscher PM, Yang J, Posthuma D, Andreassen OA, Kendler KS, Owen MJ, Wray NR, Daly MJ, Huang H, Neale BM, Sullivan PF, Ripke S, Walters JTR, O'Donovan MC, Schizophrenia Working Group of the Psychiatric Genomics C. (2022) Mapping genomic loci implicates genes and synaptic biology in schizophrenia. Nature, 604: 502-508.

13. Kovanyi B, Csolle C, Calovi S, Hanuska A, Kato E, Koles L, Bhattacharya A, Haller J, Sperlagh B. (2016) The role of P2X7 receptors in a rodent PCP-induced schizophrenia model. Sci Rep, 6: 36680.
14. Calovi S, Mut-Arbona P, Tod P, Iring A, Nicke A, Mato S, Vizi ES, Tonnesen J, Sperlagh B. (2020) P2X7 Receptor-Dependent Layer-Specific Changes in Neuron-Microglia Reactivity in the Prefrontal Cortex of a Phencyclidine Induced Mouse Model of Schizophrenia. Front Mol Neurosci, 13: 566251.
15. Huang H, Zheng S, Chen M, Xie L, Li Z, Guo M, Wang J, Lu M, Zhu X. (2021) The potential of the P2X7 receptor as a therapeutic target in a sub-chronic PCP-induced rodent model of schizophrenia. J Chem Neuroanat, 116: 101993.
16. Burnstock G, Campbell G, Satchell D, Smythe A. (1970) Evidence that adenosine triphosphate or a related nucleotide is the transmitter substance released by non-adrenergic inhibitory nerves in the gut. Br J Pharmacol, 40: 668-688.
17. Burnstock G. (1971) Neural nomenclature. Nature, 229: 282-283.
18. Burnstock G, Dumsday B, Smythe A. (1972) Atropine resistant excitation of the urinary bladder: the possibility of transmission via nerves releasing a purine nucleotide. Br J Pharmacol, 44: 451-461.
19. Unsworth CD, Johnson RG. (1990) Acetylcholine and ATP are coreleased from the electromotor nerve terminals of Narcine brasiliensis by an exocytotic mechanism. Proc Natl Acad Sci U S A, 87: 553-557.
20. Westfall TD, Kennedy C, Sneddon P. (1996) Enhancement of sympathetic purinergic neurotransmission in the guinea-pig isolated vas deferens by the novel ecto-ATPase inhibitor ARL 67156. Br J Pharmacol, 117: 867-872.
21. Robertson SJ, Edwards FA. (1998) ATP and glutamate are released from separate neurones in the rat medial habenula nucleus: frequency dependence and adenosine-mediated inhibition of release. J Physiol, 508 (Pt 3): 691-701.
22. Ho T, Jobling AI, Greferath U, Chuang T, Ramesh A, Fletcher EL, Vessey KA. (2015) Vesicular expression and release of ATP from dopaminergic neurons of the mouse retina and midbrain. Front Cell Neurosci, 9: 389.
23. Jo YH, Role LW. (2002) Coordinate release of ATP and GABA at in vitro synapses of lateral hypothalamic neurons. J Neurosci, 22: 4794-4804.
24. Huang L, Otrokocsi L, Sperlagh B. (2019) Role of P2 receptors in normal brain development and in neurodevelopmental psychiatric disorders. Brain Res Bull, 151: 55-64.
25. Stagg J, Smyth MJ. (2010) Extracellular adenosine triphosphate and adenosine in cancer. Oncogene, 29: 5346-5358.
26. Burnstock G, Meghji P. (1981) Distribution of P1- and P2-purinoceptors in the guinea-pig and frog heart. Br J Pharmacol, 73: 879-885.
27. Fredholm BB, Irenius E, Kull B, Schulte G. (2001) Comparison of the potency of adenosine as an agonist at human adenosine receptors expressed in Chinese hamster ovary cells. Biochem Pharmacol, 61: 443-448.
28. North RA. (2002) Molecular physiology of P2X receptors. Physiol Rev, 82: 1013-1067.

29. Pangalos MN, Davies CH. Understanding G protein-coupled receptors and their role in the CNS. Oxford University Press, Oxford ; New York, 2002.
30. Barnard EA. (1992) Receptor classes and the transmitter-gated ion channels. Trends Biochem Sci, 17: 368-374.
31. Brake AJ, Wagenbach MJ, Julius D. (1994) New structural motif for ligand-gated ion channels defined by an ionotropic ATP receptor. Nature, 371: 519-523.
32. Valera S, Hussy N, Evans RJ, Adami N, North RA, Surprenant A, Buell G. (1994) A new class of ligand-gated ion channel defined by P2x receptor for extracellular ATP. Nature, 371: 516-519.
33. Lalo U, Pankratov Y, Wichert SP, Rossner MJ, North RA, Kirchhoff F, Verkhratsky A. (2008) P2X1 and P2X5 subunits form the functional P2X receptor in mouse cortical astrocytes. J Neurosci, 28: 5473-5480.
34. Dal Ben D, Buccioni M, Lambertucci C, Marucci G, Thomas A, Volpini R. (2015) Purinergic P2X receptors: structural models and analysis of ligand-target interaction. Eur J Med Chem, 89: 561-580.
35. Costa-Junior HM, Sarmento Vieira F, Coutinho-Silva R. (2011) C terminus of the P2X7 receptor: treasure hunting. Purinergic Signal, 7: 7-19.
36. Kopp R, Krautloher A, Ramirez-Fernandez A, Nicke A. (2019) P2X7 Interactions and Signaling - Making Head or Tail of It. Front Mol Neurosci, 12: 183.
37. Roger S, Pelegrin P, Surprenant A. (2008) Facilitation of P2X7 receptor currents and membrane blebbing via constitutive and dynamic calmodulin binding. J Neurosci, 28: 6393-6401.
38. Donnelly-Roberts DL, Namovic MT, Han P, Jarvis MF. (2009) Mammalian P2X7 receptor pharmacology: comparison of recombinant mouse, rat and human P2X7 receptors. Br J Pharmacol, 157: 1203-1214.
39. Mikolajewicz N, Smith D, Komarova SV, Khadra A. (2021) High-affinity P2Y2 and low-affinity P2X7 receptor interaction modulates ATP-mediated calcium signaling in murine osteoblasts. PLoS Comput Biol, 17: e1008872.
40. Hattori M, Gouaux E. (2012) Molecular mechanism of ATP binding and ion channel activation in P2X receptors. Nature, 485: 207-212.
41. Allsopp RC, Dayl S, Bin Dayel A, Schmid R, Evans RJ. (2018) Mapping the Allosteric Action of Antagonists A740003 and A438079 Reveals a Role for the Left Flipper in Ligand Sensitivity at P2X7 Receptors. Mol Pharmacol, 93: 553-562.
42. Riedel T, Schmalzing G, Markwardt F. (2007) Influence of extracellular monovalent cations on pore and gating properties of P2X7 receptor-operated single-channel currents. Biophys J, 93: 846-858.
43. Alves LA, da Silva JH, Ferreira DN, Fidalgo-Neto AA, Teixeira PC, de Souza CA, Caffarena ER, de Freitas MS. (2014) Structural and molecular modeling features of P2X receptors. Int J Mol Sci, 15: 4531-4549.
44. Ugur M, Ugur O. (2019) A Mechanism-Based Approach to P2X7 Receptor Action. Mol Pharmacol, 95: 442-450.
45. Andrejew R, Oliveira-Giacomelli A, Ribeiro DE, Glaser T, Arnaud-Sampaio VF, Lameu C, Ulrich H. (2020) The P2X7 Receptor: Central Hub of Brain Diseases. Front Mol Neurosci, 13: 124.
46. Illes P, Rubini P, Huang L, Tang Y. (2019) The P2X7 receptor: a new therapeutic target in Alzheimer's disease. Expert Opin Ther Targets, 23: 165-176.
47. Francistiova L, Bianchi C, Di Lauro C, Sebastian-Serrano A, de Diego-Garcia L, Kobolak J, Dinnyes A, Diaz-Hernandez M. (2020) The Role of P2X7 Receptor in Alzheimer's Disease. Front Mol Neurosci, 13: 94.

48. Diaz-Hernandez M, Diez-Zaera M, Sanchez-Nogueiro J, Gomez-Villafuertes R, Canals JM, Alberch J, Miras-Portugal MT, Lucas JJ. (2009) Altered P2X7-receptor level and function in mouse models of Huntington's disease and therapeutic efficacy of antagonist administration. FASEB J, 23: 1893-1906.
49. Olla I, Santos-Galindo M, Elorza A, Lucas JJ. (2020) P2X7 Receptor Upregulation in Huntington's Disease Brains. Front Mol Neurosci, 13: 567430.
50. Ribeiro DE, Roncalho AL, Glaser T, Ulrich H, Wegener G, Joca S. (2019) P2X7 Receptor Signaling in Stress and Depression. Int J Mol Sci, 20.
51. Sperlagh B, Illes P. (2014) P2X7 receptor: an emerging target in central nervous system diseases. Trends Pharmacol Sci, 35: 537-547.
52. Glaser T, de Oliveira SL, Cheffer A, Beco R, Martins P, Fornazari M, Lameu C, Junior HM, Coutinho-Silva R, Ulrich H. (2014) Modulation of mouse embryonic stem cell proliferation and neural differentiation by the P2X7 receptor. PLoS One, 9: e96281.
53. Tsao HK, Chiu PH, Sun SH. (2013) PKC-dependent ERK phosphorylation is essential for P2X7 receptor-mediated neuronal differentiation of neural progenitor cells. Cell Death Dis, 4: e751.
54. Sarti AC, Vultaggio-Poma V, Falzoni S, Missiroli S, Giuliani AL, Boldrini P, Bonora M, Faita F, Di Lascio N, Kusmic C, Solini A, Novello S, Morari M, Rossato M, Wieckowski MR, Giorgi C, Pinton P, Di Virgilio F. (2021) Mitochondrial P2X7 Receptor Localization Modulates Energy Metabolism Enhancing Physical Performance. Function (Oxf), 2: zqab005.
55. Mut-Arbona P, Huang L, Baranyi M, Tod P, Iring A, Calzaferri F, de Los Rios C, Sperlagh B. (2023) Dual Role of the P2X7 Receptor in Dendritic Outgrowth during Physiological and Pathological Brain Development. J Neurosci, 43: 1125-1142.
56. Sebastian-Serrano A, Engel T, de Diego-Garcia L, Olivos-Ore LA, Arribas-Blazquez M, Martinez-Frailes C, Perez-Diaz C, Millan JL, Artalejo AR, Miras-Portugal MT, Henshall DC, Diaz-Hernandez M. (2016) Neurodevelopmental alterations and seizures developed by mouse model of infantile hypophosphatasia are associated with purinergic signalling deregulation. Hum Mol Genet, 25: 4143-4156.
57. Campos RC, Parfitt GM, Polese CE, Coutinho-Silva R, Morrone FB, Barros DM. (2014) Pharmacological blockage and P2X7 deletion hinder aversive memories: reversion in an enriched environment. Neuroscience, 280: 220-230.
58. Sperlagh B, Kofalvi A, Deuchars J, Atkinson L, Milligan CJ, Buckley NJ, Vizi ES. (2002) Involvement of P2X7 receptors in the regulation of neurotransmitter release in the rat hippocampus. J Neurochem, 81: 1196-1211.
59. Armstrong JN, Brust TB, Lewis RG, MacVicar BA. (2002) Activation of presynaptic P2X7-like receptors depresses mossy fiber-CA3 synaptic transmission through p38 mitogen-activated protein kinase. J Neurosci, 22: 5938-5945.
60. Marcoli M, Cervetto C, Paluzzi P, Guarnieri S, Alloisio S, Thellung S, Nobile M, Maura G. (2008) P2X7 pre-synaptic receptors in adult rat cerebrocortical nerve terminals: a role in ATP-induced glutamate release. J Neurochem, 105: 2330-2342.
61. Khakpay R, Polster D, Koles L, Skorinkin A, Szabo B, Wirkner K, Illes P. (2010) Potentiation of the glutamatergic synaptic input to rat locus coeruleus neurons by P2X7 receptors. Purinergic Signal, 6: 349-359.
62. Ireland MF, Noakes PG, Bellingham MC. (2004) P2X7-like receptor subunits enhance excitatory synaptic transmission at central synapses by presynaptic mechanisms. Neuroscience, 128: 269-280.
63. Cho JH, Choi IS, Jang IS. (2010) P2X7 receptors enhance glutamate release in hippocampal hilar neurons. Neuroreport, 21: 865-870.

64. Khan MT, Deussing J, Tang Y, Illes P. (2019) Astrocytic rather than neuronal P2X7 receptors modulate the function of the tri-synaptic network in the rodent hippocampus. Brain Res Bull, 151: 164-173.
65. Williams PA, Larimer P, Gao Y, Strowbridge BW. (2007) Semilunar granule cells: glutamatergic neurons in the rat dentate gyrus with axon collaterals in the inner molecular layer. J Neurosci, 27: 13756-13761.
66. Gupta A, Proddutur A, Chang YJ, Raturi V, Guevarra J, Shah Y, Elgammal FS, Santhakumar V. (2020) Dendritic morphology and inhibitory regulation distinguish dentate semilunar granule cells from granule cells through distinct stages of postnatal development. Brain Struct Funct, 225: 2841-2855.
67. Rovira-Esteban L, Hajos N, Nagy GA, Crespo C, Nacher J, Varea E, Blasco-Ibanez JM. (2020) Semilunar Granule Cells Are the Primary Source of the Perisomatic Excitatory Innervation onto Parvalbumin-Expressing Interneurons in the Dentate Gyrus. eNeuro, 7.
68. Gupta A, Dovek L, Proddutur A, Elgammal FS, Santhakumar V. (2022) Long-Term Effects of Moderate Concussive Brain Injury During Adolescence on Synaptic and Tonic GABA Currents in Dentate Granule Cells and Semilunar Granule Cells. Front Neurosci, 16: 800733.
69. Li Y, Bao H, Luo Y, Yoan C, Sullivan HA, Quintanilla L, Wickersham I, Lazarus M, Shih YI, Song J. (2020) Supramammillary nucleus synchronizes with dentate gyrus to regulate spatial memory retrieval through glutamate release. Elife, 9.
70. Tabuchi E, Sakaba T, Hashimotodani Y. (2022) Excitatory selective LTP of supramammillary glutamatergic/GABAergic cotransmission potentiates dentate granule cell firing. Proc Natl Acad Sci U S A, 119: e2119636119.
71. Ntamati NR, Luscher C. (2016) VTA Projection Neurons Releasing GABA and Glutamate in the Dentate Gyrus. eNeuro, 3.
72. Li Y, Stam FJ, Aimone JB, Goulding M, Callaway EM, Gage FH. (2013) Molecular layer perforant path-associated cells contribute to feed-forward inhibition in the adult dentate gyrus. Proc Natl Acad Sci U S A, 110: 9106-9111.
73. Houser CR. (2007) Interneurons of the dentate gyrus: an overview of cell types, terminal fields and neurochemical identity. Prog Brain Res, 163: 217-232.
74. Amaral DG. (1978) A Golgi study of cell types in the hilar region of the hippocampus in the rat. J Comp Neurol, 182: 851-914.
75. Bonthius DJ, McKim R, Koele L, Harb H, Karacay B, Mahoney J, Pantazis NJ. (2004) Use of frozen sections to determine neuronal number in the murine hippocampus and neocortex using the optical disector and optical fractionator. Brain Res Brain Res Protoc, 14: 45-57.
76. Cobb JA, Simpson J, Mahajan GJ, Overholser JC, Jurjus GJ, Dieter L, Herbst N, May W, Rajkowska G, Stockmeier CA. (2013) Hippocampal volume and total cell numbers in major depressive disorder. J Psychiatr Res, 47: 299-306.
77. Jabes A, Lavenex PB, Amaral DG, Lavenex P. (2011) Postnatal development of the hippocampal formation: a stereological study in macaque monkeys. J Comp Neurol, 519: 1051-1070.
78. Claiborne BJ, Amaral DG, Cowan WM. (1990) Quantitative, three-dimensional analysis of granule cell dendrites in the rat dentate gyrus. J Comp Neurol, 302: 206-219.
79. Yoganarasimha D, Rao G, Knierim JJ. (2011) Lateral entorhinal neurons are not spatially selective in cue-rich environments. Hippocampus, 21: 1363-1374.
80. Tsao A, Moser MB, Moser EI. (2013) Traces of experience in the lateral entorhinal cortex. Curr Biol, 23: 399-405.

81. Van Cauter T, Camon J, Alvernhe A, Elduayen C, Sargolini F, Save E. (2013) Distinct roles of medial and lateral entorhinal cortex in spatial cognition. Cereb Cortex, 23: 451-459.
82. Kinkhabwala AA, Gu Y, Aronov D, Tank DW. (2020) Visual cue-related activity of cells in the medial entorhinal cortex during navigation in virtual reality. Elife, 9.
83. McNaughton BL, Barnes CA. (1977) Physiological identification and analysis of dentate granule cell responses to stimulation of the medial and lateral perforant pathways in the rat. J Comp Neurol, 175: 439-454.
84. Colino A, Malenka RC. (1993) Mechanisms underlying induction of long-term potentiation in rat medial and lateral perforant paths in vitro. J Neurophysiol, 69: 1150-1159.
85. Petersen RP, Moradpour F, Eadie BD, Shin JD, Kannangara TS, Delaney KR, Christie BR. (2013) Electrophysiological identification of medial and lateral perforant path inputs to the dentate gyrus. Neuroscience, 252: 154-168.
86. Bramham CR, Milgram NW, Srebro B. (1991) Activation of AP5-sensitive NMDA Receptors is Not Required to Induce LTP of Synaptic Transmission in the Lateral Perforant Path. Eur J Neurosci, 3: 1300-1308.
87. Savtchouk I, Di Castro MA, Ali R, Stubbe H, Lujan R, Volterra A. (2019) Circuit-specific control of the medial entorhinal inputs to the dentate gyrus by atypical presynaptic NMDARs activated by astrocytes. Proc Natl Acad Sci U S A, 116: 13602-13610.
88. Bramham CR, Milgram NW, Srebro B. (1991) Delta opioid receptor activation is required to induce LTP of synaptic transmission in the lateral perforant path in vivo. Brain Res, 567: 42-50.
89. Bramham CR, Sarvey JM. (1996) Endogenous activation of mu and delta-1 opioid receptors is required for long-term potentiation induction in the lateral perforant path: dependence on GABAergic inhibition. J Neurosci, 16: 8123-8131.
90. Ferbinteanu J, Holsinger RM, McDonald RJ. (1999) Lesions of the medial or lateral perforant path have different effects on hippocampal contributions to place learning and on fear conditioning to context. Behav Brain Res, 101: 65-84.
91. Myhrer T. (1988) The role of medial and lateral hippocampal perforant path lesions and object distinctiveness in rats' reaction to novelty. Physiol Behav, 42: 371-377.
92. Knierim JJ, Neunuebel JP, Deshmukh SS. (2014) Functional correlates of the lateral and medial entorhinal cortex: objects, path integration and local-global reference frames. Philos Trans R Soc Lond B Biol Sci, 369: 20130369.
93. Ribak CE, Seress L, Amaral DG. (1985) The development, ultrastructure and synaptic connections of the mossy cells of the dentate gyrus. J Neurocytol, 14: 835-857.
94. Frotscher M, Seress L, Schwerdtfeger WK, Buhl E. (1991) The mossy cells of the fascia dentata: a comparative study of their fine structure and synaptic connections in rodents and primates. J Comp Neurol, 312: 145-163.
95. Scharfman HE, Myers CE. (2012) Hilar mossy cells of the dentate gyrus: a historical perspective. Front Neural Circuits, 6: 106.
96. Buckmaster PS, Strowbridge BW, Kunkel DD, Schmiege DL, Schwartzkroin PA. (1992) Mossy cell axonal projections to the dentate gyrus molecular layer in the rat hippocampal slice. Hippocampus, 2: 349-362.
97. Larimer P, Strowbridge BW. (2008) Nonrandom local circuits in the dentate gyrus. J Neurosci, 28: 12212-12223.
98. Scharfman HE. (2016) The enigmatic mossy cell of the dentate gyrus. Nat Rev Neurosci, 17: 562-575.

99. Houser CR, Peng Z, Wei X, Huang CS, Mody I. (2021) Mossy Cells in the Dorsal and Ventral Dentate Gyrus Differ in Their Patterns of Axonal Projections. J Neurosci, 41: 991-1004.
100. Hashimotodani Y, Nasrallah K, Jensen KR, Chavez AE, Carrera D, Castillo PE. (2017) LTP at Hilar Mossy Cell-Dentate Granule Cell Synapses Modulates Dentate Gyrus Output by Increasing Excitation/Inhibition Balance. Neuron, 95: 928-943 e923.
101. Vertes RP. (1992) PHA-L analysis of projections from the supramammillary nucleus in the rat. J Comp Neurol, 326: 595-622.
102. Magloczky Z, Acsady L, Freund TF. (1994) Principal cells are the postsynaptic targets of supramammillary afferents in the hippocampus of the rat. Hippocampus, 4: 322-334.
103. Pedersen NP, Ferrari L, Venner A, Wang JL, Abbott SBG, Vujovic N, Arrigoni E, Saper CB, Fuller PM. (2017) Supramammillary glutamate neurons are a key node of the arousal system. Nat Commun, 8: 1405.
104. Soussi R, Zhang N, Tahtakran S, Houser CR, Esclapez M. (2010) Heterogeneity of the supramammillary-hippocampal pathways: evidence for a unique GABAergic neurotransmitter phenotype and regional differences. Eur J Neurosci, 32: 771-785.
105. Boulland JL, Jenstad M, Boekel AJ, Wouterlood FG, Edwards RH, Storm-Mathisen J, Chaudhry FA. (2009) Vesicular glutamate and GABA transporters sort to distinct sets of vesicles in a population of presynaptic terminals. Cereb Cortex, 19: 241-248.
106. Hashimotodani Y, Karube F, Yanagawa Y, Fujiyama F, Kano M. (2018) Supramammillary Nucleus Afferents to the Dentate Gyrus Co-release Glutamate and GABA and Potentiate Granule Cell Output. Cell Rep, 25: 2704-2715 e2704.
107. Hirai H, Sakaba T, Hashimotodani Y. (2022) Subcortical glutamatergic inputs exhibit a Hebbian form of long-term potentiation in the dentate gyrus. Cell Rep, 41: 111871.
108. Ajibola MI, Wu JW, Abdulmajeed WI, Lien CC. (2021) Hypothalamic Glutamate/GABA Cotransmission Modulates Hippocampal Circuits and Supports Long-Term Potentiation. J Neurosci, 41: 8181-8196.
109. Ribak CE, Anderson L. (1980) Ultrastructure of the pyramidal basket cells in the dentate gyrus of the rat. J Comp Neurol, 192: 903-916.
110. Hefft S, Jonas P. (2005) Asynchronous GABA release generates long-lasting inhibition at a hippocampal interneuron-principal neuron synapse. Nat Neurosci, 8: 1319-1328.
111. Tallent MK. (2007) Somatostatin in the dentate gyrus. Prog Brain Res, 163: 265-284.
112. Groisman AI, Yang SM, Schinder AF. (2020) Differential Coupling of Adult-Born Granule Cells to Parvalbumin and Somatostatin Interneurons. Cell Rep, 30: 202-214 e204.
113. Jaeschke K, Hanna F, Ali S, Chowdhary N, Dua T, Charlson F. (2021) Global estimates of service coverage for severe mental disorders: findings from the WHO Mental Health Atlas 2017. Glob Ment Health (Camb), 8: e27.
114. Sadeghi D, Shoeibi A, Ghassemi N, Moridian P, Khadem A, Alizadehsani R, Teshnehlab M, Gorriz JM, Khozeimeh F, Zhang YD, Nahavandi S, Acharya UR. (2022) An overview of artificial intelligence techniques for diagnosis of Schizophrenia based on magnetic resonance imaging modalities: Methods, challenges, and future works. Comput Biol Med, 146: 105554.
115. Sharaev MG, Malashenkova IK, Maslennikova AV, Zakharova NV, Bernstein AV, Burnaev EV, Mamedova GS, Krynskiy SA, Ogurtsov DP, Kondrateva EA, Druzhinina PV, Zubrikhina MO, Arkhipov AY, Strelets VB, Ushakov VL. (2022) Diagnosis of Schizophrenia Based on the Data of Various Modalities: Biomarkers and Machine Learning Techniques (Review). Sovrem Tekhnologii Med, 14: 53-75.
116. Hartling L, Abou-Setta AM, Dursun S, Mousavi SS, Pasichnyk D, Newton AS. (2012) Antipsychotics in adults with schizophrenia: comparative effectiveness of first-

generation versus second-generation medications: a systematic review and meta-analysis. Ann Intern Med, 157: 498-511.
117. Wubeshet YS, Mohammed OS, Desse TA. (2019) Prevalence and management practice of first generation antipsychotics induced side effects among schizophrenic patients at Amanuel Mental Specialized Hospital, central Ethiopia: cross-sectional study. BMC Psychiatry, 19: 32.
118. Ohno Y, Shimizu S, Tokudome K. (2013) Pathophysiological roles of serotonergic system in regulating extrapyramidal motor functions. Biol Pharm Bull, 36: 1396-1400.
119. Fenton C, Kang C. (2023) Clozapine is the approved option in treatment-resistant schizophrenia and requires careful management. Drugs Ther Perspect, 39: 107-113.
120. Remington G, Saha A, Chong SA, Shammi C. (2005) Augmentation strategies in clozapine-resistant schizophrenia. CNS Drugs, 19: 843-872.
121. Rodrigues-Silva C, Semedo AT, Neri H, Vianello RP, Galaviz-Hernandez C, Sosa-Macias M, de Brito RB, Ghedini PC. (2020) The CYP2C19*2 and CYP2C19*17 Polymorphisms Influence Responses to Clozapine for the Treatment of Schizophrenia. Neuropsychiatr Dis Treat, 16: 427-432.
122. Nemeth G, Laszlovszky I, Czobor P, Szalai E, Szatmari B, Harsanyi J, Barabassy A, Debelle M, Durgam S, Bitter I, Marder S, Fleischhacker WW. (2017) Cariprazine versus risperidone monotherapy for treatment of predominant negative symptoms in patients with schizophrenia: a randomised, double-blind, controlled trial. Lancet, 389: 1103-1113.
123. Mailman RB, Murthy V. (2010) Third generation antipsychotic drugs: partial agonism or receptor functional selectivity? Curr Pharm Des, 16: 488-501.
124. Vasiliu O. (2022) Third-generation antipsychotics in patients with schizophrenia and non-responsivity or intolerance to clozapine regimen: What is the evidence? Front Psychiatry, 13: 1069432.
125. Zhu MH, Liu ZJ, Hu QY, Yang JY, Jin Y, Zhu N, Huang Y, Shi DH, Liu MJ, Tan HY, Zhao L, Lv QY, Yi ZH, Wu FC, Li ZZ. (2022) Amisulpride augmentation therapy improves cognitive performance and psychopathology in clozapine-resistant treatment-refractory schizophrenia: a 12-week randomized, double-blind, placebo-controlled trial. Mil Med Res, 9: 59.
126. Howes OD, Kapur S. (2009) The dopamine hypothesis of schizophrenia: version III--the final common pathway. Schizophr Bull, 35: 549-562.
127. Uno Y, Coyle JT. (2019) Glutamate hypothesis in schizophrenia. Psychiatry Clin Neurosci, 73: 204-215.
128. Hu W, MacDonald ML, Elswick DE, Sweet RA. (2015) The glutamate hypothesis of schizophrenia: evidence from human brain tissue studies. Ann N Y Acad Sci, 1338: 38-57.
129. Eggers AE. (2013) A serotonin hypothesis of schizophrenia. Med Hypotheses, 80: 791-794.
130. de Jonge JC, Vinkers CH, Hulshoff Pol HE, Marsman A. (2017) GABAergic Mechanisms in Schizophrenia: Linking Postmortem and In Vivo Studies. Front Psychiatry, 8: 118.
131. Miller BJ, Goldsmith DR. (2020) Evaluating the Hypothesis That Schizophrenia Is an Inflammatory Disorder. Focus (Am Psychiatr Publ), 18: 391-401.
132. Murphy CE, Walker AK, Weickert CS. (2021) Neuroinflammation in schizophrenia: the role of nuclear factor kappa B. Transl Psychiatry, 11: 528.
133. Crow T. (2007) Genetic hypotheses for schizophrenia. Br J Psychiatry, 191: 180; author reply 180-181.

134. Henriksen MG, Nordgaard J, Jansson LB. (2017) Genetics of Schizophrenia: Overview of Methods, Findings and Limitations. Front Hum Neurosci, 11: 322.
135. Nour MM, Howes OD. (2015) Interpreting the neurodevelopmental hypothesis of schizophrenia in the context of normal brain development and ageing. Proc Natl Acad Sci U S A, 112: E2745.
136. Tsehay B, Seyoum G. (2021) The neurodevelopmental basis of schizophrenia: clinical clues from craniofacial dysmorphology in northwest Ethiopia, 2020. BMC Neurosci, 22: 59.
137. Szeligowski T, Yun AL, Lennox BR, Burnet PWJ. (2020) The Gut Microbiome and Schizophrenia: The Current State of the Field and Clinical Applications. Front Psychiatry, 11: 156.
138. Vafadari B. (2021) Stress and the Role of the Gut-Brain Axis in the Pathogenesis of Schizophrenia: A Literature Review. Int J Mol Sci, 22.
139. Kitzinger H, Arnold DG, et al. (1949) A preliminary study of the effects of glutamic acid on catatonic schizophrenics. Rorschach Res Exch J Proj Tech, 13: 210-218.
140. Kim JS, Kornhuber HH, Schmid-Burgk W, Holzmuller B. (1980) Low cerebrospinal fluid glutamate in schizophrenic patients and a new hypothesis on schizophrenia. Neurosci Lett, 20: 379-382.
141. Perry TL. (1982) Normal cerebrospinal fluid and brain glutamate levels in schizophrenia do not support the hypothesis of glutamatergic neuronal dysfunction. Neurosci Lett, 28: 81-85.
142. Korpi ER, Kaufmann CA, Marnela KM, Weinberger DR. (1987) Cerebrospinal fluid amino acid concentrations in chronic schizophrenia. Psychiatry Res, 20: 337-345.
143. Luby ED, Cohen BD, Rosenbaum G, Gottlieb JS, Kelley R. (1959) Study of a new schizophrenomimetic drug; sernyl. AMA Arch Neurol Psychiatry, 81: 363-369.
144. Itil T, Keskiner A, Kiremitci N, Holden JM. (1967) Effect of phencyclidine in chronic schizophrenics. Can Psychiatr Assoc J, 12: 209-212.
145. Krystal JH, Karper LP, Seibyl JP, Freeman GK, Delaney R, Bremner JD, Heninger GR, Bowers MB, Jr., Charney DS. (1994) Subanesthetic effects of the noncompetitive NMDA antagonist, ketamine, in humans. Psychotomimetic, perceptual, cognitive, and neuroendocrine responses. Arch Gen Psychiatry, 51: 199-214.
146. Javitt DC, Zukin SR. (1991) Recent advances in the phencyclidine model of schizophrenia. Am J Psychiatry, 148: 1301-1308.
147. Tsai G, Passani LA, Slusher BS, Carter R, Baer L, Kleinman JE, Coyle JT. (1995) Abnormal excitatory neurotransmitter metabolism in schizophrenic brains. Arch Gen Psychiatry, 52: 829-836.
148. Egan MF, Straub RE, Goldberg TE, Yakub I, Callicott JH, Hariri AR, Mattay VS, Bertolino A, Hyde TM, Shannon-Weickert C, Akil M, Crook J, Vakkalanka RK, Balkissoon R, Gibbs RA, Kleinman JE, Weinberger DR. (2004) Variation in GRM3 affects cognition, prefrontal glutamate, and risk for schizophrenia. Proc Natl Acad Sci U S A, 101: 12604-12609.
149. Gleason SD, Shannon HE. (1997) Blockade of phencyclidine-induced hyperlocomotion by olanzapine, clozapine and serotonin receptor subtype selective antagonists in mice. Psychopharmacology (Berl), 129: 79-84.
150. Javitt DC, Jayachandra M, Lindsley RW, Specht CM, Schroeder CE. (2000) Schizophrenia-like deficits in auditory P1 and N1 refractoriness induced by the psychomimetic agent phencyclidine (PCP). Clin Neurophysiol, 111: 833-836.
151. Williams HJ, Zamzow CR, Robertson H, Dursun SM. (2006) Effects of clozapine plus lamotrigine on phencyclidine-induced hyperactivity. Prog Neuropsychopharmacol Biol Psychiatry, 30: 239-243.

152. Noda Y, Yamada K, Furukawa H, Nabeshima T. (1995) Enhancement of immobility in a forced swimming test by subacute or repeated treatment with phencyclidine: a new model of schizophrenia. Br J Pharmacol, 116: 2531-2537.
153. Noda Y, Kamei H, Mamiya T, Furukawa H, Nabeshima T. (2000) Repeated phencyclidine treatment induces negative symptom-like behavior in forced swimming test in mice: imbalance of prefrontal serotonergic and dopaminergic functions. Neuropsychopharmacology, 23: 375-387.
154. Nagai T, Noda Y, Une T, Furukawa K, Furukawa H, Kan QM, Nabeshima T. (2003) Effect of AD-5423 on animal models of schizophrenia: phencyclidine-induced behavioral changes in mice. Neuroreport, 14: 269-272.
155. Noda A, Noda Y, Kamei H, Ichihara K, Mamiya T, Nagai T, Sugiura S, Furukawa H, Nabeshima T. (2001) Phencyclidine impairs latent learning in mice: interaction between glutamatergic systems and sigma(1) receptors. Neuropsychopharmacology, 24: 451-460.
156. Jentsch JD, Dazzi L, Chhatwal JP, Verrico CD, Roth RH. (1998) Reduced prefrontal cortical dopamine, but not acetylcholine, release in vivo after repeated, intermittent phencyclidine administration to rats. Neurosci Lett, 258: 175-178.
157. Abdul-Monim Z, Neill JC, Reynolds GP. (2007) Sub-chronic psychotomimetic phencyclidine induces deficits in reversal learning and alterations in parvalbumin-immunoreactive expression in the rat. J Psychopharmacol, 21: 198-205.
158. Brigman JL, Ihne J, Saksida LM, Bussey TJ, Holmes A. (2009) Effects of Subchronic Phencyclidine (PCP) Treatment on Social Behaviors, and Operant Discrimination and Reversal Learning in C57BL/6J Mice. Front Behav Neurosci, 3: 2.
159. Zain MA, Rouhollahi E, Pandy V, Mani V, Majeed ABA, Wong WF, Mohamed Z. (2018) Phencyclidine dose optimisation for induction of spatial learning and memory deficits related to schizophrenia in C57BL/6 mice. Exp Anim, 67: 421-429.
160. Semple BD, Blomgren K, Gimlin K, Ferriero DM, Noble-Haeusslein LJ. (2013) Brain development in rodents and humans: Identifying benchmarks of maturation and vulnerability to injury across species. Prog Neurobiol, 106-107: 1-16.
161. Sircar R, Rudy JW. (1998) Repeated Neonatal Phencyclidine Treatment Impairs Performance of a Spatial Task in Juvenile Rats(a). Ann N Y Acad Sci, 844: 303-309.
162. Sircar R. (2003) Postnatal phencyclidine-induced deficit in adult water maze performance is associated with N-methyl-D-aspartate receptor upregulation. Int J Dev Neurosci, 21: 159-167.
163. Andersen JD, Pouzet B. (2004) Spatial memory deficits induced by perinatal treatment of rats with PCP and reversal effect of D-serine. Neuropsychopharmacology, 29: 1080-1090.
164. Nakatani-Pawlak A, Yamaguchi K, Tatsumi Y, Mizoguchi H, Yoneda Y. (2009) Neonatal phencyclidine treatment in mice induces behavioral, histological and neurochemical abnormalities in adulthood. Biol Pharm Bull, 32: 1576-1583.
165. Grayson B, Barnes SA, Markou A, Piercy C, Podda G, Neill JC. (2016) Postnatal Phencyclidine (PCP) as a Neurodevelopmental Animal Model of Schizophrenia Pathophysiology and Symptomatology: A Review. Curr Top Behav Neurosci, 29: 403-428.
166. Nakahara S, Turner JA, Calhoun VD, Lim KO, Mueller B, Bustillo JR, O'Leary DS, McEwen S, Voyvodic J, Belger A, Mathalon DH, Ford JM, Macciardi F, Matsumoto M, Potkin SG, van Erp TGM. (2020) Dentate gyrus volume deficit in schizophrenia. Psychol Med, 50: 1267-1277.
167. Kay Y, Tsan L, Davis EA, Tian C, Decarie-Spain L, Sadybekov A, Pushkin AN, Katritch V, Kanoski SE, Herring BE. (2022) Schizophrenia-associated SAP97

mutations increase glutamatergic synapse strength in the dentate gyrus and impair contextual episodic memory in rats. Nat Commun, 13: 798.
168. Walton NM, Zhou Y, Kogan JH, Shin R, Webster M, Gross AK, Heusner CL, Chen Q, Miyake S, Tajinda K, Tamura K, Miyakawa T, Matsumoto M. (2012) Detection of an immature dentate gyrus feature in human schizophrenia/bipolar patients. Transl Psychiatry, 2: e135.
169. Enomoto A, Asai N, Namba T, Wang Y, Kato T, Tanaka M, Tatsumi H, Taya S, Tsuboi D, Kuroda K, Kaneko N, Sawamoto K, Miyamoto R, Jijiwa M, Murakumo Y, Sokabe M, Seki T, Kaibuchi K, Takahashi M. (2009) Roles of disrupted-in-schizophrenia 1-interacting protein girdin in postnatal development of the dentate gyrus. Neuron, 63: 774-787.
170. Zhao XF, Kohen R, Parent R, Duan Y, Fisher GL, Korn MJ, Ji L, Wan G, Jin J, Puschel AW, Dolan DF, Parent JM, Corfas G, Murphy GG, Giger RJ. (2018) PlexinA2 Forward Signaling through Rap1 GTPases Regulates Dentate Gyrus Development and Schizophrenia-like Behaviors. Cell Rep, 22: 456-470.
171. Csolle C, Ando RD, Kittel A, Goloncser F, Baranyi M, Soproni K, Zelena D, Haller J, Nemeth T, Mocsai A, Sperlagh B. (2013) The absence of P2X7 receptors (P2rx7) on non-haematopoietic cells leads to selective alteration in mood-related behaviour with dysregulated gene expression and stress reactivity in mice. Int J Neuropsychopharmacol, 16: 213-233.
172. Gigg J, McEwan F, Smausz R, Neill J, Harte MK. (2020) Synaptic biomarker reduction and impaired cognition in the sub-chronic PCP mouse model for schizophrenia. J Psychopharmacol, 34: 115-124.
173. Yan Z, Khadra A, Sherman A, Stojilkovic SS. (2011) Calcium-dependent block of P2X7 receptor channel function is allosteric. J Gen Physiol, 138: 437-452.
174. Guo C, Masin M, Qureshi OS, Murrell-Lagnado RD. (2007) Evidence for functional P2X4/P2X7 heteromeric receptors. Mol Pharmacol, 72: 1447-1456.
175. Grillon C, Ameli R, Charney DS, Krystal J, Braff D. (1992) Startle gating deficits occur across prepulse intensities in schizophrenic patients. Biol Psychiatry, 32: 939-943.
176. Weike AI, Bauer U, Hamm AO. (2000) Effective neuroleptic medication removes prepulse inhibition deficits in schizophrenia patients. Biol Psychiatry, 47: 61-70.
177. Braff DL, Light GA, Ellwanger J, Sprock J, Swerdlow NR. (2005) Female schizophrenia patients have prepulse inhibition deficits. Biol Psychiatry, 57: 817-820.
178. Mena A, Ruiz-Salas JC, Puentes A, Dorado I, Ruiz-Veguilla M, De la Casa LG. (2016) Reduced Prepulse Inhibition as a Biomarker of Schizophrenia. Front Behav Neurosci, 10: 202.
179. Swerdlow NR, Light GA, Sprock J, Calkins ME, Green MF, Greenwood TA, Gur RE, Gur RC, Lazzeroni LC, Nuechterlein KH, Radant AD, Ray A, Seidman LJ, Siever LJ, Silverman JM, Stone WS, Sugar CA, Tsuang DW, Tsuang MT, Turetsky BI, Braff DL. (2014) Deficient prepulse inhibition in schizophrenia detected by the multi-site COGS. Schizophr Res, 152: 503-512.
180. Zhang Y, Huang L, Kozlov SA, Rubini P, Tang Y, Illes P. (2020) Acupuncture alleviates acid- and purine-induced pain in rodents. Br J Pharmacol, 177: 77-92.
181. Horvath G, Otrokocsi L, Beko K, Baranyi M, Kittel A, Fritz-Ruenes PA, Sperlagh B. (2019) P2X7 Receptors Drive Poly(I:C) Induced Autism-like Behavior in Mice. J Neurosci, 39: 2542-2561.
182. Szabo D, Tod P, Goloncser F, Roman V, Lendvai B, Otrokocsi L, Sperlagh B. (2022) Maternal P2X7 receptor inhibition prevents autism-like phenotype in male mouse offspring through the NLRP3-IL-1beta pathway. Brain Behav Immun, 101: 318-332.

183. Huang L, Mut-Arbona P, Varga B, Torok B, Brunner J, Arszovszki A, Iring A, Kisfali M, Vizi ES, Sperlagh B. (2023) P2X7 purinergic receptor modulates dentate gyrus excitatory neurotransmission and alleviates schizophrenia-like symptoms in mouse. iScience, 26: 107560.
184. Wong AY, Billups B, Johnston J, Evans RJ, Forsythe ID. (2006) Endogenous activation of adenosine A1 receptors, but not P2X receptors, during high-frequency synaptic transmission at the calyx of Held. J Neurophysiol, 95: 3336-3342.
185. Sperlagh B, Vizi ES. (2011) The role of extracellular adenosine in chemical neurotransmission in the hippocampus and Basal Ganglia: pharmacological and clinical aspects. Curr Top Med Chem, 11: 1034-1046.
186. Qi G, van Aerde K, Abel T, Feldmeyer D. (2017) Adenosine Differentially Modulates Synaptic Transmission of Excitatory and Inhibitory Microcircuits in Layer 4 of Rat Barrel Cortex. Cereb Cortex, 27: 4411-4422.
187. Baxter AW, Choi SJ, Sim JA, North RA. (2011) Role of P2X4 receptors in synaptic strengthening in mouse CA1 hippocampal neurons. Eur J Neurosci, 34: 213-220.
188. Sim JA, Chaumont S, Jo J, Ulmann L, Young MT, Cho K, Buell G, North RA, Rassendren F. (2006) Altered hippocampal synaptic potentiation in P2X4 knock-out mice. J Neurosci, 26: 9006-9009.
189. Montilla A, Mata GP, Matute C, Domercq M. (2020) Contribution of P2X4 Receptors to CNS Function and Pathophysiology. Int J Mol Sci, 21.
190. Hudmon A, Schulman H, Kim J, Maltez JM, Tsien RW, Pitt GS. (2005) CaMKII tethers to L-type Ca2+ channels, establishing a local and dedicated integrator of Ca2+ signals for facilitation. J Cell Biol, 171: 537-547.
191. Qian J, Noebels JL. (2001) Presynaptic Ca2+ channels and neurotransmitter release at the terminal of a mouse cortical neuron. Journal of Neuroscience, 21: 3721-3728.
192. Khan MT, Liu J, Nerlich J, Tang Y, Franke H, Illes P. (2018) Regulation of P2X7 receptor function of neural progenitor cells in the hippocampal subgranular zone by neuronal activity in the dentate gyrus. Neuropharmacology, 140: 139-149.
193. North RA. (2004) P2X3 receptors and peripheral pain mechanisms. J Physiol, 554: 301-308.
194. Stephan G, Huang L, Tang Y, Vilotti S, Fabbretti E, Yu Y, Norenberg W, Franke H, Goloncser F, Sperlagh B, Dopychai A, Hausmann R, Schmalzing G, Rubini P, Illes P. (2018) The ASIC3/P2X3 cognate receptor is a pain-relevant and ligand-gated cationic channel. Nat Commun, 9: 1354.
195. Papp L, Vizi ES, Sperlagh B. (2004) Lack of ATP-evoked GABA and glutamate release in the hippocampus of P2X7 receptor-/- mice. Neuroreport, 15: 2387-2391.
196. Alloisio S, Cervetto C, Passalacqua M, Barbieri R, Maura G, Nobile M, Marcoli M. (2008) Functional evidence for presynaptic P2X7 receptors in adult rat cerebrocortical nerve terminals. FEBS Lett, 582: 3948-3953.
197. Kukley M, Stausberg P, Adelmann G, Chessell IP, Dietrich D. (2004) Ecto-nucleotidases and nucleoside transporters mediate activation of adenosine receptors on hippocampal mossy fibers by P2X7 receptor agonist 2'-3'-O-(4-benzoylbenzoyl)-ATP. J Neurosci, 24: 7128-7139.
198. Kosmowska B, Ossowska K, Konieczny J, Lenda T, Berghauzen-Maciejewska K, Wardas J. (2020) Inhibition of Excessive Glutamatergic Transmission in the Ventral Thalamic Nuclei by a Selective Adenosine A1 Receptor Agonist, 5'-Chloro-5'-Deoxy-(+/-)-ENBA Underlies its Tremorolytic Effect in the Harmaline-Induced Model of Essential Tremor. Neuroscience, 429: 106-118.
199. Wang J, Gong Y, Tan H, Li W, Yan B, Cheng C, Wan J, Sun W, Yuan C, Yao LH. (2022) Cordycepin suppresses glutamatergic and GABAergic synaptic transmission

through activation of A(1) adenosine receptor in rat hippocampal CA1 pyramidal neurons. Biomed Pharmacother, 145: 112446.

200. Rombo DM, Dias RB, Duarte ST, Ribeiro JA, Lamsa KP, Sebastiao AM. (2016) Adenosine A1 Receptor Suppresses Tonic GABAA Receptor Currents in Hippocampal Pyramidal Cells and in a Defined Subpopulation of Interneurons. Cereb Cortex, 26: 1081-1095.
201. Wall MJ, Wigmore G, Lopatar J, Frenguelli BG, Dale N. (2008) The novel NTPDase inhibitor sodium polyoxotungstate (POM-1) inhibits ATP breakdown but also blocks central synaptic transmission, an action independent of NTPDase inhibition. Neuropharmacology, 55: 1251-1258.
202. Chancey JH, Poulsen DJ, Wadiche JI, Overstreet-Wadiche L. (2014) Hilar mossy cells provide the first glutamatergic synapses to adult-born dentate granule cells. J Neurosci, 34: 2349-2354.
203. Chiu CQ, Castillo PE. (2008) Input-specific plasticity at excitatory synapses mediated by endocannabinoids in the dentate gyrus. Neuropharmacology, 54: 68-78.
204. Kilbride J, Rush AM, Rowan MJ, Anwyl R. (2001) Presynaptic group II mGluR inhibition of short-term depression in the medial perforant path of the dentate gyrus in vitro. J Neurophysiol, 85: 2509-2515.
205. Macek TA, Winder DG, Gereau RWt, Ladd CO, Conn PJ. (1996) Differential involvement of group II and group III mGluRs as autoreceptors at lateral and medial perforant path synapses. J Neurophysiol, 76: 3798-3806.
206. Monory K, Massa F, Egertova M, Eder M, Blaudzun H, Westenbroek R, Kelsch W, Jacob W, Marsch R, Ekker M, Long J, Rubenstein JL, Goebbels S, Nave KA, During M, Klugmann M, Wolfel B, Dodt HU, Zieglgansberger W, Wotjak CT, Mackie K, Elphick MR, Marsicano G, Lutz B. (2006) The endocannabinoid system controls key epileptogenic circuits in the hippocampus. Neuron, 51: 455-466.
207. Magloczky Z, Toth K, Karlocai R, Nagy S, Eross L, Czirjak S, Vajda J, Rasonyi G, Kelemen A, Juhos V, Halasz P, Mackie K, Freund TF. (2010) Dynamic changes of CB1-receptor expression in hippocampi of epileptic mice and humans. Epilepsia, 51 Suppl 3: 115-120.
208. McNaughton BL. (1980) Evidence for two physiologically distinct perforant pathways to the fascia dentata. Brain Res, 199: 1-19.
209. Suzuki E, Sato M, Takezawa R, Usuki T, Okada T. (2011) The facilitative effects of bilobalide, a unique constituent of Ginkgo biloba, on synaptic transmission and plasticity in hippocampal subfields. J Physiol Sci, 61: 421-427.
210. Scimemi A, Schorge S, Kullmann DM, Walker MC. (2006) Epileptogenesis is associated with enhanced glutamatergic transmission in the perforant path. J Neurophysiol, 95: 1213-1220.
211. Ding F, O'Donnell J, Xu Q, Kang N, Goldman N, Nedergaard M. (2016) Changes in the composition of brain interstitial ions control the sleep-wake cycle. Science, 352: 550-555.
212. Silver IA, Erecinska M. (1990) Intracellular and extracellular changes of [Ca2+] in hypoxia and ischemia in rat brain in vivo. J Gen Physiol, 95: 837-866.
213. Jones HC, Keep RF. (1988) Brain fluid calcium concentration and response to acute hypercalcaemia during development in the rat. J Physiol, 402: 579-593.
214. Illes P, Muller CE, Jacobson KA, Grutter T, Nicke A, Fountain SJ, Kennedy C, Schmalzing G, Jarvis MF, Stojilkovic SS, King BF, Di Virgilio F. (2021) Update of P2X receptor properties and their pharmacology: IUPHAR Review 30. Br J Pharmacol, 178: 489-514.

215. Wildman SS, Unwin RJ, King BF. (2003) Extended pharmacological profiles of rat P2Y2 and rat P2Y4 receptors and their sensitivity to extracellular H+ and Zn2+ ions. Br J Pharmacol, 140: 1177-1186.
216. Suplat-Wypych D, Dygas A, Baranska J. (2010) 2', 3'-O-(4-benzoylbenzoyl)-ATP-mediated calcium signaling in rat glioma C6 cells: role of the P2Y(2) nucleotide receptor. Purinergic Signal, 6: 317-325.
217. Schneider M, Prudic K, Pippel A, Klapperstuck M, Braam U, Muller CE, Schmalzing G, Markwardt F. (2017) Interaction of Purinergic P2X4 and P2X7 Receptor Subunits. Front Pharmacol, 8: 860.
218. Hracsko Z, Baranyi M, Csolle C, Goloncser F, Madarasz E, Kittel A, Sperlagh B. (2011) Lack of neuroprotection in the absence of P2X7 receptors in toxin-induced animal models of Parkinson's disease. Mol Neurodegener, 6: 28.
219. Bartlett R, Yerbury JJ, Sluyter R. (2013) P2X7 receptor activation induces reactive oxygen species formation and cell death in murine EOC13 microglia. Mediators Inflamm, 2013: 271813.
220. Kaczmarek-Hajek K, Zhang J, Kopp R, Grosche A, Rissiek B, Saul A, Bruzzone S, Engel T, Jooss T, Krautloher A, Schuster S, Magnus T, Stadelmann C, Sirko S, Koch-Nolte F, Eulenburg V, Nicke A. (2018) Re-evaluation of neuronal P2X7 expression using novel mouse models and a P2X7-specific nanobody. Elife, 7.
221. Zhao YF, Ren WJ, Zhang Y, He JR, Yin HY, Liao Y, Rubini P, Deussing JM, Verkhratsky A, Yuan ZQ, Illes P, Tang Y. (2022) High, in Contrast to Low Levels of Acute Stress Induce Depressive-like Behavior by Involving Astrocytic, in Addition to Microglial P2X7 Receptors in the Rodent Hippocampus. Int J Mol Sci, 23.
222. Liang X, Samways DS, Wolf K, Bowles EA, Richards JP, Bruno J, Dutertre S, DiPaolo RJ, Egan TM. (2015) Quantifying Ca2+ current and permeability in ATP-gated P2X7 receptors. J Biol Chem, 290: 7930-7942.
223. Kohli S, King MV, Williams S, Edwards A, Ballard TM, Steward LJ, Alberati D, Fone KCF. (2019) Oxytocin attenuates phencyclidine hyperactivity and increases social interaction and nucleus accumben dopamine release in rats. Neuropsychopharmacology, 44: 295-305.
224. Wang P, Cao T, Chen J, Jiang Y, Wang C, Waddington JL, Zhen X. (2019) D2 receptor-mediated miRNA-143 expression is associated with the effects of antipsychotic drugs on phencyclidine-induced schizophrenia-related locomotor hyperactivity and with Neuregulin-1 expression in mice. Neuropharmacology, 157: 107675.
225. Wang X, Liu J, Dai Z, Sui Y. (2021) Andrographolide improves PCP-induced schizophrenia-like behaviors through blocking interaction between NRF2 and KEAP1. J Pharmacol Sci, 147: 9-17.
226. Mitchell EJ, Brett RR, Armstrong JD, Sillito RR, Pratt JA. (2020) Temporal dissociation of phencyclidine: Induced locomotor and social alterations in rats using an automated homecage monitoring system - implications for the 3Rs and preclinical drug discovery. J Psychopharmacol, 34: 709-715.
227. Bujas-Bobanovic M, Bird DC, Robertson HA, Dursun SM. (2000) Blockade of phencyclidine-induced effects by a nitric oxide donor. Br J Pharmacol, 130: 1005-1012.
228. Martinez ZA, Ellison GD, Geyer MA, Swerdlow NR. (1999) Effects of sustained phencyclidine exposure on sensorimotor gating of startle in rats. Neuropsychopharmacology, 21: 28-39.
229. Andreasen JT, Andersen KK, Nielsen EO, Mathiasen L, Mirza NR. (2006) Nicotine and clozapine selectively reverse a PCP-induced deficit of PPI in BALB/cByJ but not NMRI mice: comparison with risperidone. Behav Brain Res, 167: 118-127.

230. Kjaerby C, Bundgaard C, Fejgin K, Kristiansen U, Dalby NO. (2013) Repeated potentiation of the metabotropic glutamate receptor 5 and the alpha 7 nicotinic acetylcholine receptor modulates behavioural and GABAergic deficits induced by early postnatal phencyclidine (PCP) treatment. Neuropharmacology, 72: 157-168.
231. Maple AM, Call T, Kimmel PC, Hammer RP, Jr. (2017) Effects of Repeated Ropinirole Treatment on Phencyclidine-Induced Hyperlocomotion, Prepulse Inhibition Deficits, and Social Avoidance in Rats. J Pharmacol Exp Ther, 361: 109-114.
232. Sircar R, Soliman KF. (2003) Effects of postnatal PCP treatment on locomotor behavior and striatal D2 receptor. Pharmacol Biochem Behav, 74: 943-952.
233. Xu J, Chen XM, Zheng BJ, Wang XR. (2016) Electroacupuncture Relieves Nerve Injury-Induced Pain Hypersensitivity via the Inhibition of Spinal P2X7 Receptor-Positive Microglia. Anesth Analg, 122: 882-892.
234. Gao YH, Li CW, Wang JY, Tan LH, Duanmu CL, Jing XH, Chang XR, Liu JL. (2017) Effect of electroacupuncture on the cervicospinal P2X7 receptor/fractalkine/CX3CR1 signaling pathway in a rat neck-incision pain model. Purinergic Signal, 13: 215-225.
235. Honore P, Donnelly-Roberts D, Namovic M, Zhong C, Wade C, Chandran P, Zhu C, Carroll W, Perez-Medrano A, Iwakura Y, Jarvis MF. (2009) The antihyperalgesic activity of a selective P2X7 receptor antagonist, A-839977, is lost in IL-1alphabeta knockout mice. Behav Brain Res, 204: 77-81.

10. Bibliography related to the thesis and other publications

1. Huang L, Mut-Arbona P, Varga B, Torok B, Brunner J, Arszovszki A, Iring A, Kisfali M, Vizi ES, Sperlagh B. (2023) P2X7 purinergic receptor modulates dentate gyrus excitatory neurotransmission and alleviates schizophrenia-like symptoms in mouse. iScience, 26: 107560.11.2 (**IF: 5.8**)

2. Mut-Arbona P, Huang L, Baranyi M, Tod P, Iring A, Calzaferri F, de Los Rios C, Sperlagh B. (2023) Dual Role of the P2X7 Receptor in Dendritic OutgroWTh during Physiological and Pathological Brain Development. J Neurosci, 43: 1125-1142 (**IF: 5.3**)

3. Zhang Y, Huang L, Kozlov SA, Rubini P, Tang Y, Illes P. (2020) Acupuncture alleviates acid- and purine-induced pain in rodents. Br J Pharmacol, 177: 77-92. (**IF: 8.740**)

Additional publications

1. Huang L, Otrokocsi L, Sperlagh B. (2019) Role of P2 receptors in normal brain development and in neurodevelopmental psychiatric disorders. Brain Res Bull, 151: 55-64. (**IF: 3.370**)

2. Illes P, Rubini P, Huang L, Tang Y. (2019) The P2X7 receptor: a new therapeutic target in Alzheimer's disease. Expert Opin Ther Targets, 23: 165-176. (**IF: 5.473**)

3. Huang L, Sperlagh B. (2021) Caffeine consumption and schizophrenia: A highlight on adenosine receptor-independent mechanisms. Curr Opin Pharmacol, 61: 106-113.
(**IF: 4.768**)

4. Huang L, Tang Y, Sperlagh B. (2022) Glial Purinergic Signaling-Mediated Oxidative Stress (GPOS) in Neuropsychiatric Disorders. Oxid Med Cell Longev, 2022: 1075440. (**IF: 6.79**)

DOI:10.14753/SE.2024.2993

11. Acknowledgements

I would like to express my sincere gratitude to my supervisor, Professor Beáta Sperlágh, for providing me with the wonderful opportunity to start my PhD studies at Semmelweis University. Her supportive guidance, endless inspiration and thoughtful understanding throughout my studies have been instrumental in completing my PhD project.

Here, I also would like to thank Prof. E. Sylvester Vizi for the help with research design, Dr. Janos Brunner and Dr. Máté Kisfali for the help with electrophysiological recordings and analysis. I would also like to thank my colleagues, Dr. Andras Iring for the WB experiment (Figure 11B), Dr. Antónia Arszovszki for the Homer1 and vglut1 staining (15 C), Dr. Bibiána Török for the juvenile behaviours experiments (Figure 24), Bernadett Varga for the establishment of PCP model, Dr. Paula Mut-Arbona for the contribution in sholl analysis (the data did not show in my thesis).

I would also like to thank other colleagues in the group Dr. Mária Baranyi, Dr. Gölöncsér Flóra, and Tünde Oroszi in the Sperlágh Laboratory for making me feel included and supported both in my working environment and in my personal life. Without their help, my life here would have been much more difficult. I am grateful to the colleagues in Prof. János Szabadics' lab, for the invaluable advice which helped me to get through all the difficulties smoothly and calmly.

In past years, I received great help from different colleagues at the Institute of Experimental Medicine. Here I would like to express my sincere gratitude to Dr. Dóra Zelena and Dr. Gáspár Oláh for their help with immunostaining, viral injections, and Ca^{2+} imaging analysis. Many thanks also to Dr. László Barna and Dr. Pál Vági from the Microscopy Centre, Dr. Eszter Sipos from the Virus Laboratory, and Dr. Kornél Demeter from the Behavioural Research Unit, for their help and assistance with training. Without these professional training and technical support, I would not have been able to complete this project. Although I may not be able to name them all, I would like to express my special thanks to my colleagues at the Institute of Laboratory Medicine, Room 804, who were by my side whenever I had to finish my experiments late.

I would also like to express my thanks to Professor Peter Illes at the University of Leipzig and Professor Tang Yong at the Chengdu University of Traditional Chinese Medicine for providing

me with the opportunity to participate in the pain project during my PhD studies. Many thanks to Dr. Ying Zhang from Chengdu University of Traditional Chinese Medicine for her help with the pain project.

In addition, I would like to thank Marie Skłodowska-Curie and Purine DX under the European Union's Horizon 2020 Research and Innovation Programme, which funded my PhD studies abroad, enabled me to acquire skills in different disciplines, expanded my academic and social networks.

I am fortunate to have an open-minded mother in my life. Therefore, I would like to extend my sincerest gratitude to my lovely mother, Mrs. Chao-gui Zeng, for her unconditional love and endless support. I would also like to thank my lovely friends, Dr. Juliana Santana, Dr. Sarah Al Assaf, Haowei Hu, Roy Liang, Lin Cheng, Li Gu, Mrs. Stacy Carter, Mr. Wesley Carter and Mrs. Helen Grundy, for their precious company and unforgettable memories in Budapest.

Finally, I would like to thank all the animals who sacrificed their lives for this project. Without them, I would not have been able to complete my work.